ELECTRICAL COMMUNICATION

Technical Journal of the
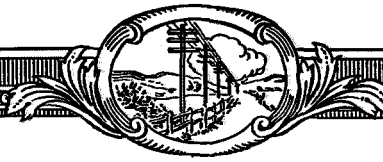*International Telephone and Telegraph Corporation*
and Associate Companies

●

HIGH-TENSION LABORATORY

SUBMINIATURE-TUBE RELIABILITY TESTING

ELECTROMAGNETIC DELAY LINES

PRECISION-APPROACH AIRFIELD RADAR

FUNCTIONAL DIAGRAMS FOR ELECTRONICS IN TELEGRAPHY

CUBIC DISTORTIONS IN RING MODULATORS

MICROSTRIP FOR BAND-PASS MICROWAVE FILTERS

COAXIAL LINE WITH HELICAL INNER CONDUCTOR

UNITED STATES PATENTS ISSUED TO THE INTERNATIONAL SYSTEM

Volume 32   **MARCH, 1955**   **Number 1**

ELECTRICAL COMMUNICATION

Technical Journal of the
International Telephone and Telegraph Corporation
and Associate Companies

Volume 32   MARCH, 1955   Number 1

CONTENTS

High-Tension Laboratory*

By AMUND BRAATEN

Standard Telefon og Kabelfabrik A/S; Oslo, Norway

DEMAND for supertension power-transmission cables in connection with the development of large water-power resources in Norway after the second world war created the necessity for a modern high-tension laboratory for cable testing and development. For economic and defensive reasons, power plants are preferably built underground, which necessitates the use of high-tension cables for linking the transformers with the outside switching plant. Furthermore, there is a tendency to use cables instead of high-tension overhead lines in suburbs and built-up areas. There is also an increasing demand for high-voltage submarine cables for the electrification of coastal districts.

A simplified plan of the building is given in Figure 1, while Figure 2 shows a general view of the laboratory proper. The main building housing the high-tension equipment is 12-sided

with a diameter of 98 feet (30 meters) and a floor-to-ceiling height of 46 feet (14 meters). The attached building has a floor space of 4300 square feet (400 square meters) and accommodates offices, physical laboratories for investigating insulating materials, instrument-maker's shop, and the control room for operation of the high-tension equipment.

The electrical installation consists of a 600-kilovolt alternating-current plant, a 2100-kilovolt surge generator, and a 1000-kilovolt direct-current set.

The alternating-current high-tension equipment is shown in Figure 3. It is capable of producing potentials up to 600 root-mean-square kilovolts and has a load capacity of 2400 kilovolt–amperes for 30 minutes. It consists of two units that may be connected in either series or parallel. Space is reserved for the future addition of a third unit that will raise the voltage to 900 kilovolts.
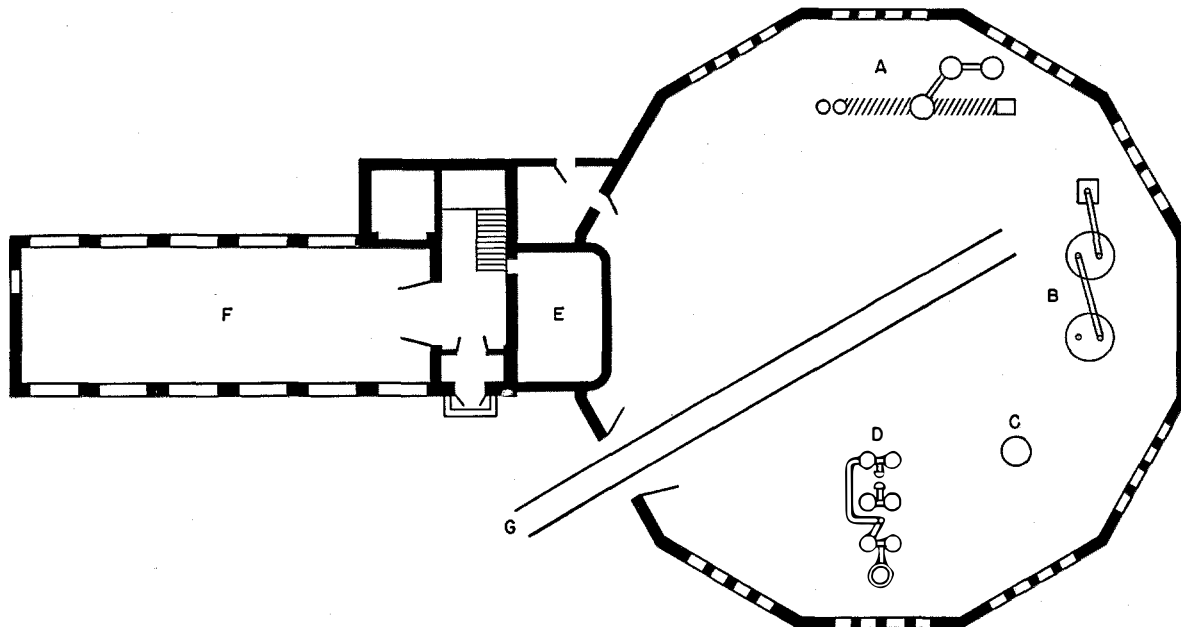

Figure 1—Plan of the laboratory. *A*—the 1 000 000-volt direct-current test set. *B*—600 000-volt alternating-current reactor set. *C*—1.5-meter-(4.9-foot-) diameter spark gap. *D*—2 100 000-volt impulse generator. *E*—the control room (on the second floor). *F*—physical laboratory, instrument shop, et cetera. *G*—railroad track.

High-voltage alternating current for testing purposes is usually obtained by using cascade-connected transformers. With capacitive loads, as is usual in the cable industry, there is always a possibility of resonance between the cable and transformer reactances. If this should happen at one of the supply-frequency harmonics, the waveform of the terminal voltage will be distorted. Another disadvantage with the cascade principle is that the transformers do not divide the potential equally among themselves because of uneven distribution of the circuit reactance.

To avoid these difficulties, it was decided to substitute for the conventional transformers a series circuit (Figure 4) having variable inductances tuned to resonate with the cable capacitance at 50 cycles per second. The series principle has the additional advantage that the short-circuit current at breakdown is reduced to a fraction of the load current. This is very important, as it avoids burning up the test specimens after breakdown. The reactors are continuously variable and are operated from the control desk.

Figure 5 and the frontispiece show the surge generator, which is a conventional two-column Marx circuit for charging capacitors in parallel and discharging them in series. The circuit is shown in Figure 6. The highest charging potential is 175 kilovolts per stage, giving the 12-stage generator a maximum discharge voltage of 2100 kilovolts. The energy per charge is 30 kilowatt–seconds at full voltage. The generator has a low self inductance and is designed to give a standard surge with a 1-microsecond front and 50-microsecond tail on short cable lengths. There is sufficient headroom to increase the generator output to 2500 kilovolts by adding two more stages.

For recording the surge, there is installed a

Figure 2—The high-voltage laboratory.
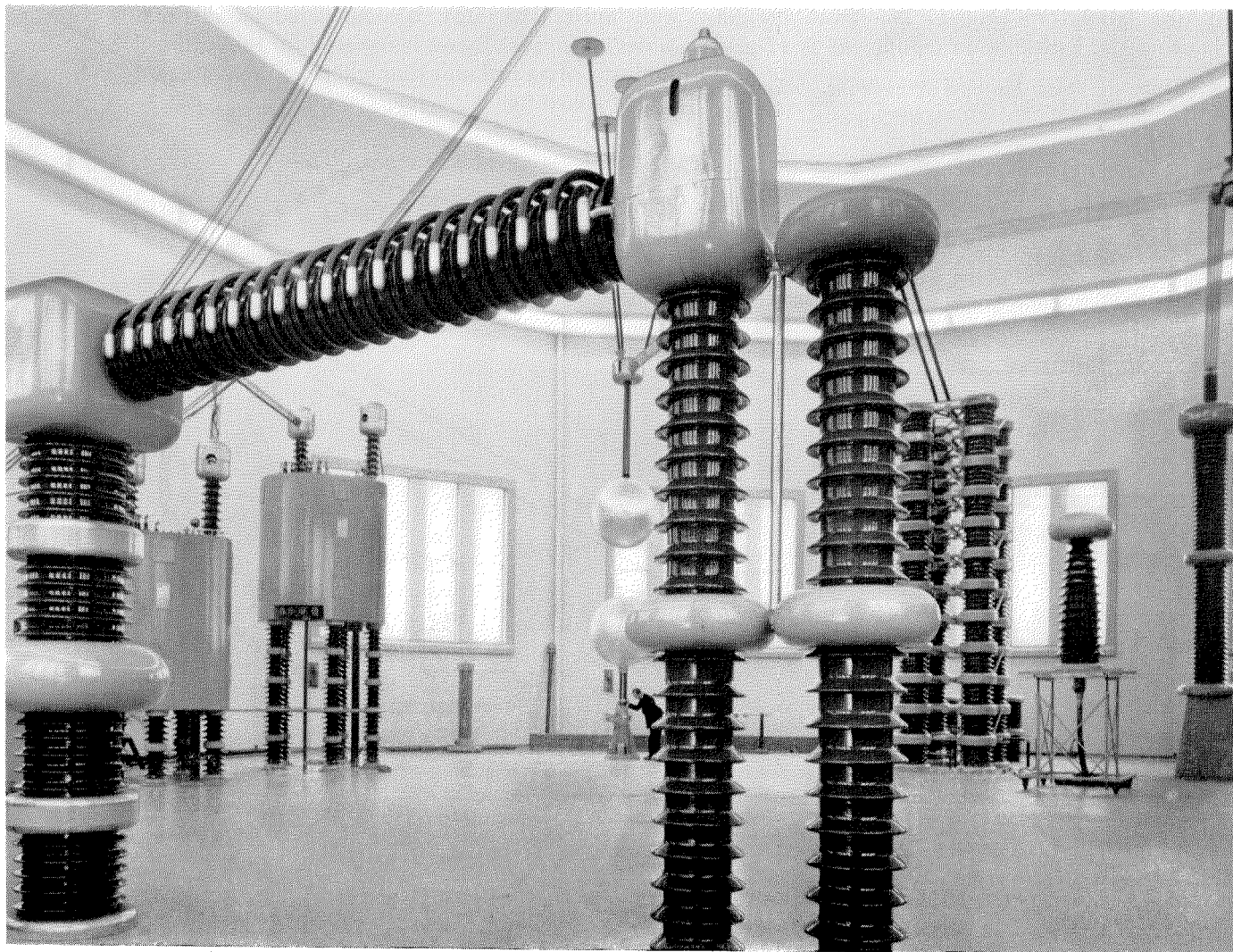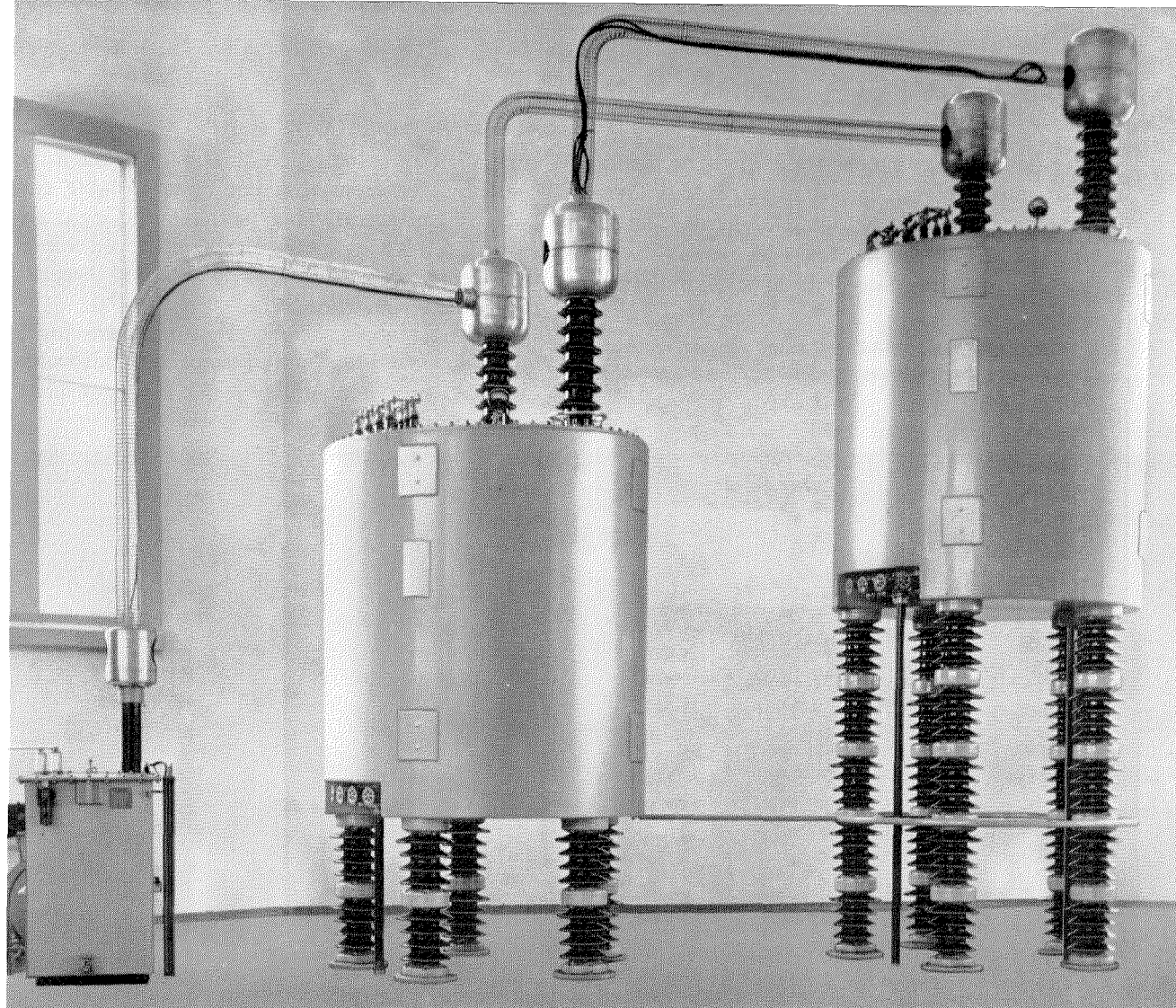
Figure 3—Above is the alternating-current set. The supply transformer is at the left. The two reactors step the voltage up to 300 and 600 kilovolts, respectively.

Figure 4—At right, simplified diagram of the alternating-current plant. The two reactors are tuned by means of moving coils to resonate with the capacitive cable load at 50 cycles.

300 KILOVOLTS

600 KILOVOLTS

CABLE LOAD

INPUT 0-5 KILOVOLTS 50 CYCLES

450 KILOVOLTS
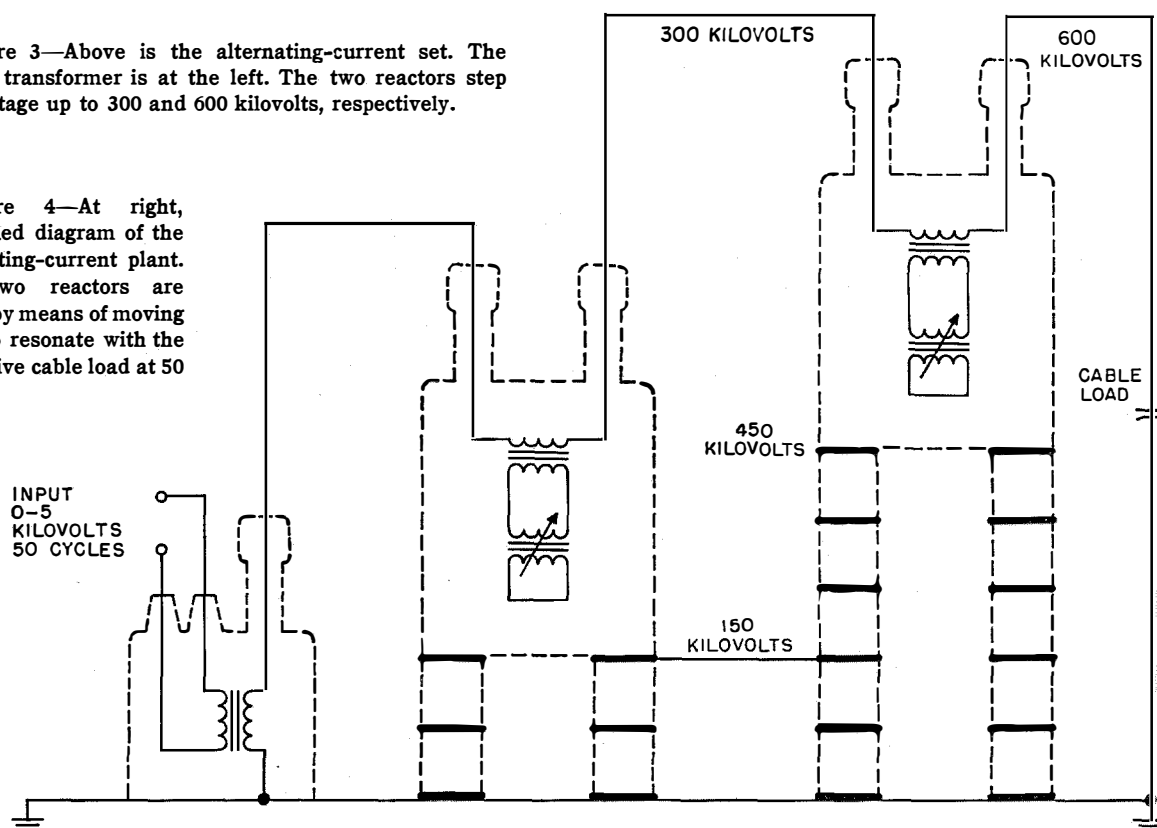
150 KILOVOLTS

two-beam continuously pumped oscillograph with an accelerating potential of 45 kilovolts, and having a writing speed of more than 6000 miles (10 000 kilometers) per second, or 10 meters per microsecond. The impulses are transmitted to the oscillograph through a coaxial cable from the foot of a variable capacitive voltage divider (seen to the right in Figure 5). The sweep can be observed on a fluorescent screen or it can be recorded directly on film.

Figure 7 shows the direct-current generator, which has a no-load potential of 1000 kilovolts and an output of 10 milliamperes. It is connected

Figure 5—The 2100-kilovolt surge generator. From left to right are the spark gap, generator columns, and capacitive voltage divider.
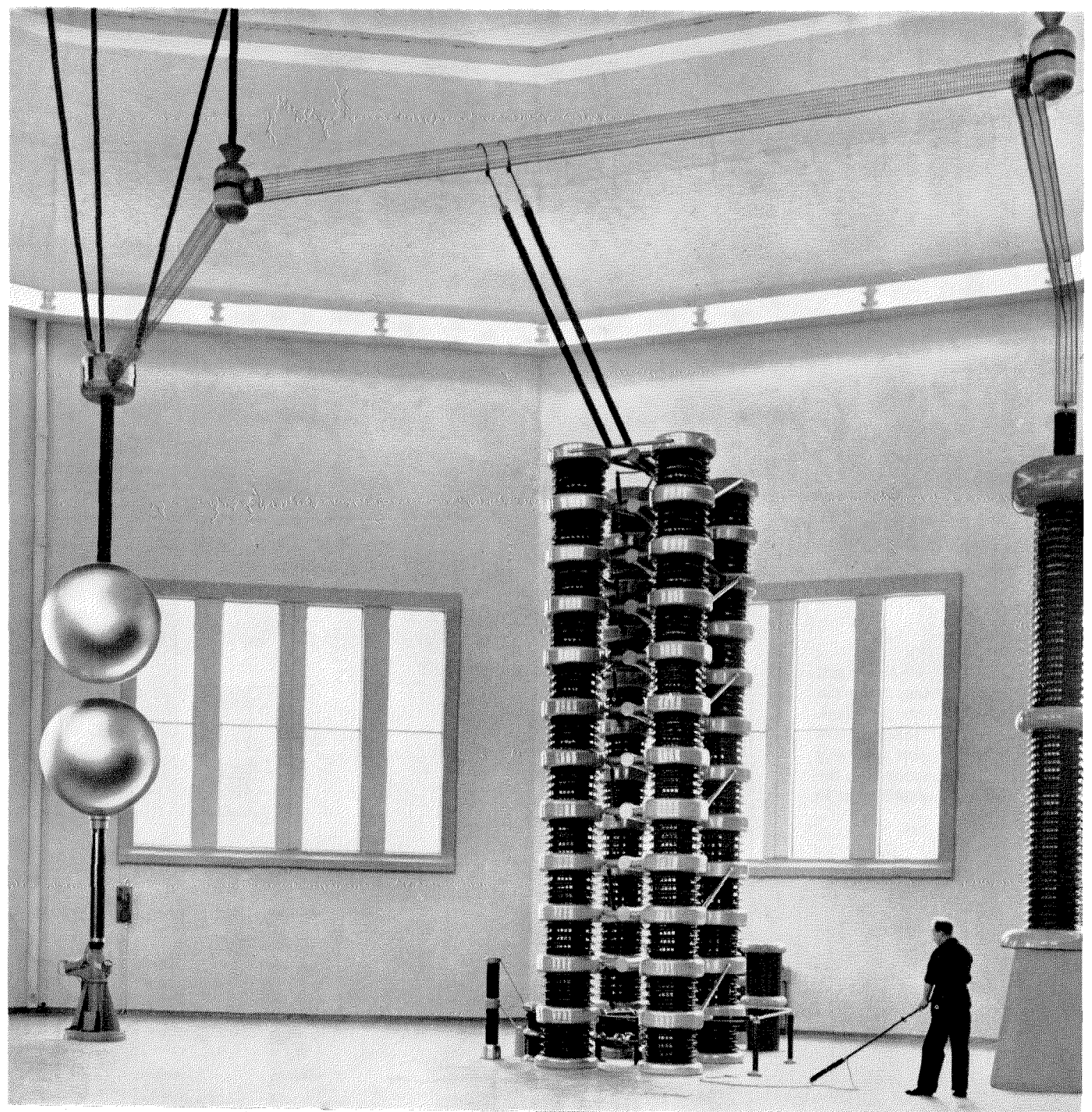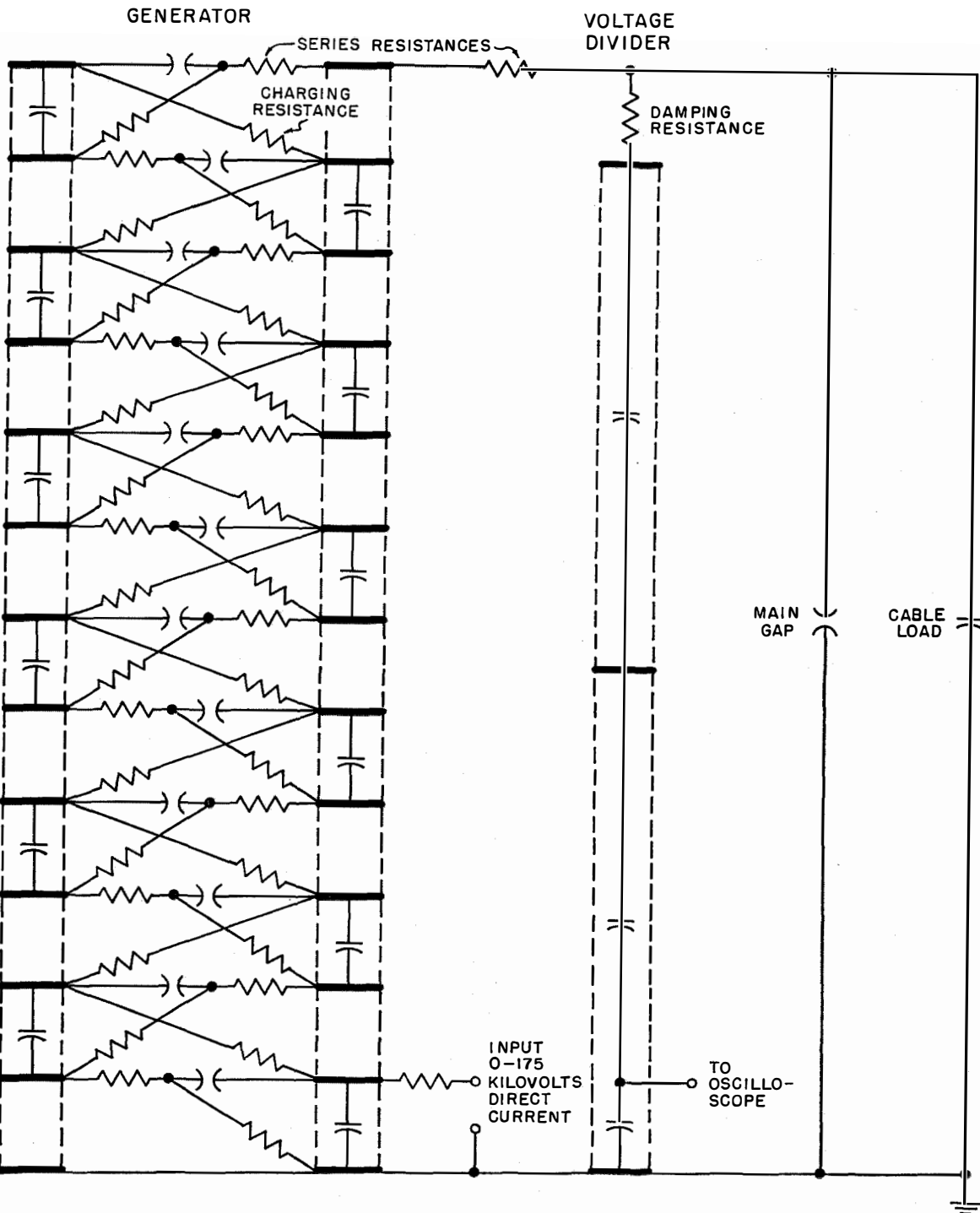
Figure 6—Schematic diagram of surge generator. The capacitors in the generator are 0.16 microfarad each. The capacitors are charged in parallel. When the gaps in the column break down, the capacitors are discharged in series across the load. The maximum surge voltage is set by the carefully calibrated main gap.

as a single Cockroft–Walton voltage-doubler circuit (Figure 8). The horizontal member contains the rectifier consisting of 64 000 selenium cells. By means of external connecting links, the rectifier column can be broken into sections for parallel connection to give higher current
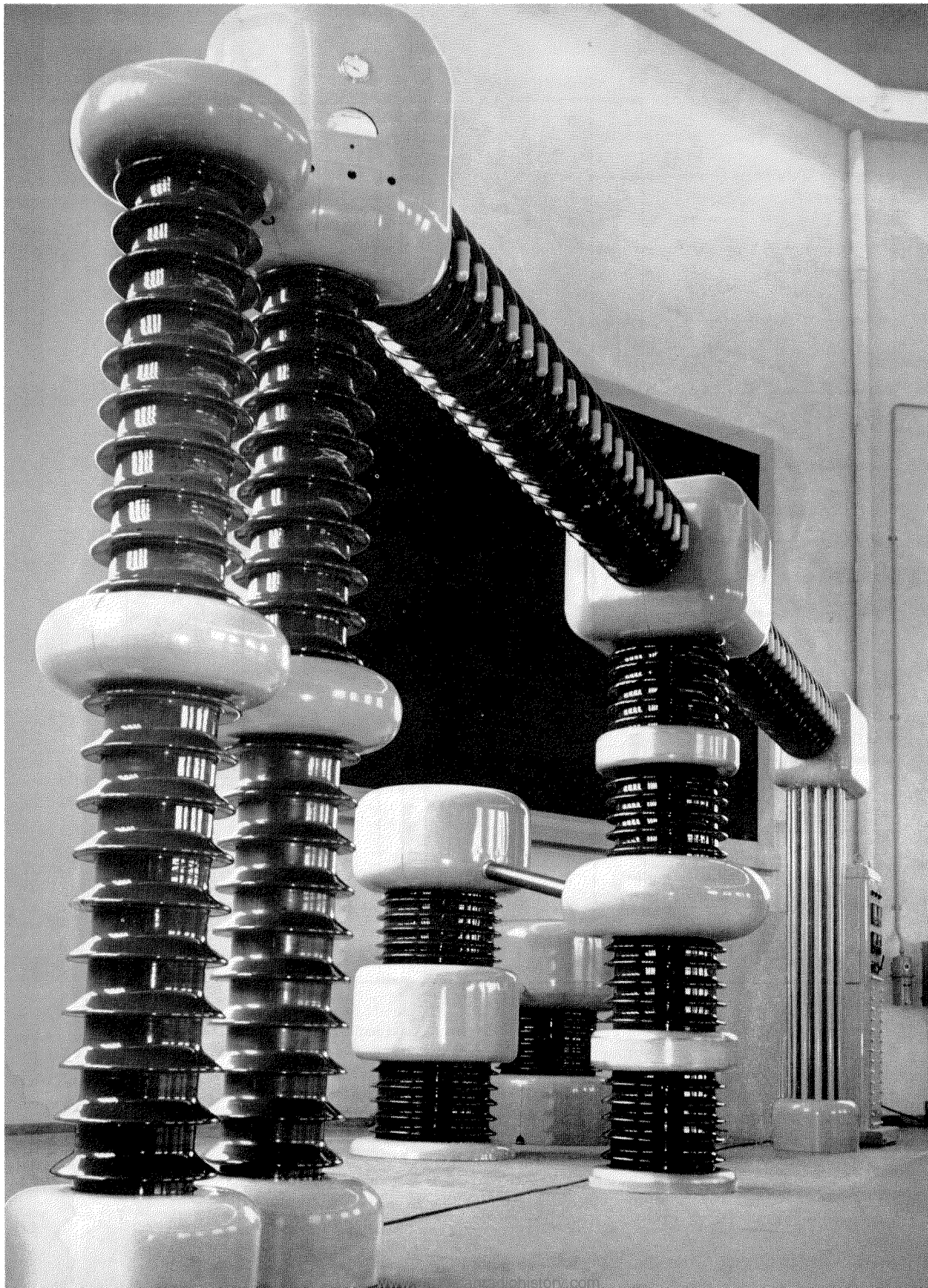
capacities at lower voltages. The same arrangement also permits change of polarity. The generator is oil cooled, a circulating pump being mounted on the right-hand cooling column.

used for measurement of alternating voltages. In this case the voltage is read in kilovolts on a direct-current instrument.

A system of bus bars is suspended from the ceiling for distribution of the potentials to the
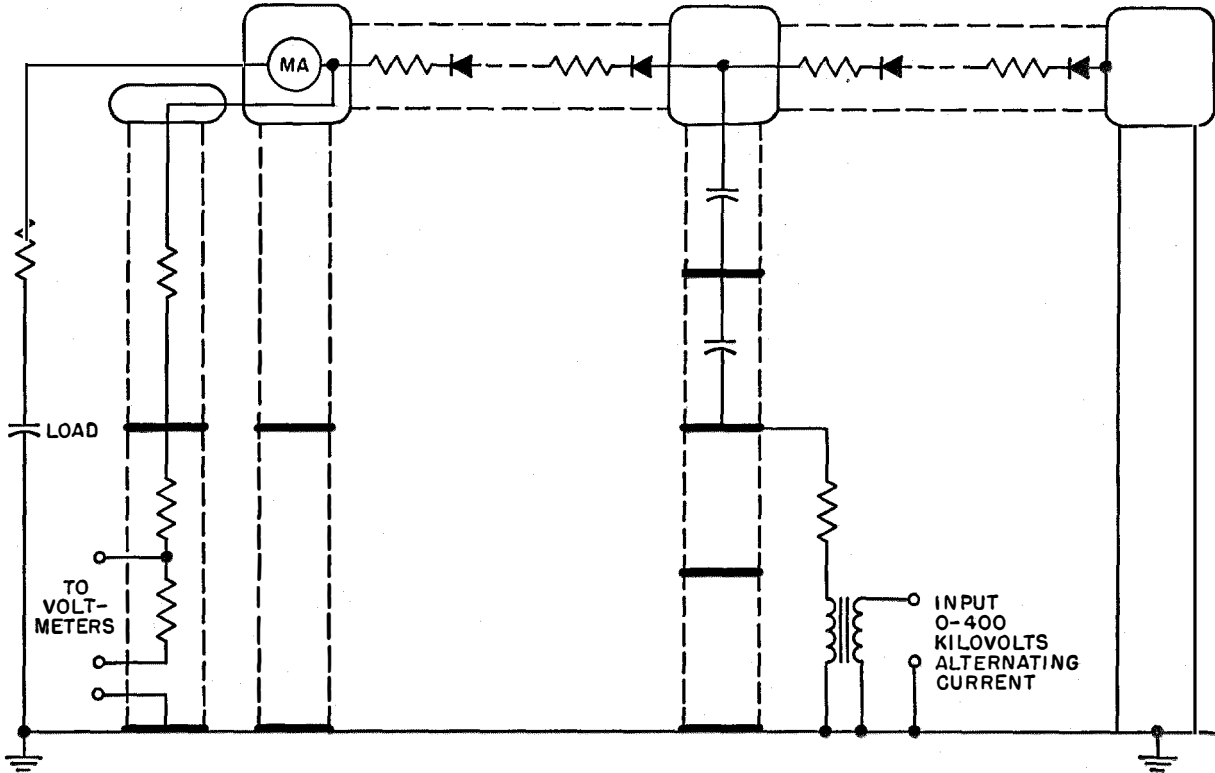
Figure 8—Circuit of the direct-current generator.

The control room is shown in Figure 9 with the oscillograph at the right. For checking high voltages and for calibration purposes, a spark gap with 1.5-meter- (4.9-foot-) diameter spheres is used. The gap distance can be adjusted remotely from the control desk, which also contains an instrument indicating the gap opening. As is well known, the spark-over voltage can be determined with good accuracy when the sphere diameter and the gap opening are known and adjustments are made for atmospheric conditions. The spheres are also

various parts of the test area. An extensive sectionalized grounding system is accessible at a number of points through wells in the floor. A railroad track is laid across the test area, making it possible to test heavy pieces.

To prevent disturbance to nearby radio receivers, especially when the surge generator is in operation, the laboratory walls and roof are electrostatically screened.

With potentials of the magnitude involved, it is often of interest to study corona discharges. These discharges emit very feeble light and

Figure 9—The control room looks into the laboratory from the second-floor level. The high-speed oscillograph is at the extreme right.

must be observed in absolute darkness. For this purpose the main building is equipped with remote-controlled blackout curtains.

The high-tension testing equipment was delivered by Ferranti Limited; Manchester, England. The selenium elements were supplied by Standard Telephones and Cables, Limited of London and the oscillograph by Trüb, Taüber and Company A/G of Zurich, Switzerland.

Standard Telefon og Kabelfabrik A/S is the only Norwegian factory making high-tension cables; the new laboratory will make it possible for the company to advance with the technical development of this field.

Subminiature-Tube Reliability Testing

By STERLING BICKEL

Farnsworth Electronics Company, a division of International Telephone and Telegraph Corporation; Fort Wayne, Indiana

FAILURE of a vital element in a guided missile during flight can so reduce the performance and the information received from the missle as to make the experiment almost worthless. In many such instances, the unreliability can be blamed on vacuum tubes. Poor workmanship during construction and variations in characteristics with time and environment make tubes a major source of circuit failure.

Especially stringent requirements are imposed by tactical environmental factors, such as; vibration, shock, acceleration, temperature extremes, et cetera, and every electronic tube installed in equipment designed or developed for missile applications must be subjected to a rigorous test program. Some of the procedures followed in the reliability testing of subminiature tubes as they are received from the manufacturer are outlined in this article.

1. Mechanical Inspection

The first step in the test and inspection procedure is to count the tubes and to inspect them visually for damage to envelopes, leads, et cetera. They are next checked for envelope diameter. For a small shipment, this is a 100-percent check, while with larger shipments only a spot check is made. If any tubes fail the spot check, the entire shipment is checked for envelope diameter. This is an important factor in insuring a proper fit in the tube mount of wired-in subminiature tubes.

All tubes passing the mechanical inspection are marked with a serial number. This procedure permits correlation of subsequent failures with data obtained during incoming inspection, a practical method of establishing minimum qualities for acceptable tubes.

2. Electrical Tests

2.1 TRANSCONDUCTANCE AND PLATE CURRENT

The transconductance of all tubes of the pentode and triode types is checked. At the same time, the plate current and screen current are checked. The operating potentials and inspection limits are those specified by the tube manufacturer. After these tests and while the tube is still in the bridge, the tube is checked for the change in plate current resulting from reducing the heater voltage by 10 percent. If the change in plate current is less than 10 percent of the value at rated voltage, the tube is acceptable; if the change in plate current is greater than 10 percent, the tube is a reject. All tubes rejected by this test are deleted from further tests and are marked and stored for later disposition.

2.2 SPECIAL TESTS

Several special tests that are performed include gas checks according to military (JAN) specifications, test of the ratio of mutual conductance to plate current under the specific operating conditions at which the tube will be used, and keyed-rectifier and leakage tests. In addition, transconductance curves of screen-grid-to-plate and suppressor-grid-to-plate are run on request of the section that will use the tube.

Diode rectifiers are checked for emission and for voltage breakdown at the rated peak-inverse potential and at the rated heater-to-cathode potential. Thyratrons and voltage-regulator tubes are checked for electrical and vibration characteristics in the actual circuits in which they are to be employed. These and other special tests are performed only as required by the users.

3. Vibration Tests

In missile use, many tube failures result from vibration, so an effort is made to screen out noisy or microphonic tubes. All triodes and pentodes passing the electrical tests are subjected to a vibration test using an electro-dynamic vibration machine. The tubes are vibrated at 40 cycles per second with an acceleration of 15 times gravity (15 g). The microphonic-noise output due to vibration is read on an oscilloscope. The tubes are then classified according

to their peak-to-peak noise-voltage output during vibration, as shown in Table 1. Any intermittent shorts will show on the oscilloscope as large noise spikes and are cause for rejection of the tube under test. Tubes falling in classes 1, 2, or 3 are color coded as indicated in Table 1 and stored for use in missiles.

4. Microscopic Inspection

4.1 PURPOSE

The tests listed above have been performed on missile tubes for the past several years. However, the number of tube failures that have occurred during the tests of the missile electronic equipment has still been excessively high. In an effort to avoid some of these failures and to reduce the chance of missile failure in flight, a procedure has been set up for visually inspecting the tubes under a binocular microscope. By this process, it is possible to sort out many tubes that are likely to fail under the rigorous requirements of missile use.

4.2 BASIS FOR ACCEPTING OR REJECTING TUBES

In a vacuum tube, there can exist many internal faults that do not affect its basic electrical operation but that, if the tube is placed in a unit where vibration is an important factor, greatly impair the function of that unit. For example, such a tube may become microphonic or fail

completely as the result of undesirable disposition of small bits of loose metal or insulating material within the envelope. Short-circuits or open-circuits may occur because of cracked insulators or defective welds. For these reasons, microscopic inspection is employed for segregating those tubes that are bad risks from the reliability standpoint. The inspection is made with a Bausch and Lomb type-*JK2* stereomicroscope, having two objectives and two sets of paired eyepieces with magnifications of 10, 15, 30, and 45. At present all subminiature tubes for missile use are being microscopically inspected for the following items.

4.2.1 Cathode Ribbons

A. A "mashed" weld, with or without discoloration, resulting in a serious reduction in thickness of ribbon material.

B. A twist at the weld that places the ribbon at right angles to the weld.

C. A sharp bend in the ribbon at the weld that results in a tear.

D. A sharp bend in any portion of the upper third of the ribbon adjacent to the weld.

E. Actual contact of the ribbon with the aluminum oxide coating of the filaments.

TABLE 1

SUBMINIATURE TUBE CLASSIFICATION CHART

Type	Load Resistance in Kilohms	Equivalent Cathode Resistance in Ohms	Plate Voltage	Screen Voltage	Limits of Noise Output in Millivolts Peak-to-Peak			
					1 Yellow	2 Red	3 Green	4 Reject
5636	10	150	100	100	40	120	120–168*	168*
5639	2	100	150	100	160	480	480–560*	560*
5718	10	150	100	—	20	60	60–70*	70*
5719	10	1500	100	—	10	30	30–70*	70*
5784	10	270	120	120	40	120	120–280*	280*
5840	10	150	100	100	30	90	90–168*	168*
5899	10	120	100	100	30	90	90–168*	168*
5902	2	270	110	110	160	420	None	420*
5977	10	270	100	—	20	60	60–140	140*
5987	2	2000	120	—	40	120	120–280*	280*
6021	10	100	100	—	20	60	60–140*	140*
6111	10	220	100	—	20	60	60–140*	140*
6112	10	1500	100	—	None	70	None	70*

* To be revised downward shortly; to be 2.8 times the manufacturer's latest root-mean-square noise limit.

F. A "taut" condition resulting from insufficient slack or too short a length of ribbon.

G. Insufficient contact area at the weld.

4.2.2 Welds in General

A. Broken or not welded.

B. Overwelding that produces either weld flakes or weld drippings.

C. Improper location of metals before welding.

4.2.3 Loose Particles in Envelope

A. Conducting materials usually from getter material or from weld flakes or drippings.

B. Nonconducting materials, such as mica flakes, dust, and aluminum-oxide heater insulation.

4.2.4 Getters

A. Underflashed, producing a tube that possibly could contain gas or could become gassy later.

B. Overflashed, leading to the presence of large pieces of getter material in the envelope.

4.2.5 Heater Insulation

A. Broken inside upper or lower edges of the cathode.

B. Heater-wire leads not properly pressed or welded in ribbons.

4.2.6 Micas

A. Cracked through.

4.2.7 Glass

A. Broken, cracked, or chipped.

4.2.8 Plates

A. Open seams in line of welds.

B. Burned from welding.
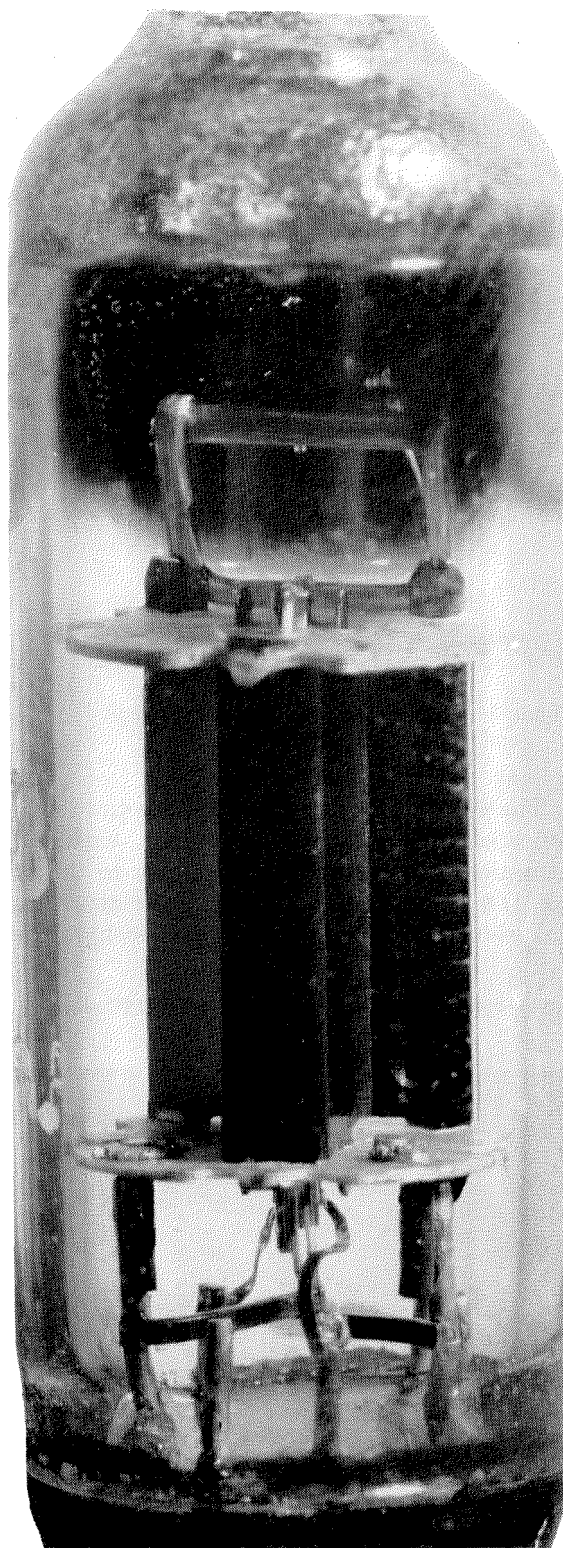
C. Splashed with weld or getter material.

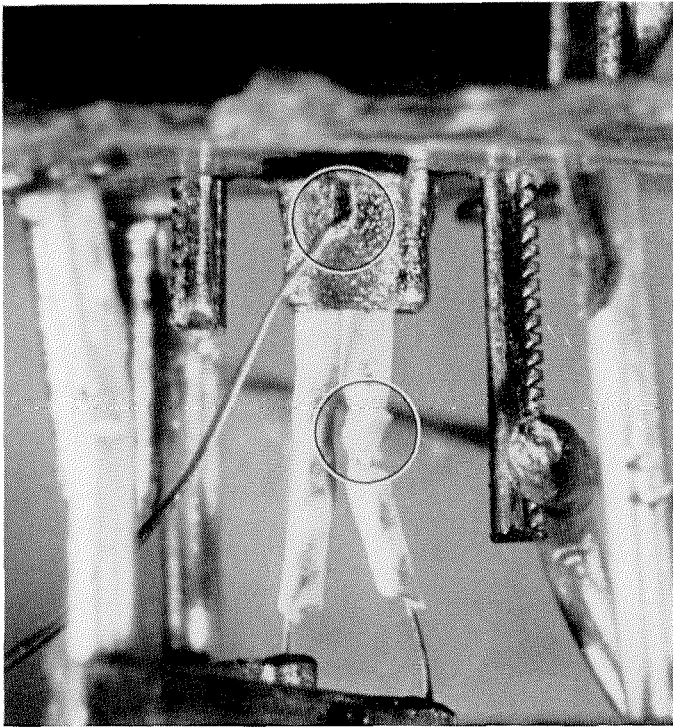**Figure 1**—A good tube that may be used as a sample for the inspector.

Figure 2—Broken heater insulation and a bent
and torn ribbon lead to the cathode.

The eight major items listed above are in the order of their relative importance, with most attention being given during testing to the first six. Data have been taken and correlation work has shown that a definite relationship exists

Figure 3—Sharp bends in ribbons that often result
in breakage during vibration.
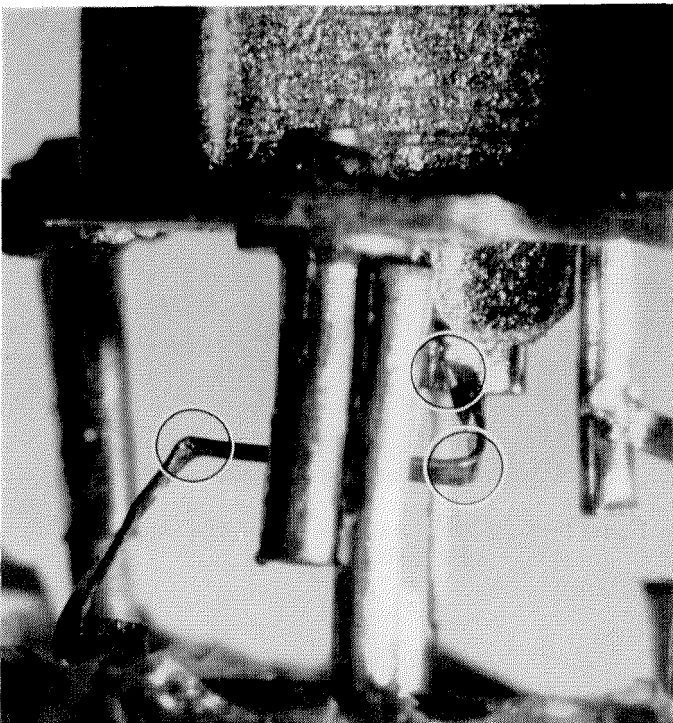
between tube failures and bad cathode ribbons, bad welds, particles, and overflashed getters.

No definite limits have yet been established for accepting or rejecting tubes by microscopic inspection. Some tubes can be readily determined to be "good" or "bad" just by observing the mentioned items under the microscope. Others will be borderline cases and can be classified effectively only by an experienced operator. An experienced operator develops an "engineering sense of sight" that enables him to separate the good tubes from the bad; it is believed that once he has achieved this attitude, tube failures in the field can be materially reduced.

At present, tubes with obvious defects are being rejected. Most of these have defective cathode ribbons, since this has been found to be one of the most serious faults encountered in the field. Other defects of a minor nature will be recorded against the serial number of the tube, and field failures will then be correlated with this inspection record.

5. Examples

Figure 1 demonstrates the appearance of a "good" tube that is suitable for the establishment of a standard.

Figure 2 reveals broken heater insulation and a bend and tear in the cathode ribbon at the cathode. Faulty heater insulation such as is shown in Figure 2 will possibly break off in service and become a noise generator. The bend and tear in the cathode ribbon at the cathode weld is cause for rejection, since in the past this has proved to be a major cause of tube failure.

Figure 3 illustrates some of the sharp bends that commonly occur in cathode ribbons. Many times the ribbons are actually kinked at these bends. Such bends cause the ribbon to break quickly during the cycling process.

An example of a bad cathode weld is shown in Figure 4. The weld has been mashed and overheated, and has a bad twist. It has been determined that such flaws at this junction will cause failure. during the early part of what would be the normal life of the tube.

Figure 5 is an illustration of a too-tight cathode ribbon. In some tubes the tautness of the ribbon has resulted in a complete break some-
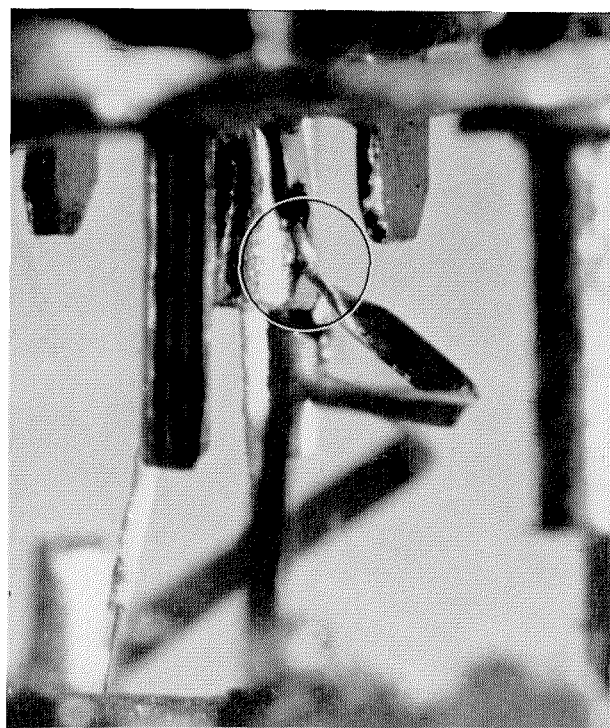
Figure 4—A bad weld.
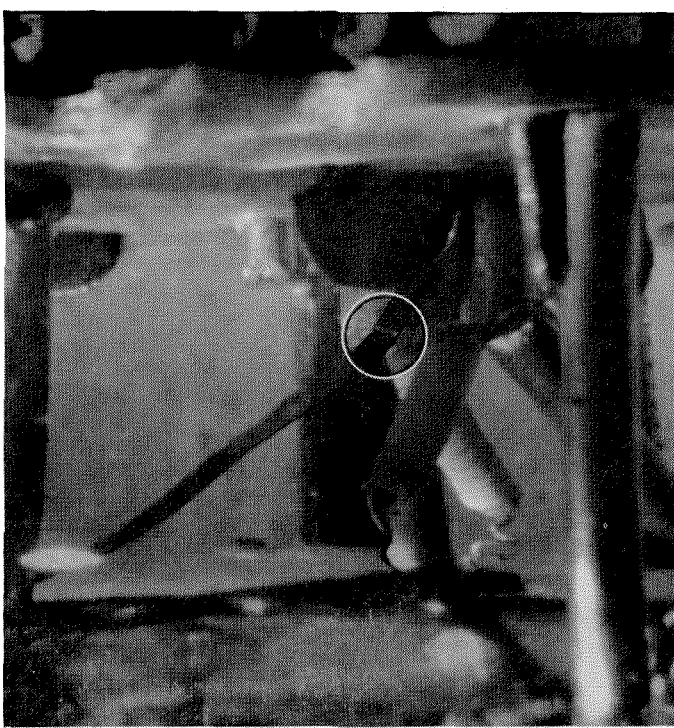
Figure 6—This overly tight cathode ribbon
has broken after a few hours of testing.

where in the upper third of its length. Such breaks result from the expansion and contraction of the ribbon with repeated heating and cooling of the cathode. As temperature changes in the cathode take place, the ribbon must move with a motion similar to that of the human elbow.

A small distance below the cathode in Figure 6, a break in the cathode ribbon can be seen. This break occurred during test after a few hours of operation. The break occurred as a result of a taut ribbon condition and could have been detected by microscopic inspection.

Figure 5—Cathode ribbon pulled too tight.
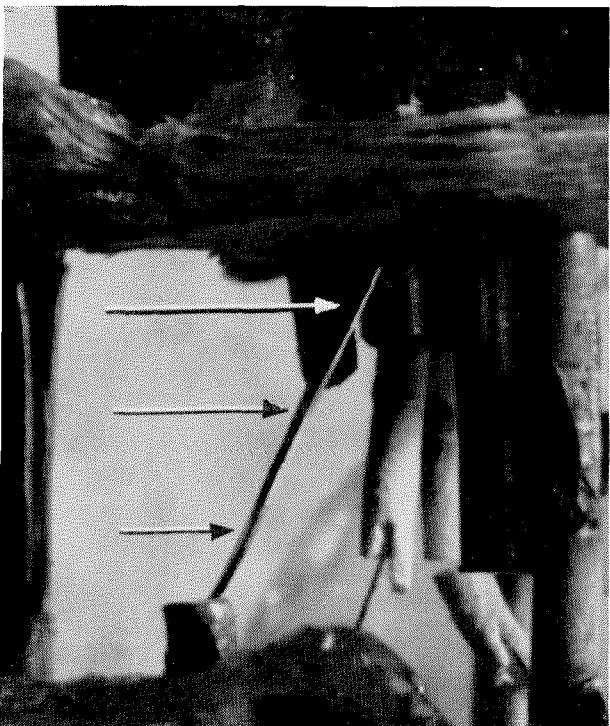
Figure 7—Broken insulation at the top of the heater.
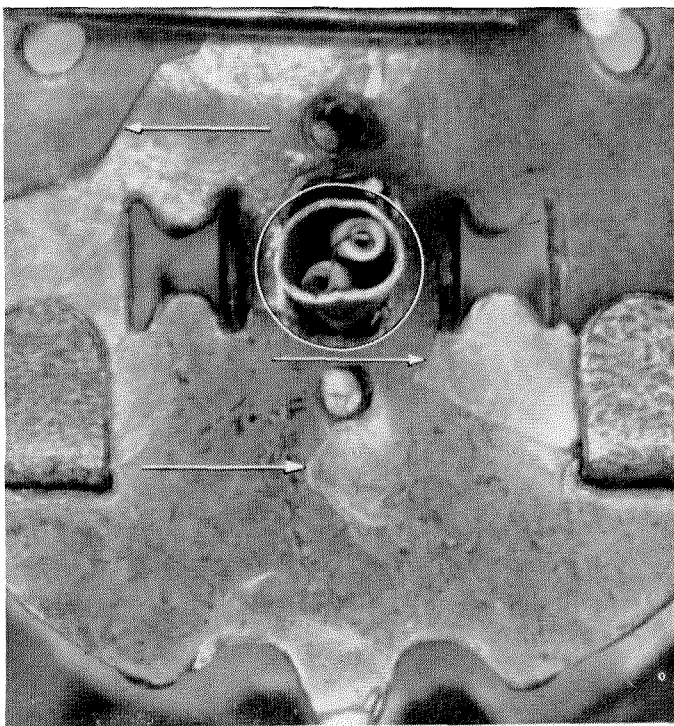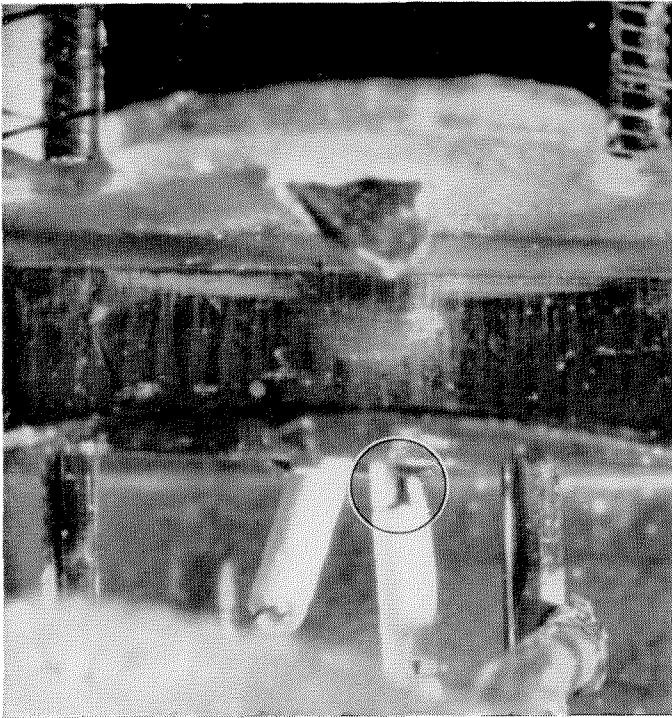
Figure 8—Broken insulation at the bottom of the heater.

Figure 10—Bad weld that has burned through
the getter support.

Figure 7 shows broken heater insulation at the top of the cathode. The heater insulation of this tube is broken down inside the upper part of the cathode resulting in a very bad heater-to-cathode short. This condition is due to poor workmanship

Figure 9—This getter strip has been overheated
and the burned-out piece will cause noise.

in coating the heaters or in installing them in the cathode. Note also the large flakes of mica beginning to peel from the upper mica support.

Figure 8 reveals a break in the heater insulation at the lower edge of the cathode. This break caused a short in the tube pictured and, if it had not been detected in time, could have caused the cathode ribbon to burn in two.

Shown in Figure 9 is an example of getter overflashing resulting from too much induction heating in the flashing process. With overflashing, there is always present a large piece of metallic getter material, either loose in the envelope or clinging to one of the elements. In the latter case, experience has shown that with service such particles break loose and cause a tube to become noisy.

Notice in Figure 10 the extremely bad weld between the getter and the plate; the getter support is burned apart. As a result of the poor weld, many spattered clinging particles are present in the envelope.

In Figure 11, a piece of loose getter material can be seen lying just below the lower mica and against the support rod of the third grid. During vibration, the motion of this piece of material

Figure 11—Piece of loose getter material.
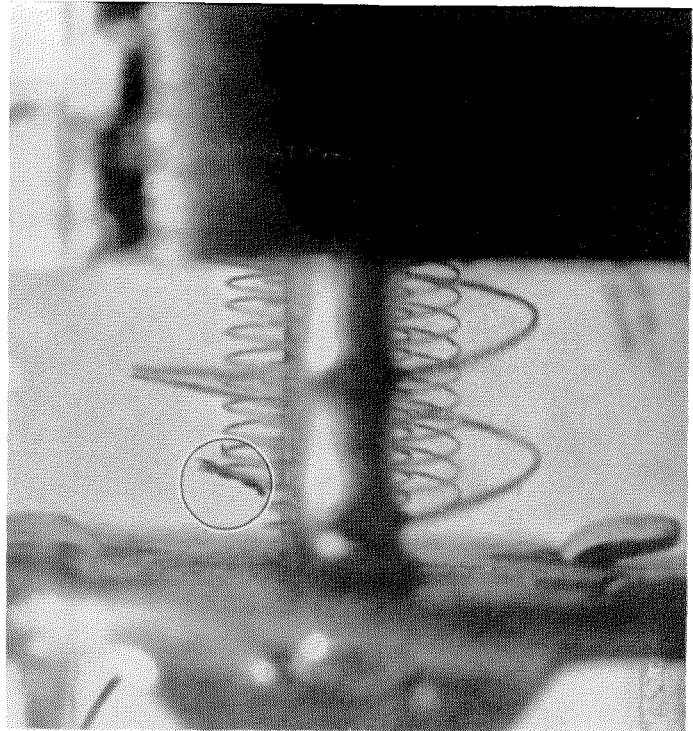
Figure 12—A piece of material short-circuiting the first and second grids.

inside the envelope of the tube will cause noise or intermittent shorts.

Close inspection of Figure 12 will reveal a piece of getter material or weld flake lying between the third turn of the inner-grid winding and the first turn of the second-grid winding, resulting in a direct short-circuit between these two grids. Such a condition is brought about by poor workmanship during production of the tube.

Lying against the envelope of the tube shown in Figure 13, there can be seen a number of particles of heater insulation, weld flakes, and getter material. Some of the particles are metallic and some are nonmetallic. Particles of this kind are a potential noise source.

Close observation of Figure 14 will reveal the presence of a piece of weld splash clinging to the weld at the lower end of the grid-support rod. During vibration tests, this metallic particle would probably break loose and cause noise or a short. Note, also, in Figure 14, the taut condition of the cathode ribbon.

Figures 1 through 14 illustrate some of the worst conditions encountered in tubes. Visual microscopic inspection can keep a large percentage of tubes having these faults out of finished equipment.

6. Desired Achievements

The ultimate goal of visual microscopic inspection is to eliminate as many as possible of the tubes having the worst conditions described

Figure 13—Collection of conducting and insulating particles within a tube.
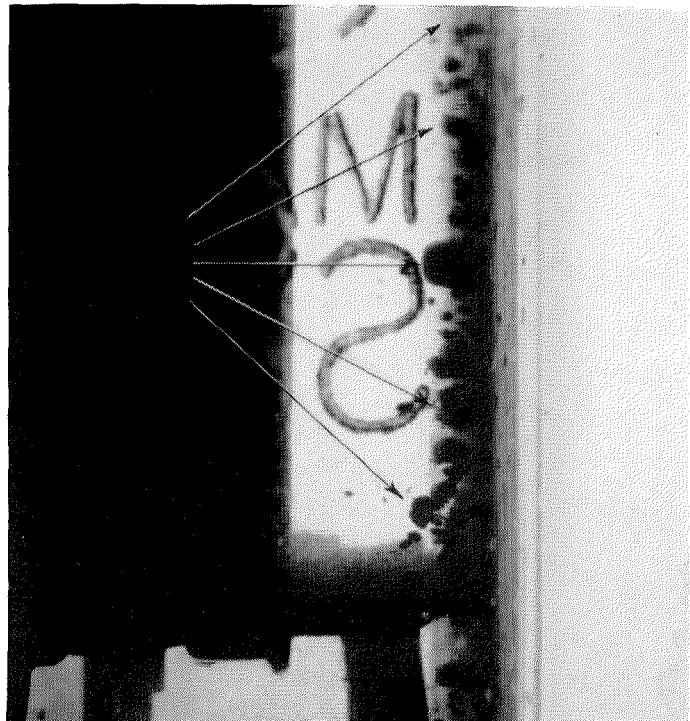
above. This is now being accomplished by means of incoming inspection. In the past, numerous tube failures in the field could have been detected with a microscope. Of course, microscopic inspection is not the final answer; the real solution to the problem can be reached only by obtaining the manufacturers' cooperation in cleaning up their production lines. This will take considerable time, however, and until it can be accomplished, visual microscopic inspection will be a useful tool.

The entire tube inspection program is necessary because even the rigorous quality control practiced by tube manufacturers is insufficient to satisfy the exacting requirements of missile use. It is hoped that at some future date it will be necessary for the user to make only spot checks in order to assure satisfactory quality, with the main burden of inspection being assumed by the tube manufacturer. Until that time, however, the microscopic 100-percent incoming inspection, as well as the described mechanical inspection, electrical tests, and vibration tests, will be continued.

Figure 14—Piece of weld splash that may break away under vibration and cause noise. Also, the cathode ribbon is too tight.

One duty will always rest with the user, that is, the duty to keep adequate records of the failures that occur in actual use. Only by reporting such failures and returning the defective tubes to the proper agencies for analysis can the causes of failure be ascertained and corrected.
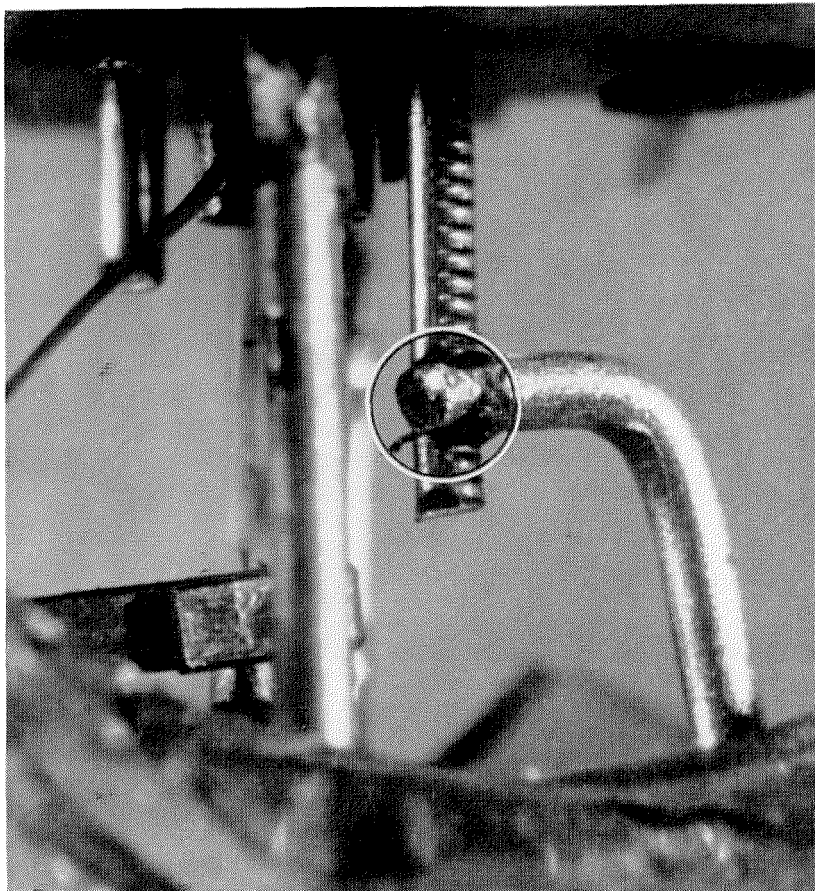
Electromagnetic Delay Lines*

By H. G. NORDLIN

Federal Telecommunication Laboratories, a division of
International Telephone and Telegraph Corporation; Nutley, New Jersey

TWO BASIC KINDS of devices are used for providing known amounts of phase shift or time delay of electrical signals. With supersonic delay devices, time delays from several microseconds to several milliseconds can be achieved. Their efficiency is, however, greatest for large time delays because of the large fixed insertion loss of the electromechanical transducers. For time delays of a fraction of a microsecond to about 10 microseconds, electrical delay devices are generally perferred because they do not have fixed insertion losses and the attenuation for a given design is proportional to the amount of time delay. In addition, the electrical delay devices are comparatively insensitive to mechanical shock and changes in temperature, which often give trouble in the supersonic delay devices.

An ideal delay line would be one in which the shift in phase from input to output is proportional to frequency and in which the voltage attenuation is a constant for all frequencies of interest. Any input wave, provided it has no components outside the prescribed frequency range, would be transmitted to the output of the ideal device without distortion. These ideal conditions cannot be realized in practice, and deviations from them are therefore a measure of the fidelity of a delay line.

Electrical delay lines in present use are of two types; lumped parameter and distributed parameter. In the usual cases, both are 4-terminal networks composed of series inductance and shunt capacitance. Resistance and dielectric dissipation are inherent properties of the inductors and capacitors, respectively. The simplest type of lumped-parameter delay line is the contant-*k* low-pass filter. This device exhibits a time delay characteristic that begins to increase with frequency about a decade below the cutoff frequency, which is directly proportional to the number of T sections in a line of a given time delay and impedance. The variation of time delay may be reduced or even reversed in direction below the cutoff frequency by causing the adjacent inductance sections to be mutually coupled to an increasing degree.

If the number of sections in the low-pass constant-*k* delay line is increased without limit, we obtain a line in which the parameters of inductance and capacitance are distributed uniformly between the input and output terminals. This resulting distributed-parameter delay line does not exhibit the sharp cutoff found with the lumped-constant devices. The useful frequency limit is approached rather slowly with increasing frequency and is evidenced by an increase in both velocity and attenuation. In general, distributed-parameter delay lines can be designed to have a greater useful bandwidth than lumped-parameter lines of equivalent size and time delay.

Our recent work in this field has been in the development of distributed-parameter delay lines of the cable type that are manufactured in continuous long sections. Some delay cables that were developed under contract with Squier Signal Laboratories of Fort Monmouth, New Jersey, will be described and data will be given on their response to rectangular pulse and sinusoidal waveforms.
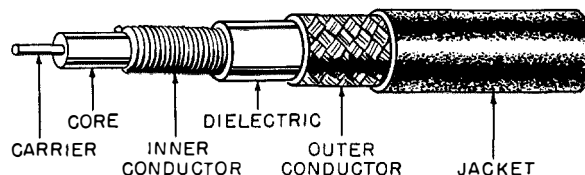

Figure 1—Distributed-parameter delay cable.

Figure 1 shows a cutaway sketch of a distributed-parameter delay cable of the type that is familiar to many electronic engineers. It consists of a flexible inner core over which are disposed

the inner conductor of insulated wire wound in the form of a closely spaced single-layer solenoid, a dielectric layer that may be extruded or formed with a tape, an outer conductor that may be either a braid or serving of insulated or bare copper wire, and a vinyl-type jacket that acts to prevent loosening of the outer conductor and also as a protection against physical damage and moisture. An outstanding advantage of the distributed-parameter delay cable lies, of course, in the fact that a required amount of time delay can be obtained merely by cutting off a piece of cable of the necessary length.

The original cable of this type, *RG-65/U*, was developed from a design originated at the Massachusetts Institute of Technology. It was intended as a high impedance cable, but since it has a time delay of 0.04 microsecond per foot (0.13 microsecond per meter), about 27 times that of a polyethylene-insulated coaxial cable, it has been used frequently as a broad-band distributed-parameter delay cable.

Three recently developed types, *A*, *B*, and *D* will be referred to in this paper. Types *A* and *B* were designed for highly stable operation over a wide frequency range at impedance levels of 1000 ohms and 250 ohms, respectively. Special manufacturing techniques were devised to insure a high degree of precision and uniformity in their production. The *D* cable is currently in an advanced stage of development. It represents the results of an effort to obtain high efficiency with regard both to voltage attenuation and concentration of time delay, as well as a reasonably high fidelity up to a frequency of 10 megacycles per second.

The *A* cable has a nominal time delay of 0.2 microsecond per foot (0.7 microsecond per meter) and a nominal characteristic impedance of 1000 ohms. Its overall diameter is 0.405 inch (10.3 millimeters). The inner conductor is size-32 (American Wire Gage) type-*F*-Formex-coated magnet wire, and the outer conductor is a conventional braid of size-34 *F*-Formex-coated magnet wire. The response of the *A* cable to rectangular pulse and sinusoidal waveforms is illustrated in Figure 2. The time delay is constant from 1 to 10 megacycles per second and decreases by about 5 percent from 10 to 30 megacycles. The attenuation of the cable is 3 decibels per microsecond of delay at about 10 megacycles.

The oscillograms show how a rectangular pulse is distorted after passing through 6 feet (1.8 meters) of cable terminated in its characteristic resistance. The picture on the left shows the shapes of the input and output pulses as well as
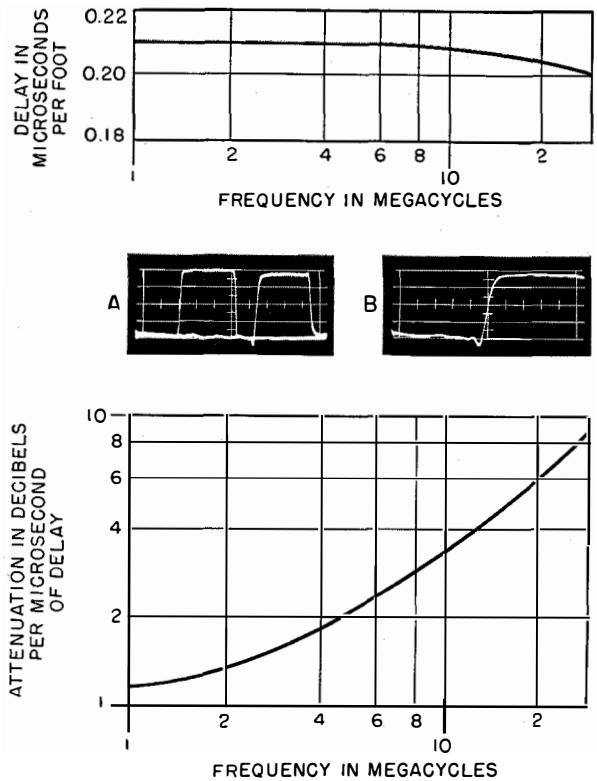
Figure 2—Type-*A* delay cable. The delay–frequency characteristic is shown at top and the attenuation–frequency relation at the bottom. Oscillograms are for a 1-microsecond pulse through 6 feet (1.8 meters) of cable with timing divisions of 0.3 microsecond at *A* and 0.1 microsecond at *B*. At *A*, the input pulse is at the left and its output form is at the right.

their relative positions on a time scale. In this case, the delay is about 1.3 microseconds. The picture on the right shows the leading edge of the output pulse with the time scale expanded to 0.1 microsecond per division. The rise time of the pulse between the 10- and 90-percent points is 0.06 microsecond.

Similar information is shown for the *B* cable in Figure 3. This cable has a nominal time delay of 0.1 microsecond per foot (0.3 microsecond per meter) and a nominal characteristic impedance of 250 ohms. Its over-all diameter is 0.405 inch (10.3 millimeters). The inner conductor is

size-23 (American Wire Gage) F-Formex-coated magnet wire and the outer conductor is size-34 F-Formex wire. The variation of time delay in the frequency range shown is about 5 percent and the attenuation curve is nearly the same as
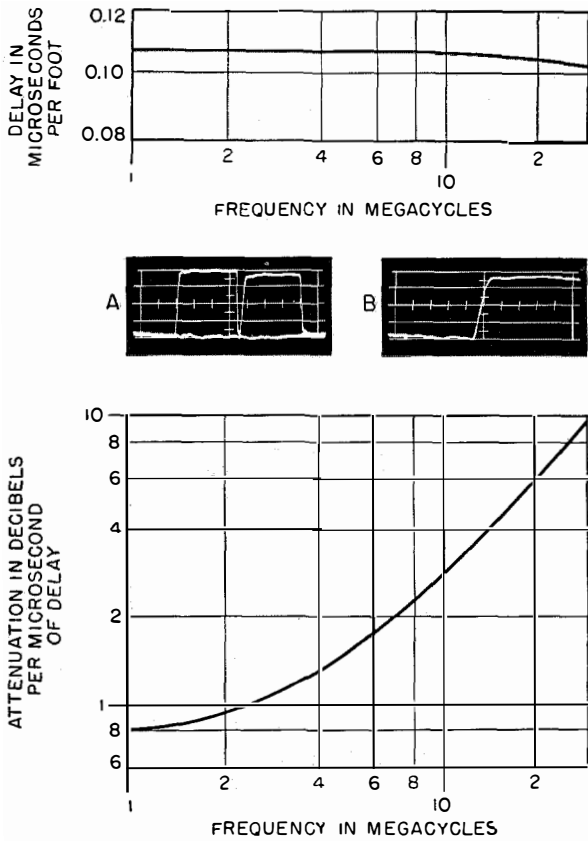
Figure 3—Type-B delay cable. The oscillograms are for a 1-microsecond pulse transmitted over 10 feet (3 meters) of cable with timing divisions of 0.3 microsecond at A and 0.1 at B.

for the A cable. The rise time of the pulse, delayed through 10 feet (3 meters) of cable, is 0.06 microsecond.

In the course of the development work on the A and B cables, investigations were made of the magnetic properties of plastic compounds containing powdered ferrite materials with a view toward employing them in the core structure of the delay cables for the purpose of obtaining a lower attenuation per unit of time delay. We concluded that the losses introduced by the magnetic compound would overshadow the reduction in conductor losses at frequencies above about 10 megacycles but that a consider-

able improvement in efficiency could result in the 10-megacycle range. In addition to the possibility of improved efficiency, the use of magnetic materials makes it possible to increase the amount of time delay in a given volume of cable. Because the A and B cables were designed for the highest possible operating frequency, no magnetic materials were used in their construction.

We are presently in the final stage of the development of a D cable utilizing the desirable properties of ferrites. The objective is a cable of high quality having a nominal time delay of 1 microsecond per foot (3 microseconds per meter) length, low attenuation, and minimum amplitude and phase distortion in the frequency range up to 10 megacycles. Referring momentarily back to the data on the A and B cables, it will be recalled that the time delay on those cables is constant up to at least 10 megacycles, decreasing slowly at higher frequencies. This drop-off of time delay with increasing frequency has been shown in the literature to be due to the nature of the magnetic coupling between each turn of the inner conductor and neighboring turns. At low frequencies, the fields coupled in this manner are substantially in phase and the mutual coupling tends to enforce the general magnetic field. As the frequency is increased, coupling occurs to an increasing extent between turns in which the currents are not in phase and cancellations occur in the general magnetic field with a resulting decrease in inductance. It can readily be seen that for a greater concentration of time delay or, in other words, a larger phase constant, the out-of-phase coupling will occur to an important extent at a lower frequency.

In the D cable, the central core is composed of a thermoplastic compound containing a commercial ferrite in powder form. The core is extruded over a Fiberglas cord at a rate somewhat slower than is normally used for polyethylene. It has good flexibility and does not crack or break as a result of normal handling, although breakage will occur if the core is repeatedly bent in a radius of less than about 0.5 inch (12.7 millimeters). The inner conductor is size-40 F-Formex-coated magnet wire. Over this, a dielectric tape is wrapped with a 50-percent overlap. The outer conductor is a braid of size-36 F-Formex-coated magnet wire. The

over-all diameter of the cable including the jacket is approximately 0.25 inch (6.4 millimeters).

The response of the basic D cable to sinusoidal and rectangular pulse waveforms is shown in

occurrence of oscillations or ringing preceding the 2 step changes in voltage on the pulse. In addition, the rise time of the pulse has increased to 0.12 microsecond after transmission through a 1-foot (0.3-meter) length of the cable. The
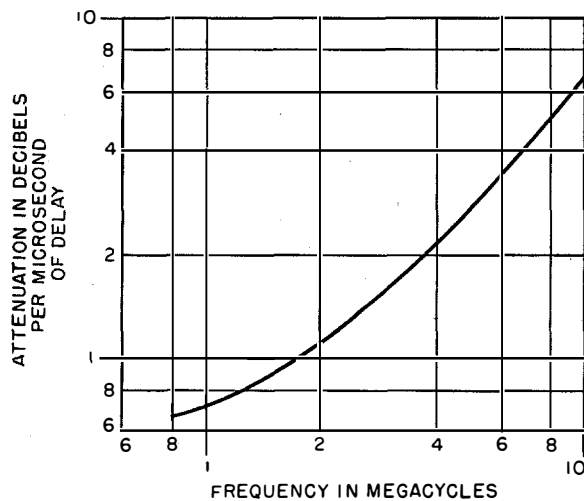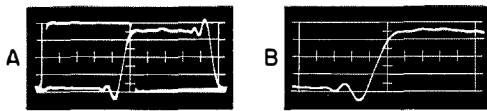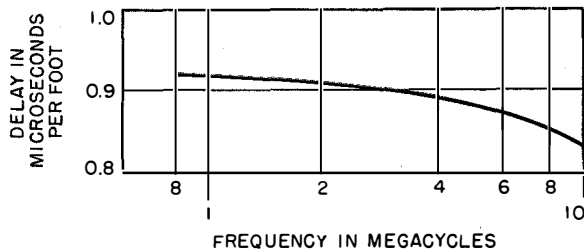
Figure 4—Type-D delay cable without compensation. The oscillograms are for a 1-microsecond pulse transmitted over 1 foot (0.3 meter) of cable with timing divisions of 0.2 microsecond at A and 0.1 at B.
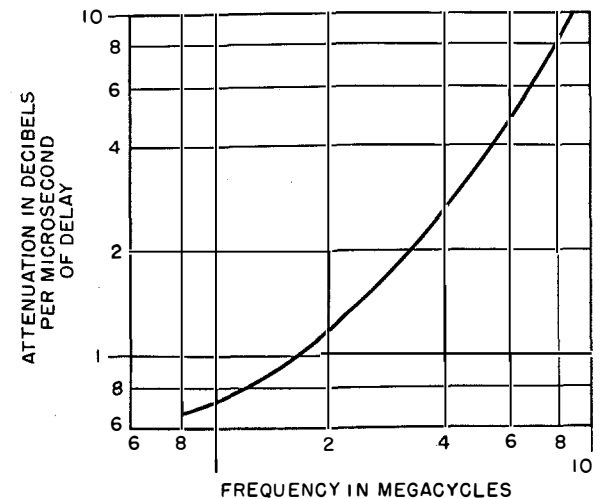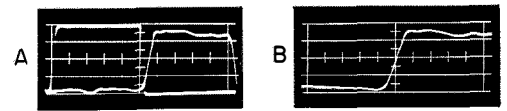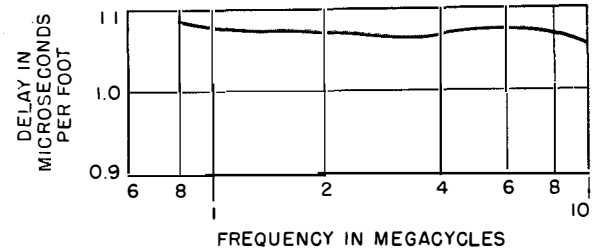
Figure 5—Type-D delay cable with metallized-film compensation. The oscillograms are for a 1-microsecond pulse through 1 foot (0.3 meter) of cable with timing divisions of 0.2 microsecond at A and 0.1 at B.

Figure 4. Whereas the A and B cables have a constant time delay between 1 and 10 megacycles, the time delay of this cable decreases about 10 percent in that frequency range. Although the attenuation at one megacycle per second is lower than for either the A or B cables, the increase at higher frequencies is greater, with the 3-decibel-per-microsecond point occurring at about 6 megacycles. The effect of phase distortion on the pulse response is seen to be the

nominal characteristic impedance of this basic D cable is 1750 ohms.

A method of compensating for the decrease in time delay of distributed-parameter devices by the use of floating metallic "patches" that are insulated from the helical inner conductor, from each other, and from the outer conductor, was described by Kallmann.[1] The decrease in time delay at high frequencies resulting from a

[1] H. E. Kallmann, "Equalized Delay Lines," *Proceedings of the IRE*, volume 34, pages 646–657; September, 1946.

decrease in inductance is thereby compensated for by a rise in the effective capacitance. Kallmann demonstrated the method by using rectangular pieces of metallic foil that were inserted one by one under the inner conductor during the construction of a delay-line section. It was shown that the time delay can be made nearly constant up to a frequency at which the patches are each about a half wavelength long. The degree of equalization is a function of the width of the patches and of the dielectric constant and thickness of the insulation between the patches and the inner conductor. The capacitance patches have no effect at low frequencies, where negligible phase difference exists along the length of each patch. As the frequency is increased and the phase shift increases, current flows through the patches and the effective capacitance of the cable is increased. This technique would suffice for the manufacture of small units but it would be difficult to devise a means of automatically installing such patches on a cable-type delay line in factory production.

A compensated form of the basic D cable was developed utilizing this method of time-delay compensation in a form that is adaptable to continuous factory production. Metallized Mylar film of the type employed for capacitors is used. This film is available in a range of thicknesses down to 0.25 mil (0.00025 inch or 0.006 millimeter) with an evaporated coating of aluminum or silver on one side. Conducting patches are formed on a tape of the material by creating dividing lines on the metallic film with a low-current arc or as a modification of the evaporation process. The tape thus prepared is wound on the delay-cable core before applying the helical inner conductor and with the metallized surface facing the core. The frequency band in which the compensation is effective is determined by the length of the patches along the tape and by the pitch of the tape winding on the core. The degree of compensation is affected by the width of the tape and the thickness of the Mylar insulation. The Mylar tape, even in the 0.25-mil (0.006-millimeter) thickness, has enough strength to allow the use of conventional taping machinery.

The response of a compensated version of the D cable is illustrated in Figure 5. This cable has a nominal characteristic impedance of 1900 ohms. The total variation of time delay from 1 to 10 megacycles is less than 3 percent. The attenuation is somewhat higher than for the basic D cable, the 3-decibel point occurring at about 5 megacycles. This may be improved to some extent if the metallized Mylar can be obtained with a higher metallic-film conductivity. The effect of the time-delay compensation on the rectangular-pulse response is quite obvious. The rise time of the transmitted pulse is reduced to 0.06 microsecond, and the undesirable oscillations are substantially eliminated.

Precision-Approach Airfield Radar
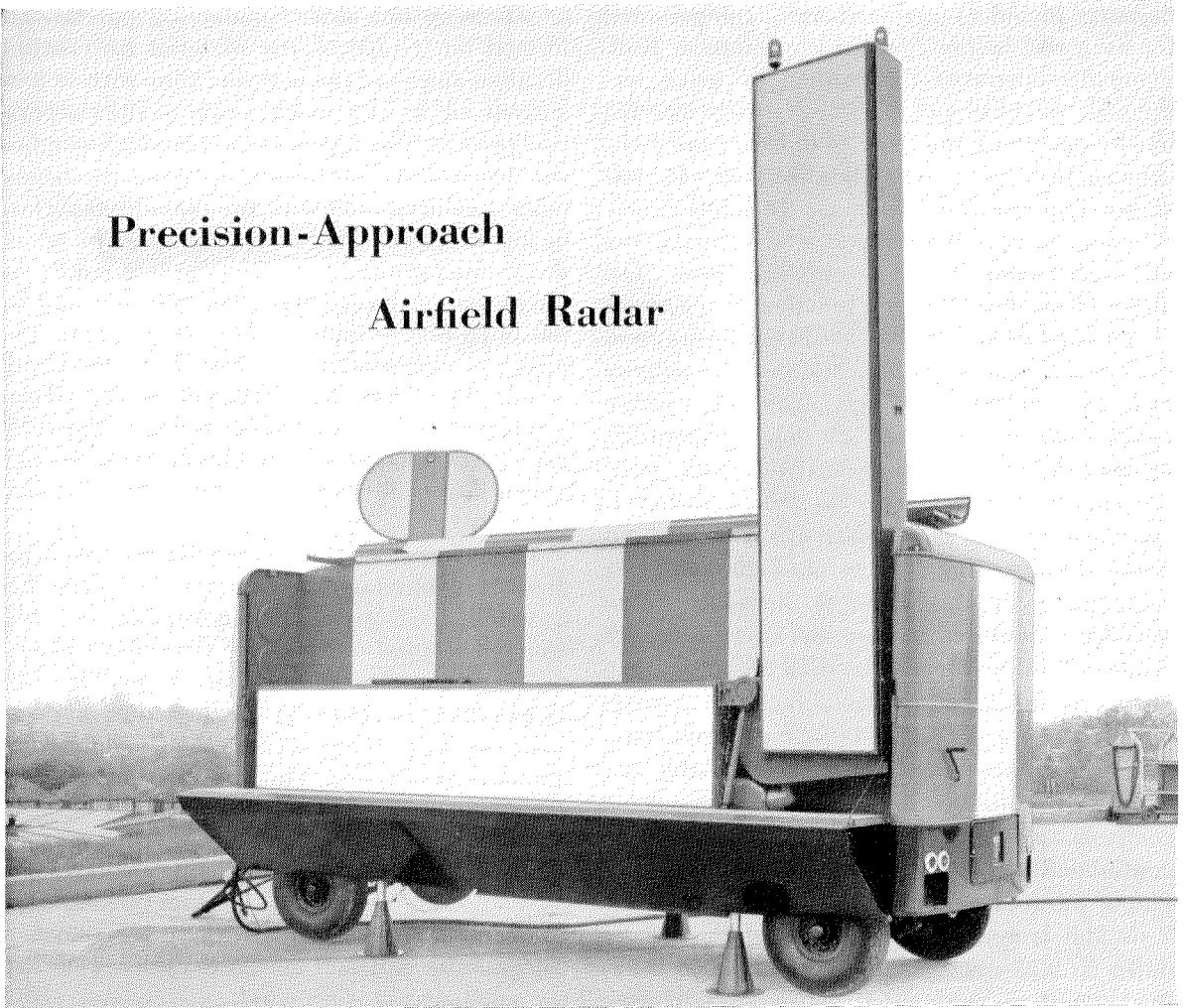
DURING the annual Society of British Aircraft Constructors' exhibition, held at Farnborough, England, the radio division of Standard Telephones and Cables, Limited, presented an operational display of their precision-approach radar equipment. This equipment, probably the most comprehensive of its type in the world, is already in operation at two airfields of the British Ministry of Supply, the International Airport of Zurich, Switzerland, two airfields of the Royal Netherlands Airforce in Holland, and at the Royal Canadian Navy's base at Shearwater, Nova Scotia.

The equipment provides the ground controller at an airfield with visual three-dimensional information about aircraft approaching the runway; distance, azimuth, and elevation are all indicated. This information, vital during inclement weather, enables the controller to convey to the pilot over the normal radiotelephone channel, all instructions necessary to fly the aircraft to the approach end of the runway, whence a safe visual landing can be made.

The radar section of the equipment is installed in an unattended vehicle normally positioned at the side of the runway facing down-wind. Two 50-kilowatt pulse-type radar transmitters operating in the 3-centimeter band radiate fan-shaped

beams from two antennas in the direction of the descent path. The 10-mile (16-kilometre) working range of the equipment thus represents a swept space of approximately 3 miles by 1 mile (4.8 by 1.6 kilometres) in which an aircraft can be detected. Radar echoes from the aircraft are interpreted by the receiving equipment in the vehicle and transmitted by a radio link to the airfield control tower, where they are presented to the controller on azimuth/range and elevation/range cathode-ray tubes.

The control tower display console showing the elevation/range cathode-ray tube indicator on the left and the azimuth/range indicator on the right.
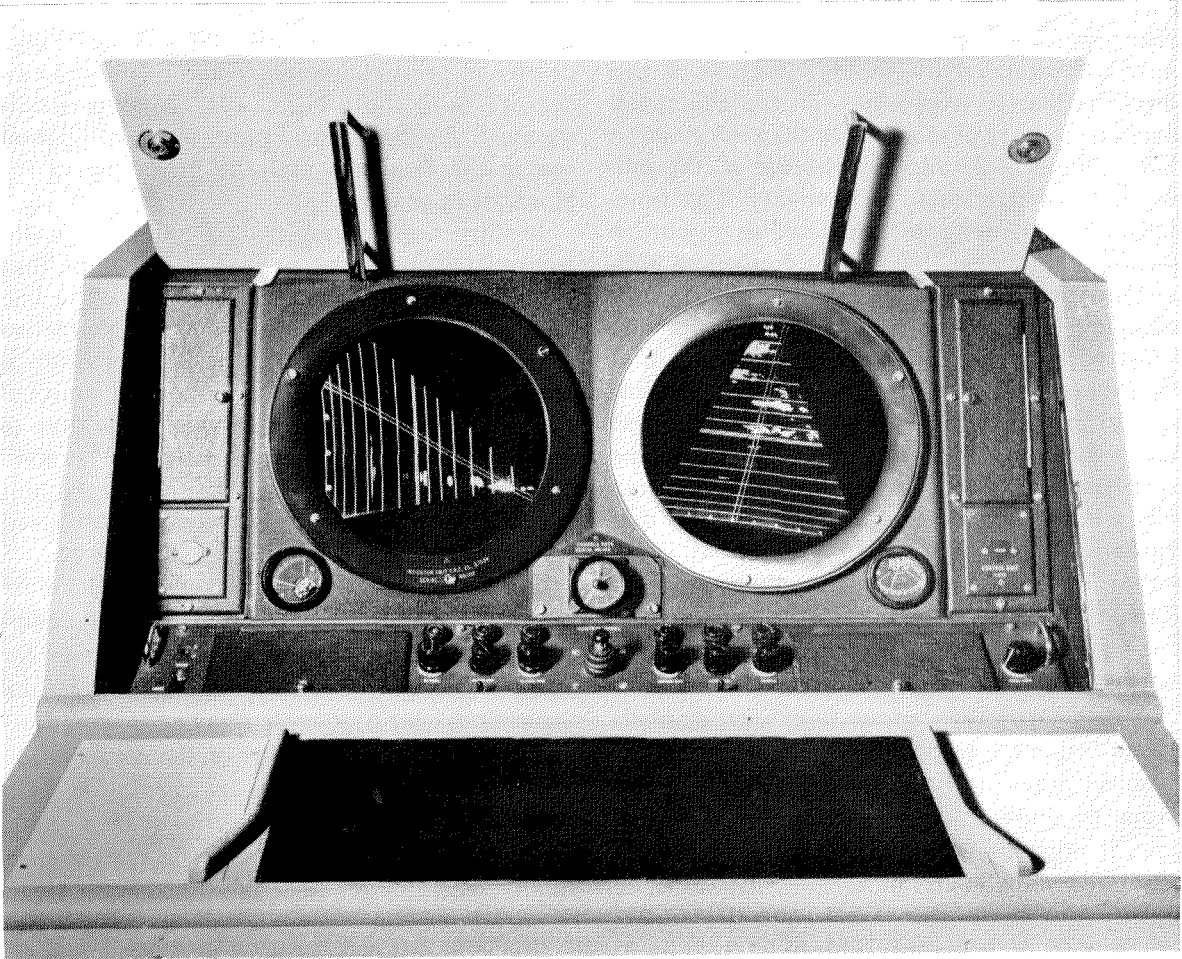
Functional-Diagram Approach to Electronics in Telegraphy

By E. P. G. WRIGHT and D. S. RIDLER

Standard Telecommunication Laboratories, Limited; London, England

DESIGNERS of electronic digital computers have provided telecommunication engineers with an attractive method of expression which, on account of its inherent simplicity, is likely to be widely adopted in the future. The basis of this new form of expression comprises a small number of symbols representing clear-cut and frequently used functions. These symbols can be grouped together in different combinations to produce functional diagrams that express the philosophy of the design.

It must be appreciated that such functional diagrams do not attempt to describe the circuit arrangement or even the type of components that it is intended to employ. Because of this simplification, it is possible for the functional diagrams to be read more easily than information that requires a detailed knowledge of the employment of particular components. The functional diagrams may be considered as an outline drawing that is capable of being coloured subsequently to produce a picture. The process of colouring is roughly analogous to filling in the detail with particular components although it will be appreciated that there will be standardized arrangements for many of the functions so that the work of filling in involves chiefly the consideration of interconnecting standard units.

The advantage of the use of functional diagrams is the removal of the detail that is essential for actual operation but unnecessary to describe the general method of operation. It is a striking example of providing a better view of the wood by removing some of the trees.

In this paper the various functional symbols are applied to telegraph systems and the reader is given an opportunity of judging whether these claims to simplicity are justified. At the same time, it must be pointed out that simple functional diagrams will not necessarily translate directly into simple practical circuits by the mere substitution of component blocks. The circuit designer must still use his art although the

functional diagram may assist him in the thought process necessary in the evolution of the design.

1. Symbols for Functional Diagrams

1.1 SIMPLE TELEGRAPH SYSTEMS

It will be already understood that in automatic telegraphy it is usual to transmit characters in the form of combinations of 5 units, each unit being either a "mark" or a "space." The 32 combinations available are insufficient to include both alphabet and numerals and for this reason use is made of two combinations known as "figures" and "letters." The reception of one of these combinations causes the receiving teleprinter to print characters from one only of two "cases" until the other "shift" combination is received. As the names imply, one combination covers the numerals and the other covers the alphabet in general.

In start–stop telegraphy the 5 units are usually transmitted serially at a speed of 50 bauds; that is, each unit lasts for 20 milliseconds. The line rests in the mark condition when no characters are being transmitted and each combination is preceded by one additional starting unit of space, which causes the receiving teleprinter to undergo a single cycle of operations. The combination is concluded by another additional unit of mark, which makes allowance for any speed difference between transmitter and receiver.

When a character is being received, the start space must be recognised by the receiving equipment to initiate the cycle of operations for reading the character. During this cycle the theoretical centre of each element is examined to ascertain the constitution of the combination of 5 information elements received. To help visualise an arrangement that might be suitable for carrying out these functions, a trigger such as *1F* and a counter such as *1C* in Figure 1 can be postulated. The trigger is a device having two stable states indicated by the compartments labelled *1* and *0*, which may be set up to the

exclusion of each other by signals on the appropriate input leads indicated by arrowheads pointing towards the compartments. The counter, on the other hand, has 140 stable states and is advanced from one state to the next by a signal applied to the single input. The outputs in both cases are indicated by arrowheads pointing away from the compartments. The symbol $1G$ denotes a gate, and the encircled 2 indicates that 2 simultaneous inputs are necessary to produce an output.

It is assumed for simplicity that, as the line alternates between mark and space during the course of a character, a signal will appear on an M lead when the line is in mark and on the S lead when it is in space. In these circumstances, the arrival of the start space will trigger compartment 1 of $1F$ to give an output, which by convention will be called $1F1$. D is a source of driving pulses always present so that $1F1$ causes pulses from D to pass through $1G$ and to step counter $1C$ in response. The counter will continue to step at intervals determined by D and to provide outputs timed in relation to the start space until further action is taken.

In case the reader may suspect that these symbols express something more than what first meets the eye, it may be noted that a trigger such as $1F$ represents the function performed by an electro-magnetic relay with a locking winding arranged so that it may be maintained in either operated or unoperated condition according to some external control. The output $1F1$ from the trigger $1F$ represents a break contact. The 2-input "and" gate $1G$ can be provided by 2 contacts in series, whereas the 2-input "or" gate $4G$ described later can be provided by 2 contacts in parallel; the counter $1C$ represents the type of function provided by a telephone stepping switch.

With 50-baud transmission, each element in the telegraph character is 20 milliseconds in duration and with the start and stop elements added to the 5 information elements, each character will require a period of 140 milliseconds in all. It is, therefore, desirable that the counter $1C$ should take a period of this order to make a complete cycle. The pulses from source D are, therefore, made to occur at a rate of 1000 per second, and at the conclusion of the cycle of operations the counter $1C$ can be arranged to reset the trigger $1F$ from 1 to 0 at 140 milliseconds, thereby disconnecting the drive to the counter, which will cease until the arrival of a subsequent character causes the cycle of operations to be repeated.

It is desirable to inspect the incoming line when the counter is in positions $1C30$, 50, 70, 90, and 110, as those 5 time positions will represent the theoretical centre of each of the 5 information elements. Inspection at these times will permit the use of a signal of greatest distortion without causing misoperation.
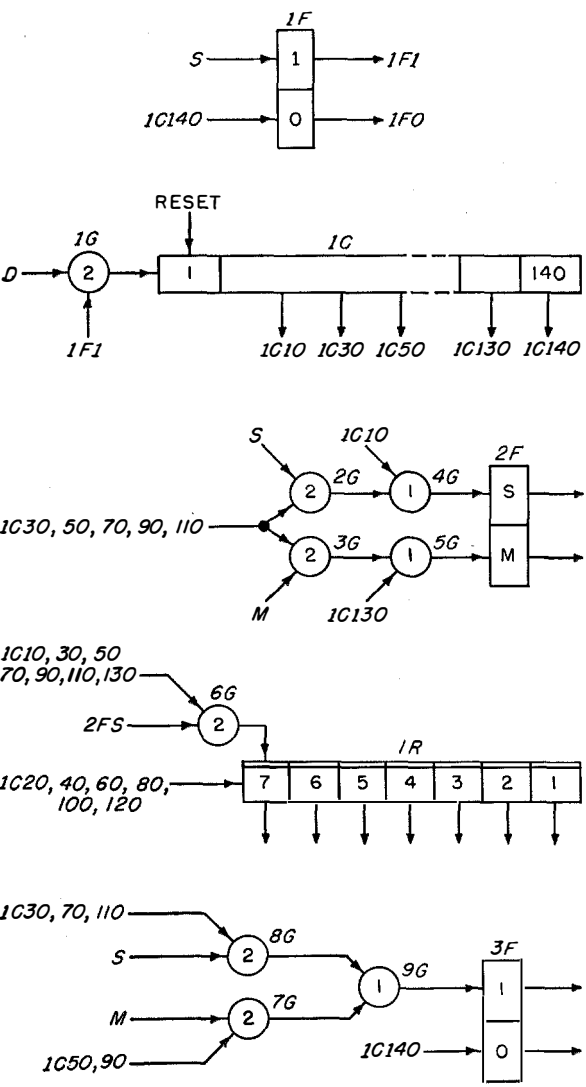

Figure 1—Elements of a start–stop automatic telegraph system. S represents a space, M is a mark, and D is a driving source.

The ability to read a telegraph character may be used for retransmitting or recording a message. It will be appreciated that in the former case it may be desirable to regenerate the signals to correct distortion due to line or atmospheric conditions. In the case of regeneration, a second trigger, 2F, may be incorporated, having two stable conditions M and S representing mark and space respectively, the trigger 2F being altered at the examination times by an input from 2G or 3G if it is found that the condition of the line has changed since the last examination. As the start element is always a space and the stop element is always a mark, these two conditions can be applied to 2F (without reference to the condition of the line) through gates 4G and 5G respectively. Furthermore, as the line is to be examined at the centre, as opposed to the beginning, of each elemental period, the trigger 2F will be changed half an element in time later than the changes are received from the line, and for this reason the start element is applied to the trigger 2F at 1C10 and the stop element at 1C130. The gates 2G and 3G provide joint control according to the condition of the line and at the proper times of examination, and the output of 2F represents the mark or space condition to be applied to the outgoing line.

On the supposition that it is desired to read and record the characters, there must be introduced a device that is capable of storing any one of the 32 different combinations that may be produced by the 5 different elements. A suitable device is provided by a stepping register such as 1R, the symbol for which shows a 7-element register enabling the condition of the start and stop elements to be registered in addition to that of the 5 information elements. The way in which this register is operated is as follows. Each of the register elements is capable of being set in either of 2 conditions, and in particular the element numbered 7 is shown arranged to be set by an input coming in from above. The arrow shown coming in to the side of element 7 represents the stepping means that causes the pattern of the symbol as a whole to make a step forward from left to right so that the condition of element 7 will be advanced to element 6 and so on. Now it will be clear that, if the normal condition of each element represents a mark condition and the operated condition of each element represents

a space condition, then the result of the periodic inspection of the line can be applied to element 7 as 7 discrete inputs at the times indicated, the composite pattern representing the character being obtained eventually by providing a step to the register between each examination time. As previously described, the line passing from mark to space starts the counter or time scale 1C, which can provide examination pulses at 1C10, 30, 50, 70, 90, 110, and 130, an input being presented to 1R7 at these times if the line is found to be in space. At intermediate times such as 1C20, 40, 60, 80, 100, and 120, a step is provided so that the pattern of marks and spaces gradually extends across the register and at the conclusion of the character its complete identity is available. It will be appreciated that on completion the start element that was initially inserted into 1R7 will have stepped forward to 1R1, the 5 information elements will be in 1R2, 3, 4, 5, 6, and the stop element will be present in 1R7, where it was introduced but not subsequently moved. The register function has no single mechanical analogy, the function often being performed by a combination of switches and relays.

The four symbols introduced above represent basic functions that can be used in many different combinations to describe a variety of systems not only in telecommunications, but also in industrial applications such as digital computers. To appreciate the possibilities of such systems, it is only necessary to master the
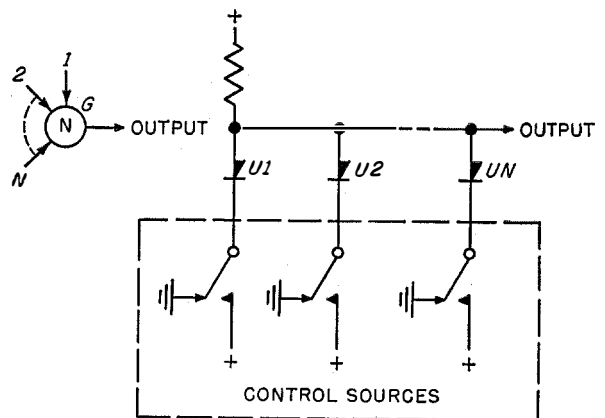

Figure 2—Coincidence (and) gate that produces output only when all control sources apply positive potential to the rectifiers.

simple functions represented by these four symbols. The numbers associated with the symbols may vary to suit the requirements and the components to be used. The number of inputs applied to a gate must depend on the determining factors. The capacity of the counter and register must be chosen to suit their application. Similarly there will be occasions when a trigger device may serve a useful function with more than two elements, provided not more than one is operated at a time.

1.2 CIRCUIT METHODS

Having briefly introduced the symbols by way of well-established functions, it is now proposed to describe some of the circuit components and methods by which the symbols may be realized. Necessarily this must be in the nature of a brief review since the advances during the last decade or so have been as numerous as they have been rapid.

It is interesting to note that the computer engineer has made a substantial contribution towards new methods of realizing the functional diagram in much the same way that he has promoted its use. Because the hard valves used in the early digital computers were found to be unsuitable in some respects, it became necessary to seek new methods. The search produced several new solutions that were readily accepted and tried out in this new field.

1.2.1 Gate Circuits and Components

The rectifier, or diode, is perhaps the most commonly used circuit element in gates on account of its inherent simplicity and low cost. A typical coincidence rectifier gate arranged to give an output when a positive potential is applied to all inputs at the same time is shown in Figure 2. The positive voltage from the supply source passes through the rectifiers U1, U2 . . . UN to the control sources, shown schematically. If any control is at zero potential, the common connection will be held near zero (the potential drop across the rectifiers). On the other hand, if all sources are simultaneously positive, the common connection will become positive to indicate coincidence. The corresponding mixing (or) circuit is shown in Figure 3 in which any

single positive control source will cause a positive output across the resistance. These circuits might make use of hard valves or metallic rectifiers such as selenium or germanium for example according to the design requirements in respect of cost, reliability, speed, et cetera.
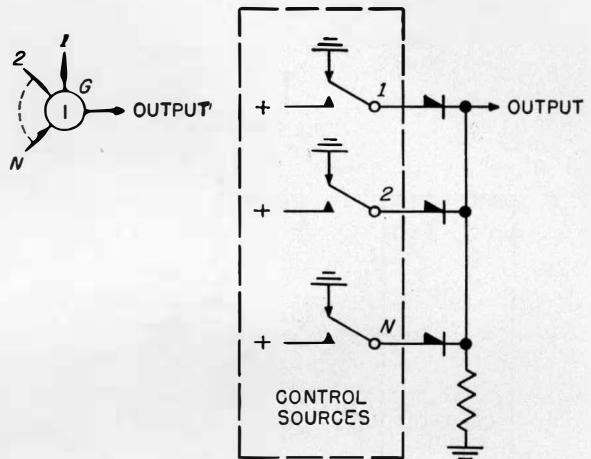
Figure 3—Mixing (or) gate that produces output if any one control source applies a positive potential to the rectifiers.

It is characteristic of the rectifier gate that it produces an overall power loss. Often this does not inconvenience the designer since the trigger-circuit components may contain an inherent gain, or if this is not so a suitable pulse regenerator may be inserted. Nevertheless, a useful class of gating circuit is that in which a supply of pulses can be switched from a low-impedance source without appreciable loss while the control source uses only a minimum of power.

For example, a gate circuit might comprise a hard valve with a cathode-connected source of negative pulses that can be "switched" to the anode by means of a suitable control voltage on the grid. Alternatively, a cold-cathode gas trigger tube can be used in much the same way. A third example using a more-recently developed component is shown in Figure 4 in which use is made of the switching properties of a point-contact transistor.[1] Negative pulses from a low-impedance source are applied to the collector and may be switched to a load R1 in the emitter under the control of a potential applied to the base resistance R2. If this potential is positive,

---

[1] British Patent Application 29848/53

no current will flow into the emitter, and in consequence the collector current, when the pulse is on, will reach only a small value. On the other hand, if the control potential is negative and the current gain sufficient, then, when a pulse is present a small initial current in the emitter will

Figure 4—Arrangement of a point-contact transistor to produce a coincidence (and) gate.

cause a larger current to flow in the collector, thus further reducing the base potential until the transistor "bottoms" and is held on by the difference between the emitter and collector currents flowing in $R1$. In these circumstances an effective low impedance will be maintained between collector and emitter and the pulse current will be determined mainly by the load.

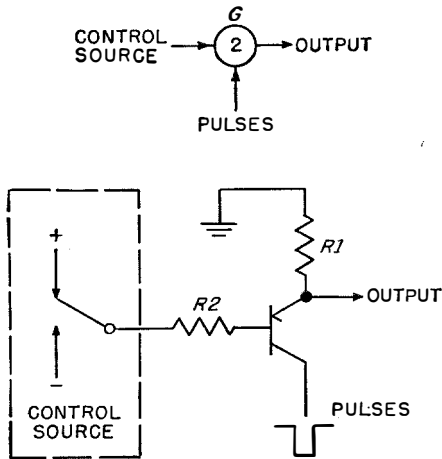Junction transistors can also be used for this class of gate although the technique of using them is rather different from that outlined for the point-contact type.

Mention should be made of the magnetic gate, which may have considerable importance in the future on account of its ruggedness, speed of operation, and low cost. Use is made of the properties of the rectangular hysteresis loop shown typically in Figure 5. If a suitable constant-current pulse source is applied to one input winding of a toroid such that the hysteresis loop is only traversed between point 1 and point A, then only a very small electromotive force will be induced in the output winding since there can be very little change of flux. On the

other hand, if the control winding is energized with a similar value of ampere-turns at the same time as a pulse occurs, then the hysteresis loop will be traversed to point B and an output pulse will be induced in the output winding. In this way a single pulse has been gated through. Steps must be taken to restore the magnetic state of the core from state 0 to state 1 in order that the cycle may be repeated. This can conveniently be achieved by interposing pulses of opposite polarity between those from the pulse source.

In practice, magnetic gates can use ferrite toroids producing rectangular hysteresis loops, which permit operation at very high speeds. Furthermore, the windings are often formed by only single turns so that the construction is very simple.

1.2.2 Trigger Circuits and Components

In the last decade so many solutions have been proposed for what may be called the trigger group that only a few of the more-promising components need be discussed in any detail.

Hard-valve trigger circuits, such as the Eccles–Jordan, are well known and extensively used and probably represent the best of current practice. However, there is much interest in replacing
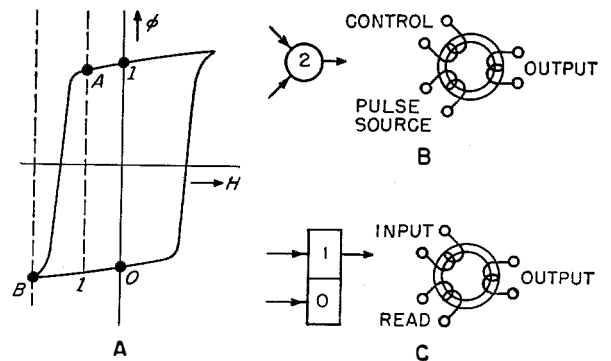

Figure 5—Typical hysteresis loop A on which the magnetic versions of the gate B and trigger C are based.

them for reasons of power and heat dissipation, reliability, life, initial cost, and general convenience.

For comparatively slow-speed circuits the gas tube is attractive since the properties of the gas discharge are well adapted to a 2-state device

and since the visibility of discharge can be a valuable aid to maintenance. The development of gas-tube circuits has also provided some experience with useful techniques that can similarly be applied to some transistor circuits that will be outlined later.

Since a discharge in a gas can be extinguished only by disconnecting or reducing the anode voltage, it has become common to use tubes in

by U1, U2, and R3 produces an output to trigger tube CT2 since only the positive plate of U1 is positive due to the drop across R2. The resultant current passing through the main gap of CT2 depresses the voltage on the common anode connection due to the presence of R1 and, since C1 was charged and C2 not, the potential drop across CT1 is reduced below the glow-maintaining value. With proper choice of constants, tube
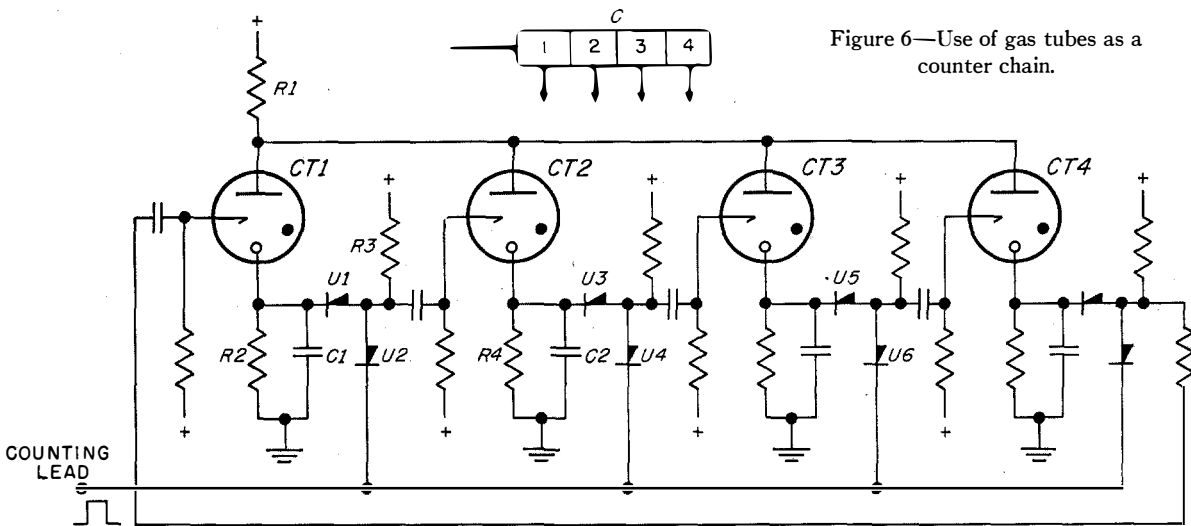
Figure 6—Use of gas tubes as a counter chain.

pairs or groups, the firing of one gap being used to extinguish another. This is not, however, an inconvenience, since two outputs corresponding to 1F1 and 1F0 of Figure 1 are thereby provided. When one tube of the pair is rendered conducting by the application of a triggering potential, the instantaneous flow of current can be used to depress the voltage across the other and thereby extinguish it.

The process can be made clearer by reference to a rather-more-complex circuit. Figure 6 shows 4 cold-cathode trigger tubes CT1–4 arranged as a ring counter. Assume that one tube, say CT1, is conducting and that current is flowing from the positive supply through the common anode load resistor R1, the main gap of CT1, and resistor R2 to earth. Capacitor C1 will have charged to the potential across R2, which also determines in conjunction with R1 the anode voltage supply to the other tubes. If, now, a pulse is applied to the common counting lead, then only the rectifier coincidence gate formed

CT1 will extinguish while C2 charges with a time constant:

$$\frac{R1 \cdot R4 \cdot C2}{R1 + R4}.$$

Meanwhile, C1 discharges through R2. When these charge and discharge processes are complete, the glow discharge may be further advanced from CT2 to CT3 by the application of a second pulse and so on.

A more-compact and convenient counter can be made by the inclusion of the gas gaps within a single envelope[2] if use is made of directional ionization coupling among, say, 10 main cathodes and 10 commoned transfer cathodes. Figure 7 illustrates a typical arrangement for 4 main cathodes.

Each cathode has geometrical asymmetry, so that, for instance, if current is initially flowing through the common resistor R1, gap AK3, and

[2] G. H. Hough and D. S. Ridler, "Multicathode Gas-Tube Counters," *Electrical Communication*, volume 27, pages 214–226; September, 1950.

resistor *R3* to earth, only the transfer-cathode gap *AK4* will have a low breakdown potential due to the proximity of the discharge. Therefore, if a negative pulse is applied to the transfer cathodes, only gap *AK4* will break down and gap *AK3* will extinguish, due to the additional voltage drop across *R1*. Now, since the gap *AK5* will come under the influence of the glow on *AK4* while gap *AK3* deionizes, when the pulse goes off, gap *AK5* will break down and conduct.

In this way a pulse applied to the commoned transfer electrodes will have caused the discharge to take a step forward.

Gas-tube trigger circuits may be considered practical up to a speed range in the region of 10 000 steps per second although higher speeds have been attained for stepping registers. The input and output characteristics of the circuits are convenient, particularly for rectifier gates. For a further increase in speed, the transistor is probably the most convenient and versatile element.

The point-contact transistor is a most-convenient type for trigger circuits since it has the property of being able to hold itself conducting in a suitable circuit and can, therefore, conveniently fit one compartment of the functional
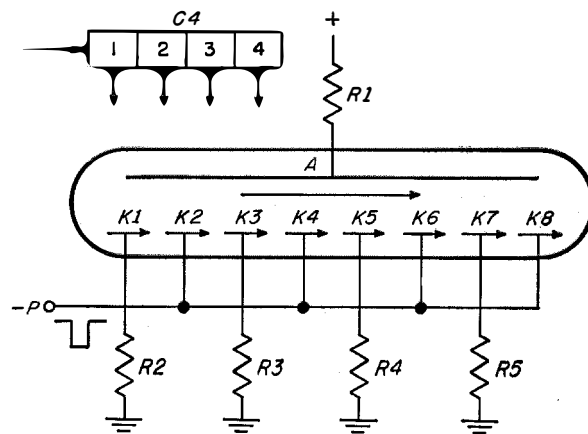

Figure 7—In this counter, several sets of gas gaps are mounted in a single envelope.

symbol. However, it is apparent that there is a considerable field for the junction type, which is less sensitive to temperature than the point-contact unit and, therefore, more likely to find favour where the ambient range is wide. The issue is by no means decided, and it is probable that there will be an extensive field of application for both types and perhaps for some new varieties. Whereas the circuits of junction types have much in common with those for hard valves, the approach to the use of the point-contact transistor is rather novel and will be described in view of its greater interest.
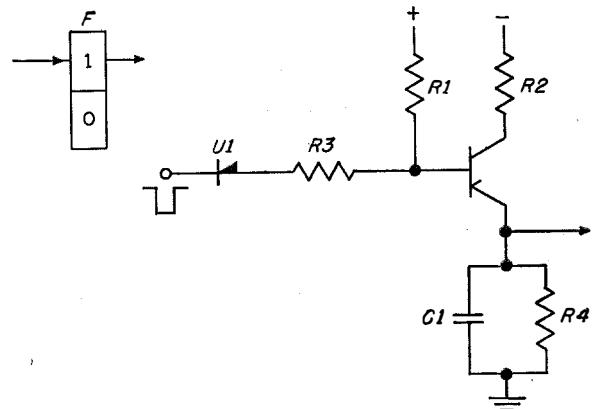
Figure 8—Trigger circuit using a point-contact transistor.

The most suitable point-contact transistors for trigger functions should have a current gain between the emitter and the collector at least greater than unity and should have a low standing current in the collector with zero or a small negative voltage on the emitter. Given these conditions, satisfactory trigger circuits can be evolved. Figure 8 shows one simple example of such a circuit, which is somewhat analogous to the gas-tube trigger and has similar desirable properties from the point of view of ease of interconnection.[3] In the "off" condition, the current flowing through *R1*, *R3*, and *U1* is arranged to be somewhat larger than the small collector-to-base current and of opposite polarity so that the base is slightly positive and the collector, therefore, presents a high impedance. If, now, a negative triggering pulse is applied such that emitter current flows, then current will also flow in the collector and the circuit will take up a second stable state in which the transistor is held on by the difference in current between emitter and collector that maintains the base negative. The circuit can be triggered back to the off condition by momentarily reducing the collector supply to zero, which can be conveniently achieved by means of a second transistor trigger circuit.

[3] British Patent Application 33618/53.

In much the same way that the output from the cathode circuit of a gas tube may be used to control the triggering of a further tube as shown in Figure 6, so the output from R4 in parallel with C1 in the emitter of the transistor in Figure 8 may be used to control the triggering of a further transistor via the base. Again this may be illustrated by considering the transistor ring counter in Figure 9.

Assume that one particular transistor such as T1 has been triggered into the "on" condition so that the current flowing through it will result in a negative potential across R1. If, now, a stepping pulse is applied to the common counting lead, then only the coincidence gate formed by the rectifiers U1 and U9 will produce a negative output pulse since the other gates will be held at earth through the emitter loads. Transistor T2 will, therefore, trigger and the additional current necessary to charge C2 will cause the potential across L to rise and restore T1 to the off condition.

tor circuits, which are in many respects similar, has been influenced by the functional diagram in the sense that they are flexible elements easily interconnected by virtue of their input and output characteristics. At the same time it is necessary to regard the functional diagram itself as flexible and capable of alternative interpretations. For instance, the counter 1C of Figure 1 might in practice be broken down into 3 stages, the count of 140 milliseconds being derived by counting pulses occurring at a rate of 5000 per second, firstly in tens to derive 2-millisecond periods, then this output in tens again to obtain 20-millisecond periods, and finally in sevens to obtain 140 milliseconds. The interconnection of the three counters necessary for this process is simply achieved by means of gates, and any time interval may be obtained by outputs in combination. Even so, the most economical circuit may not result when the functional elements are directly replaced by circuit elements, and it is here that the circuit designer
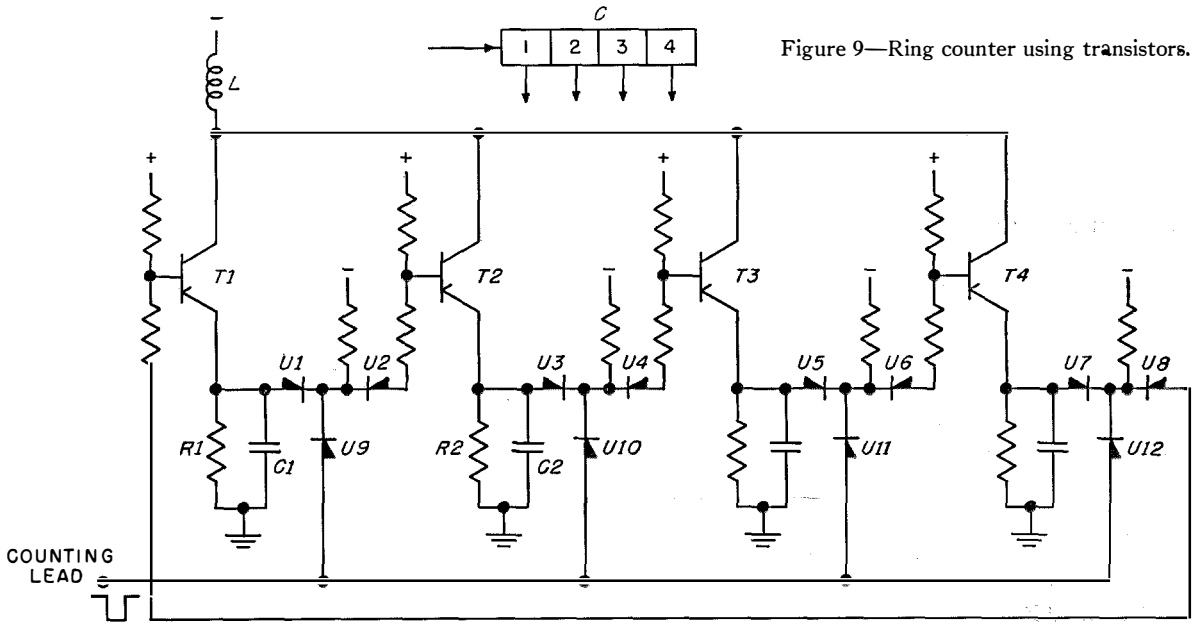
Figure 9—Ring counter using transistors.

It is desirable to use a common inductance rather than a common resistance, as in the case of the gas-tube counter, since the variation in the off-condition collector current between transistor samples would give rise to an unpredictable collector supply voltage on account of the potential drop across the common resistance.

The design of these basic gas-tube and transis-

must use skill in the arrangement of components.

In addition to the types of trigger already described, the static magnetic trigger, like the magnetic gate, is an element of growing importance, although circuits using this device differ in some respects from circuits using gas tubes and transistors and may not fit so easily into the functional diagrams outlined.

Magnetic triggers make use of the two states of remanent magnetism denoted *1* and *0* on the hysteresis loop shown in Figure 5. The main feature of this loop is that the remanent flux is very nearly the same as the saturation flux. If a suitable pulse is applied to the input winding of a core made from material with this type of hysteresis loop, then it will be left in either state *1* or *0*, dependent on the polarity of the pulse. There is no standing indication of the remanent state, and to provide an output, it is necessary to pulse the core a second time and to observe the output winding for the presence of an electromotive force indicating a change of flux. If this second, or reading, pulse has the same polarity as the original input pulse, then the flux change will be small and only a small electromotive force will be induced across the output, or reading, winding, whereas if the original pulse were of opposite polarity the hysteresis loop would be traversed towards the other remanent state and a resultant output pulse would be induced in the reading winding. A simple trigger built on this basis has the disadvantages that there is no standing output and that any interrogation results in a return to a particular state. On the other hand it has the advantage of no standing power drain.

Research is now being directed towards methods of reading the polarity of the remanence without destroying it, and there would appear to be reasonable hope of success. If these methods prove simple, then there can be little doubt that magnetic elements will be very versatile, very rugged, and have a long life.

2. Functional Diagrams Applied to Telegraph Systems

Some of the less-well-known operations in telegraphy will now be described by means of functional diagrams that will use the symbols outlined in section 1.

2.1 CHARACTER IDENTIFICATION

For supervisory purposes a message in process of transmission may have to be scanned for a particular character, which may, for example, represent the end of the message. It would clearly be possible to record each character in turn on a register such as *1R* in Figure 1 and when the time scale has given the sixth step to *1R* to examine the significant positions for the particular combination that requires special attention. However, this function can be performed much more simply in the following manner.

It is possible with a trigger such as *3F* to indicate with certainty if a character received is *not* the one requiring special attention; thus, if an indication from *3F* is not given, it follows that it was in fact the special character. The functional operation may be described in more detail as follows. Supposing that the particular character to be observed is *M S M S M*, then if the first element of the character is a space it is certain that it is not part of the special character and a transfer can take place from *3F0* to *3F1*. Similarly, if the second element is a mark, which cannot possibly be a part of the special character, then the trigger *3F* can be transferred from *3F0* to *3F1*. In a similar manner the third and fifth elements can be treated as the first element, and

Characters Transmitted—

      S M S M S M M *M M M* **S M S M M S M** *M M M* **S M M M M S M** *M M M M M* **S M M S S S M**

Additional False Start—

      S M S M S M M *M M* <u>**S**</u> *M* **S M S M M S M** *M M M* **S M M M M S M** *M M M M M* **S M M S S S M**

Characters Received—

      S M S M S M M *M M* **S M S M S M M S M M M M S M** *M M M* **S M M M M M M** *M* **S M M M S S S M**

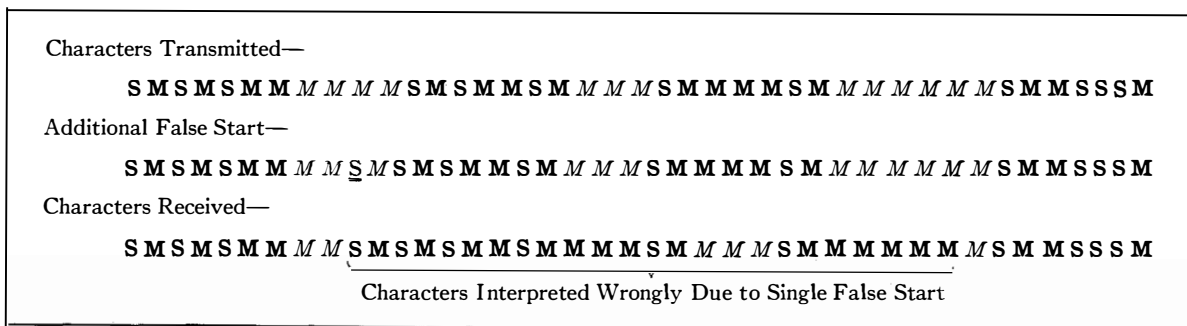Characters Interpreted Wrongly Due to Single False Start

Figure 10—Effect of a false start element introduced by interference. Each 7-element character shown in boldface starts with a space S and ends with a mark M. The spurious start signal is underscored and causes the reception of three wrong letters in the place of the two transmitted characters.

the fourth element can be treated in the same way as the second element. If, after the last examination at $1C110$, there remains an output from $3F0$, then the special character $M\ S\ M\ S\ M$ has just been received.
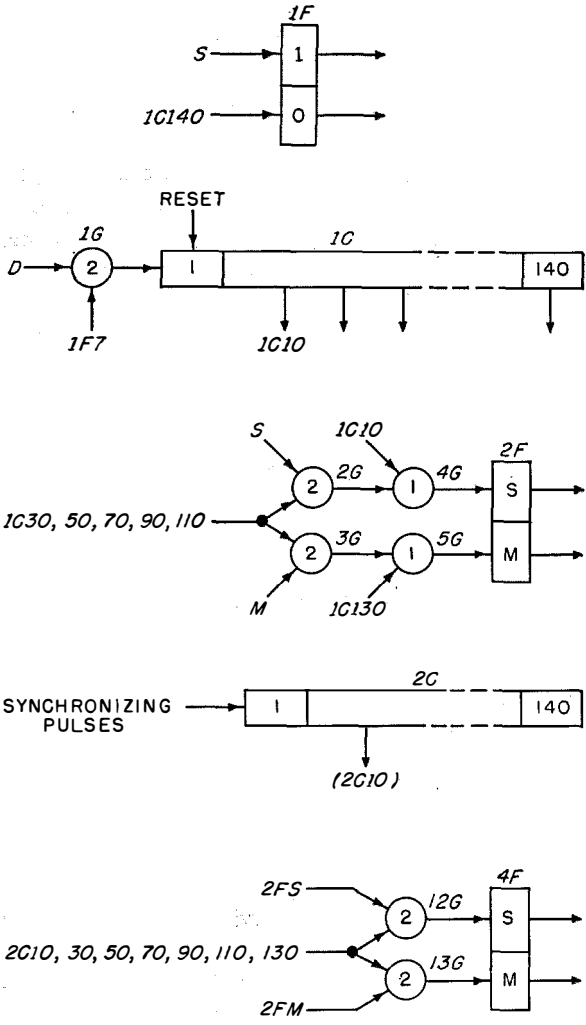

Figure 11—Transmitting end for element synchronization.

2.2 Synchronous Telegraph Systems

It is well known that in start–stop telegraph systems one of the most-damaging effects of interference is to cause the receiver to become out of phase with the transmitter, with the consequence that the transmitted characters are misinterpreted until correct phase is regained (see Figure 10). One satisfactory method of avoiding the false start signals, which are responsible for this trouble, is to make use of synchronous transmission, that is to run the receiver in phase with the transmitter independently of the start–stop signals. With such an arrangement it is possible to disregard apparent starts that occur at improper times. Either element synchronization or character synchronization can be used. Element synchronization is advantageous on account of its ability to reduce loss of synchronism, but character synchronization altogether eliminates such trouble although the equipment needed is somewhat greater than that required for element synchronization, as illustrated below.

For element synchronization it is necessary to include triggers such as $1F$ and $2F$ and a counter such as $1C$ (Figure 1) for the recording in turn of each element of the start–stop character. A second counter such as $2C$ in Figure 11 is employed to give the synchronous time, and an extra trigger $4F$ can be used to transfer the condition from $2F$ under control of the synchronous time scale. In this way each element of each character is re-aligned to fit the synchronous times. At the incoming end (Figure 12) a synchronous time scale allows the trigger $5F$ to
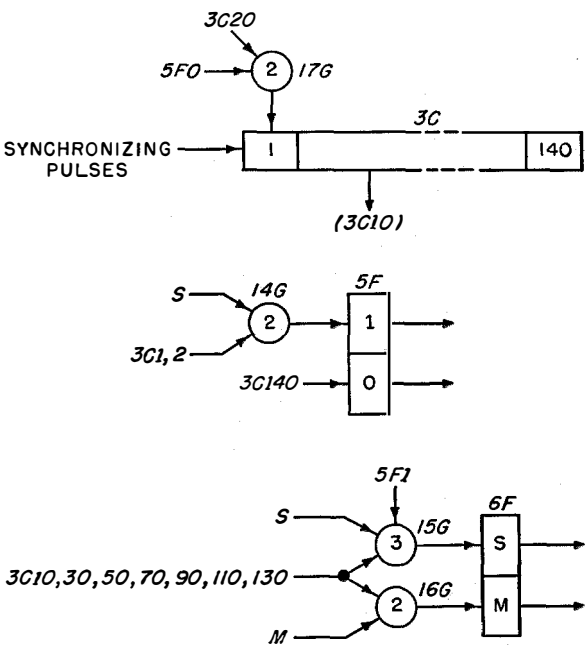

Figure 12—Receiving end for element synchronization.

change over from *0* to *1* only if space is being received at the acceptable inspection time. If there remains an output from *5F* after this period ceases, the time scale can be reset at the proper time to maintain synchronism in preparation for the receipt of a character possibly commencing in the next element position.

With character synchronization it is necessary to store the whole character at the outgoing end to provide for an adverse relation between the start–stop and synchronous time scales. This can be achieved by storing the element values on 7 separate triggers, *11F* through *17F* of Figure 13, which are operated under control of the start–stop time scale *1C* and subsequently read by the synchronous time scale *2C*. It is evident that these triggers must be restored to normal after they are read so that they may be available without delay for re-use by a subsequent character. At the incoming end (Figure 12) no time-scale-reset requirement arises as the trigger *5F* can only pass from *0* to *1* at the start of each cycle of *3C*.

2.3 ERROR-INDICATING SYSTEMS

It will be appreciated that character synchronization virtually eliminates message distortion due to false start elements. However, disturbances on radio, and even line, circuits may occur and result in an incorrect character being received. Various systems have been devised to indicate if a character received contains an incorrect element. The simplest process introduces a parity check; such a check is achieved by ensuring that each character contains an even number of marks or spaces. Suitable equipment can be employed to indicate any character received that fails to satisfy the parity check. The following method may be used to ensure that all characters have an even number of marks.

It is evident that, of the 32 different combinations provided by 5 information elements, 16 of the 32 will contain an odd number of marks, but if the characters formed from these 16 combinations use mark for the stop element, these characters will then have an even number of marks. The other 16 combinations can use a space for the stop element, thereby retaining also an even number of marks. The polarity of the stop element is not important, provided there is
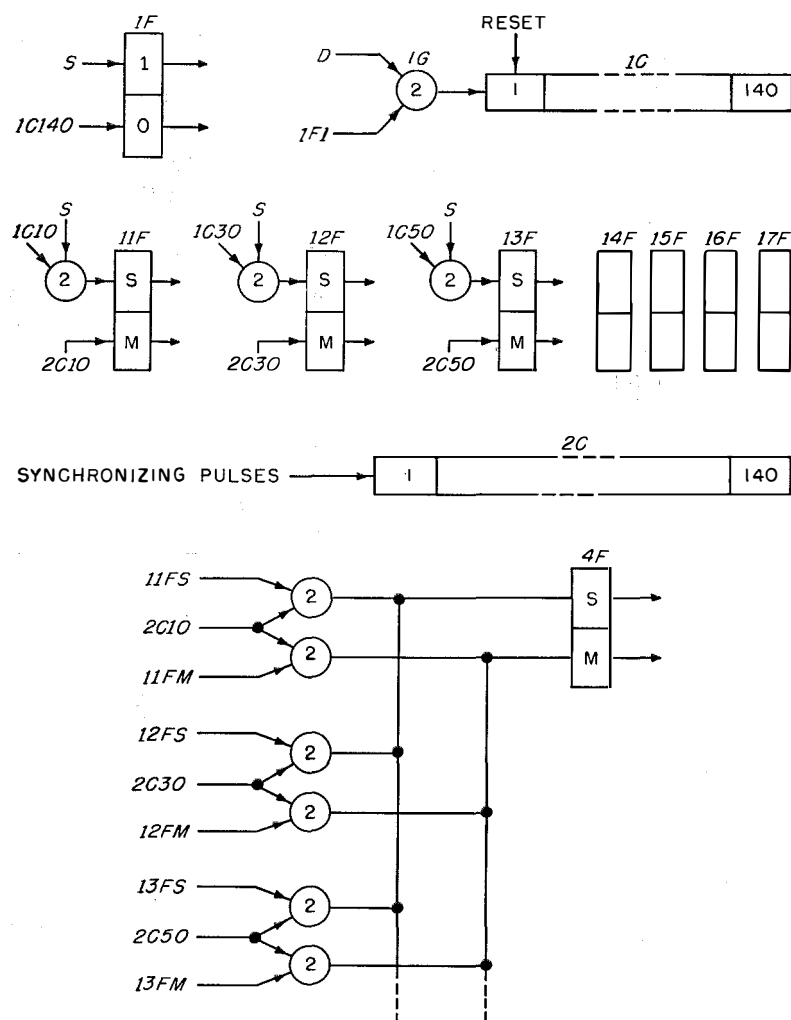

Figure 13—Receiving end for character synchronization.

always a transition of polarity for the start element of the following character. It will be appreciated that a 2-position counter can determine the appropriate stop and start elements so that each character can be made to contain an even number of mark elements and to ensure that each start element differs from the previous stop element.

For character-synchronous systems in which it is necessary to store each character, the checking principle can be further developed using both start and stop elements for checking purposes. One favoured system is to transmit 32 different combinations of 7 units, each comprising 3 spaces and 4 marks or vice versa. Each character can be checked for the total of marks and spaces and, unless there has been a transposition of a mark element to a space and also a space to a mark in the same character, any normal fault can be indicated. Such systems need to make a character translation from the 5-unit to the 7-unit base and a further re-translation at the receiving end. As a consequence, two relatively involved terminal equipments are needed.

An alternative, and simpler, arrangement is achieved by scanning the 5-unit characters in turn to avoid translating all those characters that contain 1, 2, or 3 spaces and to obtain the constant total by the addition of the appropriate combination of balancing elements to replace the start and stop elements. The seven 5-unit character combinations containing 0, 4, or 5 spaces cannot be treated in this way and must be translated.

2.4 Error-Correcting Systems

Another arrangement aims to determine an element received incorrectly and to correct it so that there is no need to use a channel in the reverse direction to seek a repetition.[4,5] As in the error-indicating systems, it is accepted that certain error combinations will remain undetected, but it is confirmed by statistics that a large percentage of all errors are isolated and could, therefore, be corrected automatically. This alternative is described hereafter as an exercise in the use of functional diagrams to describe a system.

The system considers each pair of characters as a unit for which there are 4 check elements

(2 start and 2 stop elements) available for check and correction. These 4 elements provide 16 different combinations that, being transmitted with a pair of characters, describe their constitution on a parity basis.

Assume that the 5 information elements of the first of a pair of characters are lettered $11R1$ . . . $11R5$, that those of the second of the pair are lettered $12R1$ . . . $12R5$, and that the check elements are numbered $21C$, $22C$, $23C$, and $24C$. A space occurring in the information elements is used to control the check elements as shown in Table 1.

TABLE 1

CONTROL OF CHECK ELEMENTS

Space In	Provides Impulses To
$11R1$	$21C$, $22C$
$11R2$	$21C$, $23C$
$11R3$	$21C$, $24C$
$11R4$	$21C$, $22C$, $23C$
$11R5$	$21C$, $22C$, $24C$
$12R1$	$21C$, $23C$, $24C$
$12R2$	$22C$, $23C$
$12R3$	$22C$, $24C$
$12R4$	$22C$, $23C$, $24C$
$12R5$	$23C$, $24C$

The information elements of a pair of characters are examined in transmission, and 4 check elements are prepared according to the above list. If, now, a check element ($21C$, $22C$, $23C$, or $24C$) receives an odd number of impulses, a mark is transmitted; otherwise a space is transmitted. If the information elements are similarly examined on reception and check elements again prepared, then the two groups of check elements may be compared to indicate and correct a possible fault. Since an impulse is sent to two or three check elements when a space is present, then if one, and only one, check element compares incorrectly it can be assumed that it is the check element that is wrong, and no correction is necessary. Any one of the 6 different combinations of 2 check elements wrong or of the 4 different combinations of 3 check elements wrong indicates that a particular information element needs correction in accordance with the list above, whereas all check elements wrong indicates several errors that are beyond correction.

Turning now to the functional diagram of Figure 14 and assuming $11F$ to be the trigger, $11C$ the start–stop time scale, and $12C$ the

---

[4] British Patent 710258; September 22, 1954.
[5] British Patent Application 34415/53.

synchronous time scale as before, *11R* and *12R* comprise a couple of character registers introduced alternately by the 2-element counter *13C*, which is driven once as each character arrives. The registers *11R* and *12R* record the space elements encountered under control of the start–stop time scale *11C* as described before. In Figure 15, *31F* provides a sequence control and
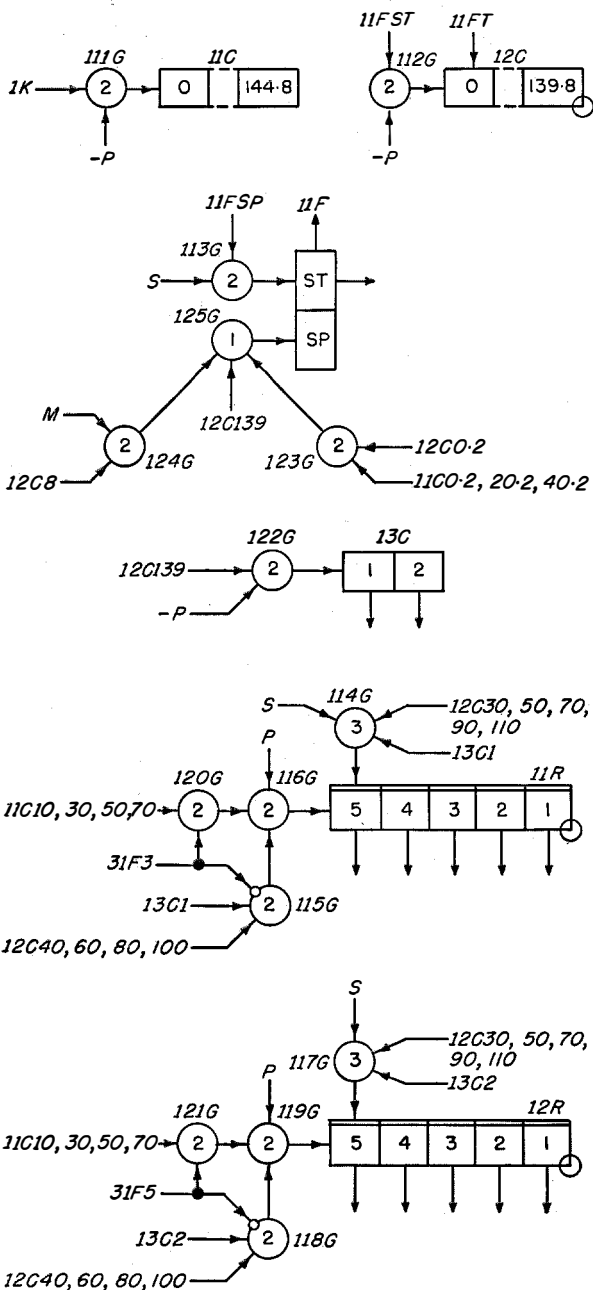
Figure 14—Error-correcting-system character reception, outgoing terminal.
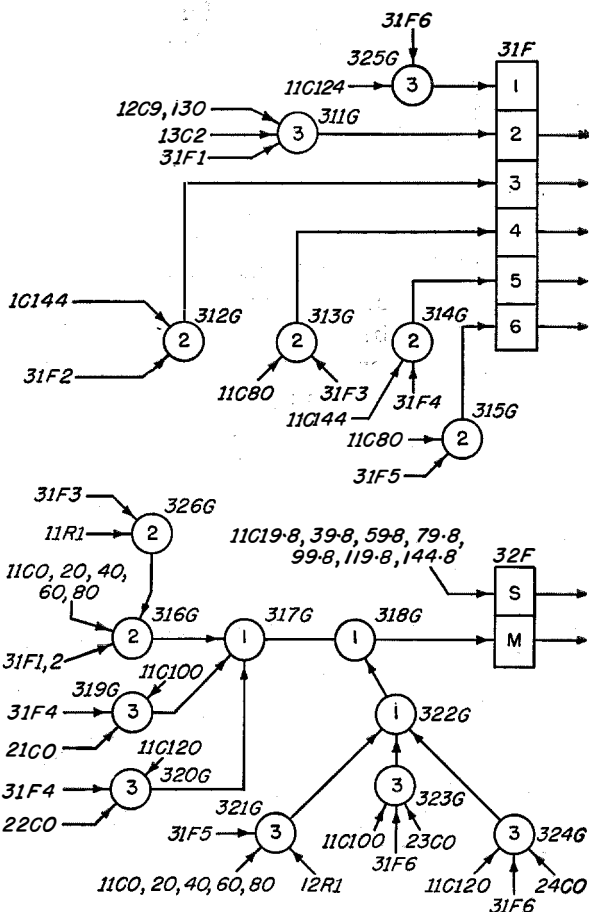
Figure 15—Error-correcting-system character emission, outgoing terminal.

is in form similar to the trigger *11F* except that there are 6 positions, only 1 of which may be operated at a time. Normally in position *31F1*, it advances to *31F2* when the second of a pair of characters is in process of being received. It then awaits the end of a synchronous cycle when it advances to *31F3* in which the 5 information elements in *11R* are emitted; thereafter it passes into *31F4* for 2 check elements. *31F5* and *31F6* control the emission of the second of the pair of characters in a similar way, after which *31F* advances to *31F1* to await the time when a further pair of characters can be transmitted.

The counters *21C*, *22C*, *23C*, and *24C* of Figure 16 are operated in accordance with the arrangement described above during the time cycle of *12C* (Figure 14) while *31F* (Figure 15) is in position *3* or *4*, that is while the first of a pair of characters is in process of transmission.

The trigger *32F* performs the function of *2F* in earlier examples; it reads the space condition of the registers *11R* and *12R* and of the counters *21C* through *24C* under the sequence control *31F* and the time scale *12C*. *32F* is shown biassed to mark for each element but is changed to space as required.

At the receiving end, the synchronous time scale *41C* of Figure 17 and the registers *41R* and *42R* for a pair of characters follow the technique already explained; the changeover between these two registers is controlled by *42C* which only passes to *42C3* when the trigger *41F* confirms that a character has been received in *41R*. The check counters *43C–46C* are pulsed from *41R* and *42R* during the cycle when the second character is being received. The check elements are also counted, and, if no failures have taken place, each counter will be in its *1* condition: the counter *51C* (Figure 18) will in consequence transmit on the two following cycles the exact contents of *41R1–5* and *42R1–5* through *502G*, et cetera, the standard start and stop elements being inserted. If any combination of 2 or 3 of the counters is in its *0* condition, the appropriate element will be corrected by a pulse applied to *51C*. The trigger *51F* is used to indicate the total number of incorrect counters and to ensure through *506G–509G* that the only correction effected is determined by the precise arrangement of all the counters *43C–46C* that register disagreement through *510G–519G*. If all 4 counters are wrong, there is no correction but the condition can be alarmed and the doubtful character indicated. It should be explained that the registers *11R* and *12R* (Figure 14) are stepped both from the start–stop time scale *12C* and from the synchronous time scale *11C*, the control being vested in *31F3* and *31F5*. The

circles surrounding these inputs to *115G* and *118G* indicate that the operation of these gates is inhibited by and not associated with these inputs. It is undesirable that the gates *114G* and *120G* should conduct simultaneously, and such an event is avoided by *123G*, which prevents the unwanted phase relation between *11C* and *12C*. This correcting system needs no translation or message storage before transmission.
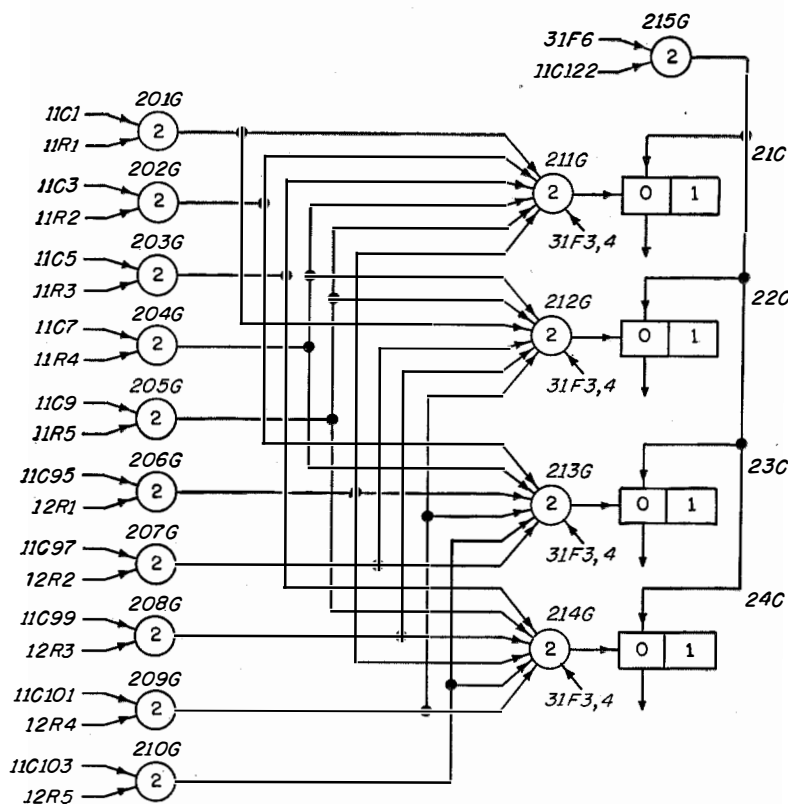
Figure 16—Error-correcting-system check-element determination.

2.5 EXTENSION OF UNIPERIOD OR ELEMENT LENGTH

It will be appreciated that another way of using the 140 milliseconds of available time in a synchronous system is to extend each of the 5 elemental periods to 28 milliseconds. The characters can be stored in pairs, as described, and the synchronous time scale used to examine the stored values every 28 milliseconds. The longer elements would allow, say, three examinations at the receiving end, and the majority condition would be accepted.

3. Miscellaneous Applications

3.1 Flexible Time Scale

A flexible time-scale arrangement is useful for several requirements in telegraph operation.

Figure 17—Error-correcting-system character reception, incoming terminal.

For example, a false-start condition is unlikely to persist for 20 milliseconds, and if it is found to have ceased after a few milliseconds the time scale can be reset and the false character rejected. For passing supervisory signals over a telegraph channel, it is common practice to allow the line to rest in space instead of mark. If then the time scale is arranged to examine the 7 elemen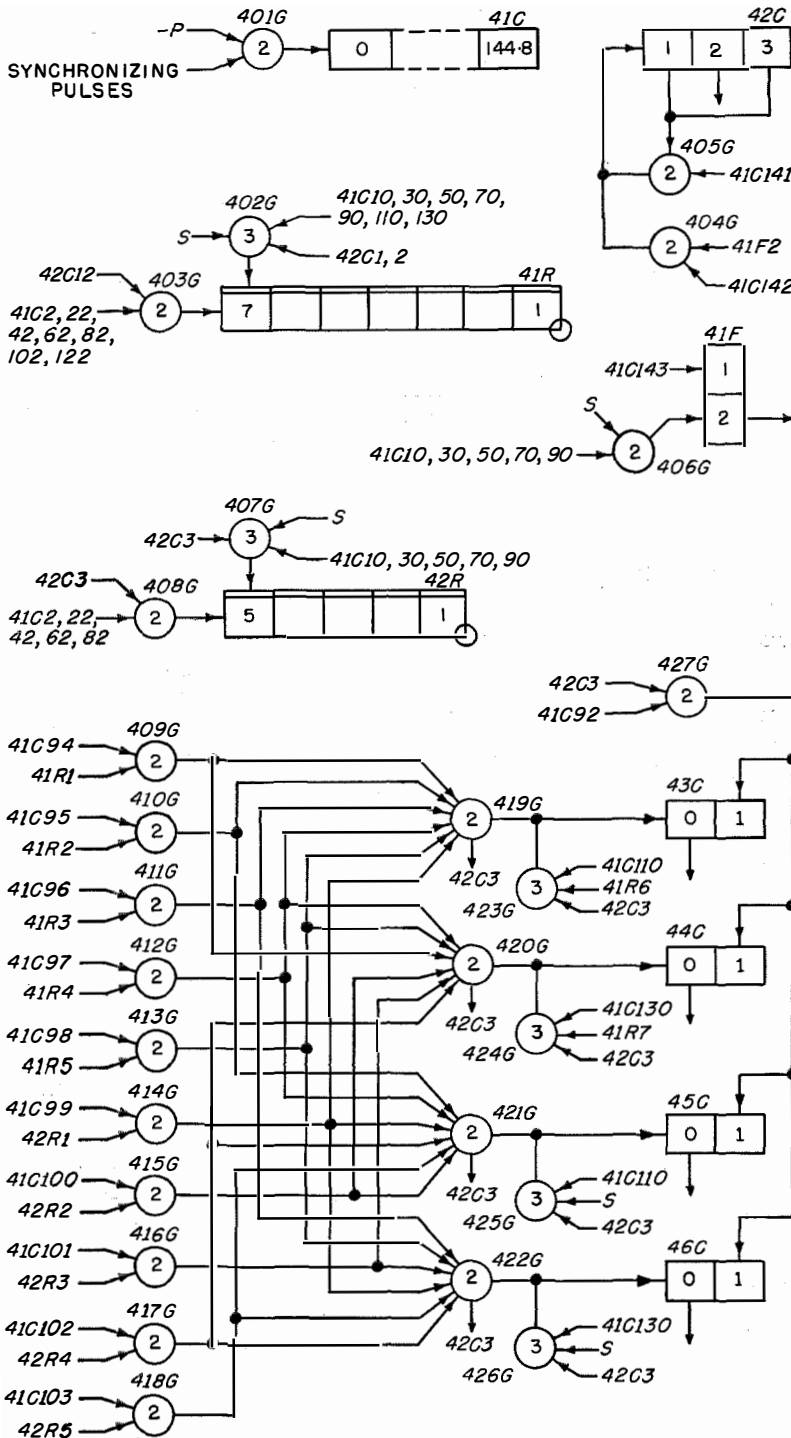ts, it can ensure that the space condition is maintained until mark reappears before allowing the line to revert to normal operation. When no such signals are in use, it may be desirable to insert the mark for the stop element, disregarding the condition of the incoming line.

Many of these time-scale conditions can be easily varied for experimental and statistical examination to ascertain the most suitable values in different line conditions. For exact comparison work, it has been found essential to make high-quality magnetic recordings of typical distorted messages that can be re-read without further distortion due either to random or systematic variations in tape-reading speed. Tapes can be perforated to determine the different parameter values by the use of special measuring equipment.

3.2 Multiple Regeneration

Although originally introduced to avoid excessive distortion on long telegraph connections, it seems likely that there will be some application for regenerators on quite short lines provided that, as a consequence, the terminal machines can be guaranteed improved operating conditions.

Such improvement would allow the machines more margin, with a consequential decrease in maintenance. However, for such a policy to be attractive it would be necessary to find a very cheap and reliable regenerator with low maintenance expense. One attractive method of meeting these requirements is a form of multiple regenerator in which 20, 40, or 60 circuits could share not only a common power plant but also other common facilities.[6]

For example, with a memory type of store, in which the elements are examined periodically and in sequence, a group of time scales could be built in which the individual parts might be of extremely simple construction. In principle each scanning of the memory could be made to accumulate a counting operation that had been initiated by a trigger such as *1F*. If the repetition rate of scanning is high, the relative position of scanning when the trigger operates represents an error that can be neglected. With a repetition frequency of 0.625 millisecond, a total of 32 scans would mean 20 milliseconds, and 7 periods of 20 milliseconds would cover the normal time cycle. Counting in binary notation, the whole scale could be provided by 8 elements, a number of circuits could be provided on a single memory device and the individual portion of the circuit would be limited to triggers such as *1F* and *2F*.

3.3 MESSAGE STORING AND RETRANSMISSION

The memory type of store may be conveniently utilized for the storage of messages and take the place of a reperforator. In a similar way the transmission of a telegraph message stored electronically involves only the reading of the stored information and means to control the signal sent to line as already described. The scanning speed will normally be far greater than that essential for telegraph purposes, and as a consequence an annex system may be introduced to provide a ready means of altering the time scale. It will be evident that such an arrangement provides facilities for the transmission of messages at different speeds to suit the different conditions that arise. Associated with the need to store telegraph messages, there will naturally be the need to number the messages and to handle them sequentially. Both these functions

[6] British Patent Application 34415/53.

can be adequately carried out by the memory type of storage using the facility for rapid scanning to achieve the rapid selection of number or message that is naturally desirable for efficient operation.[7]

4. Memories

Mention has been made of the use of a memory type of storage that could be provided by mercury delay lines, magneto-strictive lines,[8]

[7] British Patent Application 34415/53.
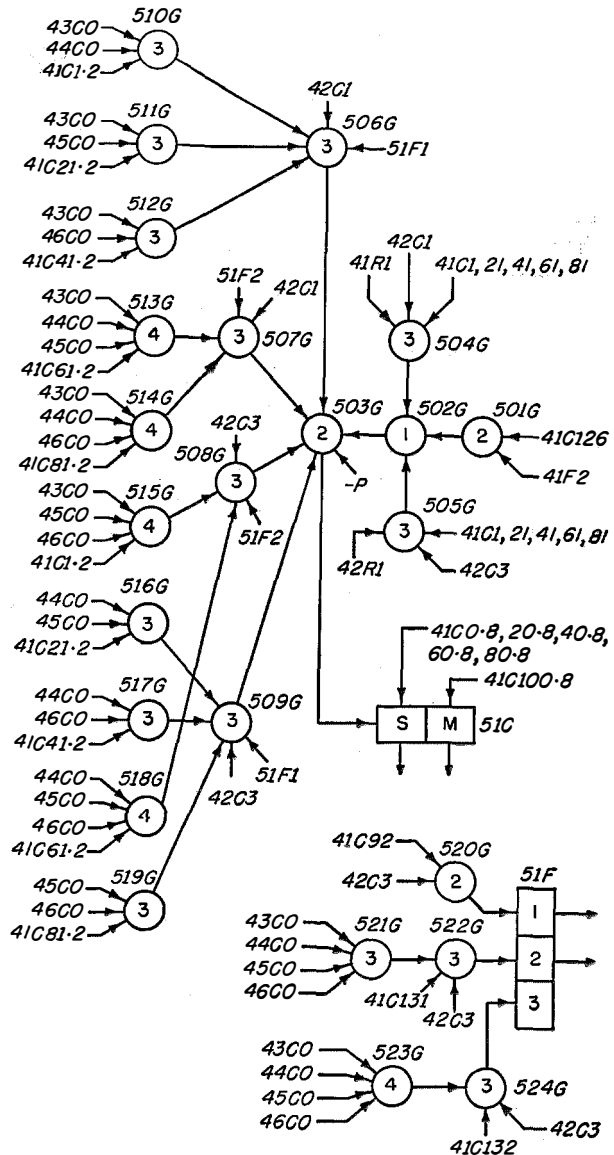[8] British Patent Application 3433/54.

Figure 18—Error-correcting-system character emission, incoming terminal.

or cathode-ray tubes, each of which would produce a repetition rate of approximately 1 millisecond. An alternative approach is possible with a magnetic drum having a rotational time of, say, 20 to 50 milliseconds. In each case the contents of the memory are scanned by sequential examination of the elements, and as a consequence their condition can only be read or modified at specific instances of time indicated by a special series of pulses produced for this purpose. A group of elements in a memory corresponds closely to the register indicated as *1R* in Figure 1. Each single element can be used to represent a trigger such as *1F*, and with some auxiliary equipment a group of elements can be caused to act as a decimal or binary counter.

The first cost and life of a memory element compares very favourably with any individual component that needs to be packaged, tested, and wired into a circuit. It will be appreciated, therefore, that in making any economic comparisons it is essential to study the associated equipment needed to use the memory to represent a variety of different functions; the timing, or clock, pulses already mentioned form one example. Circuits for writing, reading, and amplifying form another group, and in addition there may be control circuits for performing simple arithmetic. In any case, it will be essential to drive the scanning arrangement. Some of these expenses may be common to a number of groups of elements, whereas others may be individual to a single group like the track on a magnetic drum. The extent of the charges for the common equipment per storage element will naturally depend on the facilities provided and on the number of elements forming the memory. For many applications the number of storage elements will be large and as a consequence the speed of examination will be high, requiring that hard valves or transistors be employed. There is no question that there is likely to be an optimum scanning speed because the expense of the memory as a whole must necessarily be influenced by the power consumption, which will tend to increase rapidly with the frequency of operation.

It is a matter of some interest that a register shown on a functional diagram may in general be a series of static devices, like valves, or a memory. If a memory is arranged to perform a number of different functions as that of a counter, trigger, or register, there arises a need to express the state of the memory by a waveform or as a binary number. This is analogous to the technique of describing pulse supplies by their waveform, but it should be appreciated that, whereas static devices are invariable, memories vary according to the circuit condition.

Cubic Distortions in Ring Modulators*

By LEOPOLD CHRISTIANSEN

Mix & Genest, a division of Standard Elektrizitäts-Gesellschaft A.G.; Stuttgart, Germany

THE IDEAL ring modulator shown in Figure 1A with its equivalent circuit at 1B may be thought of as being a polarity-changing switch. If the terminals to which the carrier wave E_c is applied were connected to a battery and the left-hand terminal were positive, the two rectifiers shown on the horizontal lines would be highly conductive and the rectifiers on the diagonal lines would be relatively nonconductive. A signal wave E_s applied at the input would pass through the input transformer, the horizontal rectifiers, and the output transformer to the load. If the battery polarity were reversed, the diagonal rectifiers would be conductive and the horizontal rectifiers would be nonconductive. The signal wave would then pass to the load through the diagonal rectifiers but the polarity of the wave at the load would be the reverse of the previous case.

Assuming the carrier frequency to be several times that of the signal and its waveform and amplitude to be such as to switch the rectifiers rapidly between conducting and nonconducting conditions, a waveform of the type shown in Figure 1C would result.

The frequency spectrum across the load resistor R_l is the product of the signal voltage E_s and the switching function α. Only sidebands

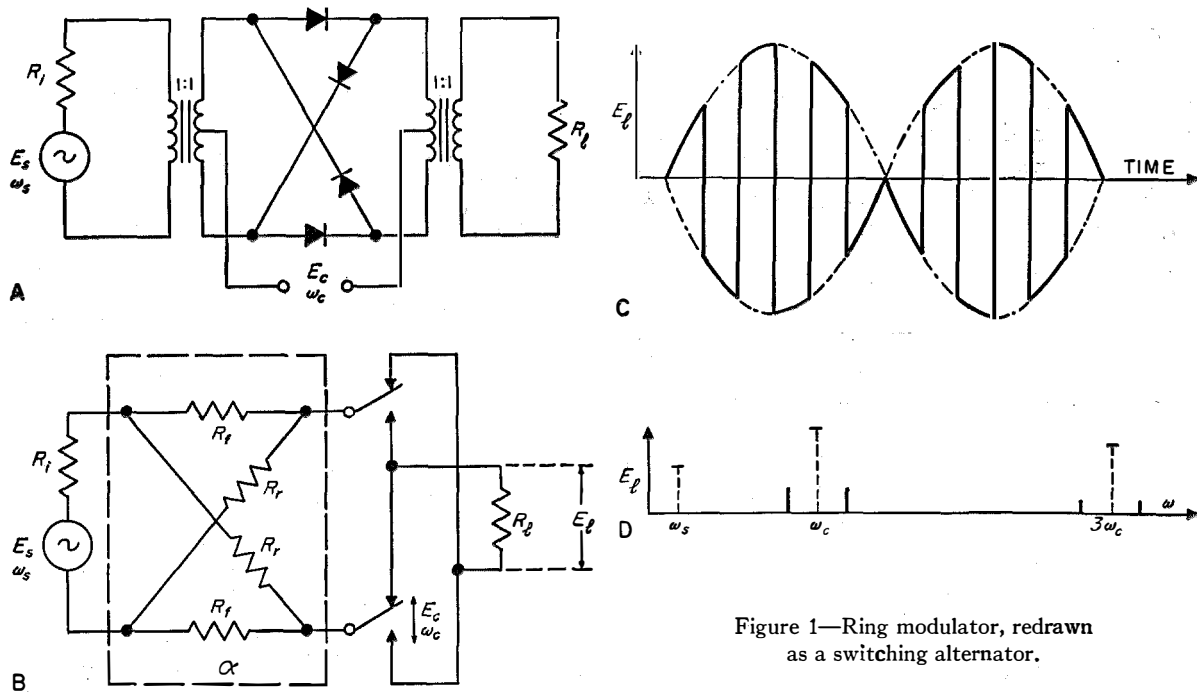Figure 1—Ring modulator, redrawn as a switching alternator.

$$\alpha = \ln \frac{(R_f/R_r)^{\frac{1}{2}} + 1}{1 - (R_f/R_r)^{\frac{1}{2}}} = \text{attenuation of switching alternator,}$$

$$E_l = \frac{E_s e^{-\alpha}}{2} \cos \omega_s t \times \boxed{+1} \boxed{-1} = \frac{E_s e^{-\alpha}}{\pi} \cos (\omega_c \pm \omega_s) t - \frac{E_s e^{-\alpha}}{3\pi} \cos (3\omega_c \pm \omega_s) t \pm \cdots$$

of the first order of the carrier wave and its odd harmonics will appear as indicated by $3\omega_c$. The deviation of the actual from the ideal case is determined by three factors.

A. Nonideal switching action of the rectifier.

B. Incomplete symmetry of the network.

C. Interaction of signal voltage and rectifier circuit.

In this paper, only the action of the signal voltage on the performance of a modulator in its ideal conception will be analyzed. This action of the signal (even for complete symmetry of the circuit) produces cubic distortion in the modulator. This happens even if the carrier wave has the ideal shape. The most disadvantageous distortion comes from sidebands of the third order of the signal frequency that is, sidebands located at three times the signal frequency from the carrier frequency. These sidebands are particularly unwanted in multichannel telephony because they generate both intelligible and unintelligible crosstalk.

The following considerations are actually limited to ring modulators consisting of rectifier elements with small capacitances (for instance, germanium modulators). It is more complicated to consider rectifiers in which the capacitance varies with the impressed voltages as is the case with copper-oxide and selenium rectifiers.

1. Generation of Cubic Distortion

Since the individual nonlinear elements of the network are subjected to different operating conditions in a ring modulator, it seems appropriate to differentiate between forward and reverse distortions. Forward distortion occurs when a rectifier element is passing current, while reverse distortion originates in elements that block the current.

1.1 FORWARD DISTORTION

Figure 2 shows the dependence of the forward (current-passing) resistance R_f of a rectifier element in the signal-voltage circuit on the voltage across the element. The curve shown is the first derivative of the reverse function of the direct-current characteristics $i = f(e)$ of the rectifier element.
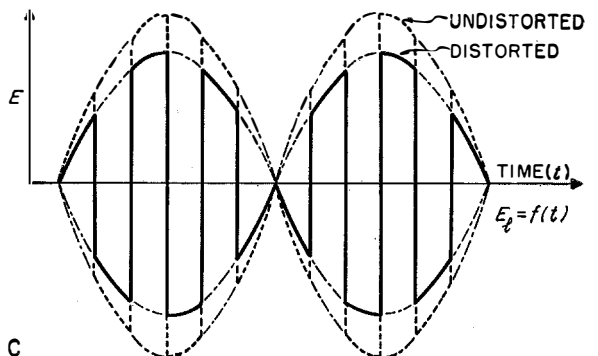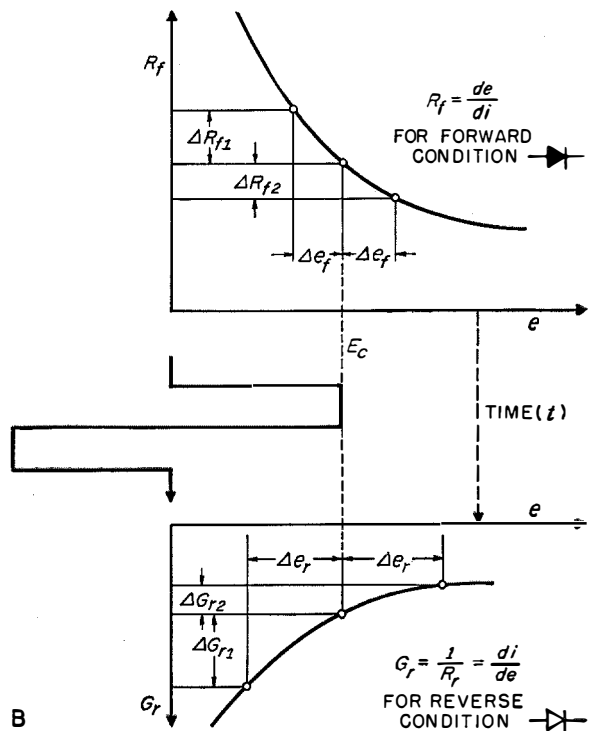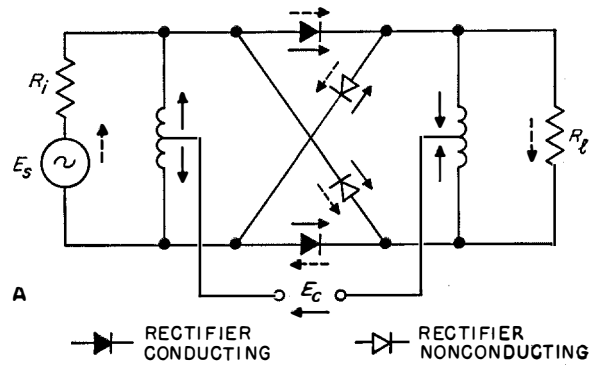

Figure 2—Generation of cubic distortion in conducting and blocking rectifier elements.

The following observations refer to the duration of one switching position, that is, one half-wave of the carrier voltage, which is assumed to be rectangular to simplify the conditions of operation.

The operating point on the line $R_f = g(e)$ is determined by the carrier voltage applied to the element. At insignificantly small signal voltages, the resistance of the element for the signal circuit equals R_f. When the signal voltage rises, it adds to the carrier voltage in one element and reduces the carrier voltage by the signal-voltage value in the other one. The voltage at the element is thus increased and decreased cyclically by Δe_f, in which Δe_f is approximately equal to the product of the signal current and the differentiated resistance of the rectifier element.

Corresponding to the nonlinear relation between R_f and e, the sum of the two rectifier-element resistances forming part of the signal circuit will, hence, change with the instantaneous value of the signal voltage across the element. The shape of the output voltage indicates that the distortion is cubic because the odd harmonics of the envelope, with the polarity changed, point to odd sidebands.

From the graph of Figure 2B, it may be deduced directly that the forward cubic-distortion factor D_{3f} is proportional to the difference in the change of resistance $\Delta R_f = \Delta R_{f1} - \Delta R_{f2}$ of the rectifier element divided by the sum of the resistances ΣR in the signal circuit.

$$D_{3f} \sim \Delta R_f / \Sigma R. \tag{1}$$

Applying Taylor's theorem for the slope of the characteristic $R_f = g(e)$ in the vicinity of the operating point E_c as determined by the carrier voltage,

$$R_f - \Delta R_{f2} = g(E_c + \Delta e_f)$$
$$= R_f + \frac{(dR_f)}{(de)} \frac{\Delta e_f}{1!} + \frac{(d^2R_f)}{(de^2)} \frac{\Delta e_f^2}{2!} + \cdots, \tag{2}$$

$$R_f + \Delta R_{f1} = g(E_c - \Delta e_f)$$
$$= R_f - \frac{(dR_f)}{(de)} \frac{\Delta e_f}{1!} + \frac{(d^2R_f)}{(de^2)} \frac{\Delta e_f^2}{2!} - \cdots, \tag{3}$$

and, by addition of (2) and (3),

$$\Delta R_f = \Delta R_{f1} - \Delta R_{f2}$$
$$= \frac{(d^2R_f)}{(de^2)} \Delta e_f^2. \tag{4}$$

The effects of the higher derivatives of the characteristic are neglected. The forward cubic distortion contributed by the conducting rectifier elements is approximately proportional to the square of the signal-voltage component Δe_f on the conducting rectifier element and directly proportional to the curvature of the $R_f = g(e)$ characteristic at the operating point determined by the carrier voltage applied to the conducting rectifier element. By curvature, the second derivative of the resistance characteristic is meant.

1.2 Reverse Distortion

Analogous considerations apply to the reverse distortion, except that the conductance takes the place of the resistance. Starting with the characteristic of the differential conductance $G_r = (1/R_r) = f(e)$, it will be found that the distortion factor is proportional to the change in conductance in relation to the total conductance in the signal circuit. The results are analogous to (4).

$$\Delta G_r = \frac{(d^2G_r)}{(de^2)} \Delta e_r^2. \tag{5}$$

The cubic-distortion factor contributed by the blocking rectifier elements also varies as the square of the signal-voltage component on the blocking rectifier element Δe_r and the curvature of the characteristic $G_r = f(e)$ at the operating point, determined by the carrier voltage applied to the blocking rectifier element.

As will be shown later, the signal-voltage component on the blocking rectifier element is, however, very different from that on the conducting rectifier element.

It may be seen readily that the distortions in both the conducting and the blocking elements have the same direction when the rectifier element in its blocking period acts in accordance with the characteristic of differential conductance indicated in Figure 2B. This is the case with germanium diodes. Barrier-layer rectifiers have different curvatures for the blocking period. In

germanium modulators, therefore, the distortion factors will have to be added.

All endeavor to decrease the distortion in ring modulators must, hence, aim at the reduction of two quantities; the signal voltage applied to the rectifier element and the degree of curvature of the characteristic for resistance and conductance, respectively, which is influenced by the carrier voltage.

2. Signal-Voltage Component

The signal-voltage component that appears across the rectifier element during one period of a switching alternation results from the additional current sent through the rectifier-element resistance by the signal-voltage source. It is, therefore, nearly equal to the product of the signal current and the differential resistance at the operating point set by the carrier. The signal-voltage component may then be computed from the signal-voltage distribution across the line and cross resistances of the modulator.

Assuming a large switching ratio of the rectifier element, that is $R_f < R_l < R_r$, the following equations are obtained.

$$\Delta e_f \approx \frac{R_f}{R_i + R_l} E_s, \qquad (6)$$

$$\Delta e_r \approx \frac{R_l}{R_i + R_l} E_s, \qquad (7)$$

where

R_i = internal resistance
R_l = load resistance
E_s = terminal voltage of the signal circuit.

The quantities Δe_f and Δe_r are proportional to the terminal voltage of the signal circuit, provided the carrier voltage and the circuit of the network are constant. Indeed, all measurements on ring modulators always show the square-law character of the cubic-distortion factor predicted by (4) and (5).

From (6) and (7), it follows that the signal voltage across the blocking rectifier element of a ring modulator is higher than across the conducting element by the factor

$$R_l/R_f = (R_r/R_f)^{1/2},$$

in other words by the square root of the switching ratio. This equation explains the fact, established by measurements, that in the case of germanium

modulators, too, the reverse distortion is always higher than the forward distortion in the matching condition. It is because of this fact that a controlled mismatching of the ring modulator, called undermatching, is effective as a means for linearizing the action.

3. Curvature of Resistance Characteristic and Conductance Characteristic

The curvature of the related characteristics for resistance and conductance depends on the type of rectifier. If the direct-current characteristic $i = f(e)$ can be represented by a parabola, then the curvature of the resistance characteristic $R_f = g(e)$ follows the equation $T \sim 1/e^3$, where T is the degree of curvature. The cubic-distortion factor thus varies inversely with the cube of the carrier voltage. With a direct-current characteristic in the form of an exponential function, the curvature of the resistance characteristic and, consequently, the cubic-distortion factor will decrease as an exponential function together with carrier voltage. In the first case, there is a linear relation between the distortion attenuation and the carrier level and in the second case between the distortion attenuation and the carrier voltage. Here, distortion attenuation stands for the natural logarithm (ln) of the reciprocal distortion factor.

Measurements on germanium modulators have shown that distortion attenuation increases in proportion to nearly three times the carrier level when the carrier voltage is low, and nearly to twice the carrier level when the carrier voltage is higher. It is therefore evident that the differential-resistance characteristic $R_f = g(e)$ must be a hyperbola for low carrier voltages and a negative logarithm of the form $R_f = C - \ln_e$ for higher carrier voltages. From this information on the resistance characteristic, it follows further that the direct-current characteristic of the germanium diode can be plotted as a parabola only when the voltage is small and that its curvature is less pronounced when the voltage is increased. This is confirmed by measurements on direct-current characteristics.

4. Linearization of a Modulator

The effectiveness of all methods employed to reduce cubic distortion in ring modulators

can easily be predicted by the above considerations. It is only necessary to determine the effect the applied method will have on the signal-voltage component across the rectifier element in the conducting and blocking conditions and on the setting of the operating point, determined by the carrier voltage, for both the conducting and blocking conditions of the rectifier element. Then, the effects on the forward and reverse distortions may be analyzed separately and the over-all results can be qualitatively estimated. It may be stated that a nonlinear network of the ring modulator is linearized when the distortion attenuation has increased, while the output power level and the carrier power level have remained constant.

Data on distortion attenuation that are supported by voltage-level values only are not sufficient to define a degree of distortion suppression. Linearizing action frequently results in the distortion remaining nearly unchanged at constant carrier voltage, while the carrier input resistance is increased. An improvement can only be obtained when the carrier voltage is increased so as to yield the original carrier power. An unequivocal criterion for the nonlinear action of the modulator is the graph of distortion attenuation plotted against the carrier power level for a predetermined power level at the modulator output terminals.

5. Measurement Results

Some of the best-known methods for linearizing action were tested experimentally and will be discussed against the background of the above nonlinear relations. All measurements were made on germanium rectifiers. It should be noted that the condition of mathematically precise square-wave carrier voltage could not be fulfilled and that the terminal resistance, too, was not a real one for all frequencies but consisted of the input resistance of a filter impedance. This departure from theoretical conditions made it impossible to obtain exact verification of the factors causing distortion. Nevertheless, the quality of various relations can be clearly observed, as shown by the results. For the purpose of the discussion, however, a graph of the distortion attenuation is plotted against both the carrier voltage and the carrier power; the first provides for the application of the above-

described considerations under conditions of constant carrier voltage, while the second points to an effective method of linearization. Reference level of zero nepers is 1 milliwatt in 600 ohms (0.7749 volt).

Figure 3 shows the effect of inserting a resistor in series with each rectifier element. The distortion in the blocking condition is unchanged for a constant carrier voltage applied to the modulator. The distortion in the forward direction is increased despite the fact that the series resistance R_s reduces the signal voltage across the rectifier element, because it also reduces the carrier voltage and thus sets the operating point on a more-curved portion of the characteristic. The two effects do not entirely cancel each other. This is especially true for large values of series resistance, where the distortion due to the reduction of the carrier voltage across the element predominates and the curvature
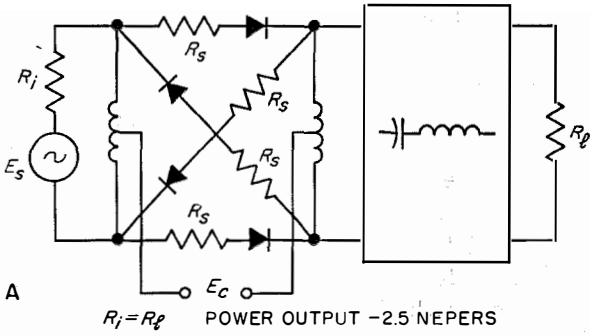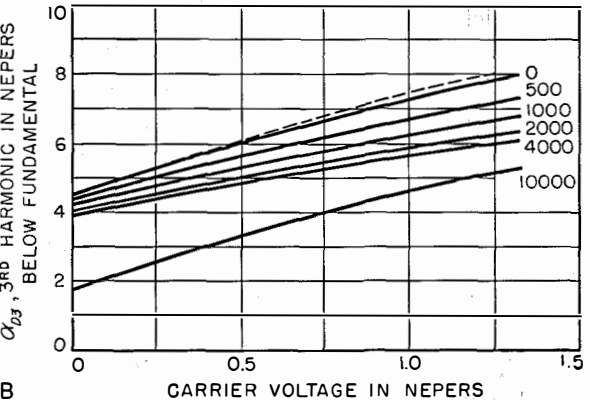

Figure 3—Measured distortion attenuation in a germanium modulator as a function of the carrier voltage level for the indicated values of R_s in ohms. The dashed curve is for 10 000 ohms in parallel with the rectifiers.

increases, as discussed in the previous section. This increased curvature, the carrier voltage remaining low, is clearly seen from the slope of distortion attenuation plotted against the carrier voltage level, when R_s equals 0. If a low carrier voltage is applied to the modulator, the series
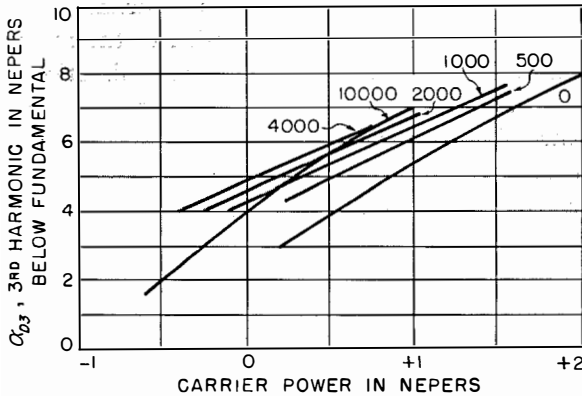

Figure 4—Measured distortion attenuation of the circuit of Figure 3 as a function of carrier power level for the indicated values of R_s in ohms.

resistance has little effect since the voltage drop from the carrier current is correspondingly small. The distortion, however, has decreased as may be seen when the curve of attenuation is plotted against the carrier power as in Figure 4. This is accounted for by the increase in carrier input resistance due to the added series resistor.

The network of Figure 3 is not always suitable because the over-all attenuation of the modulator increases rapidly. A resistance R_p placed in parallel with the rectifier elements does not change the distortion relations so long as this resistance is high with respect to the load resistance, because no change then occurs in the factors that determine the distortion. Similarly, there is no change in the carrier power requirements.

An arrangement commonly used for linearization is shown in Figure 5. The series resistors R_s are inserted at the signal-input side; they are outside the rectifier network. This circuit differs from the previous one in that the voltage across the blocking rectifier element is reduced by the drop due to the current flowing through the resistance of the conducting rectifier. This is also true for the signal voltage at the blocking element. However, the two changes again do not

completely cancel each other. If the carrier voltage is kept constant, the distortion attenuation decreases. The result of this linearizing action would again be most evident from a graph of the attenuation plotted against the carrier power and would not differ markedly from Figure 4. Similarly, this circuit is not too practical because of the substantial increase in attenuation of the entire modulator output.

Figure 6 is for a split-ring arrangement. In this modulator, the four rectifier elements do not constitute a closed ring but two push–pull systems supplied from separate windings of the input transformer. Both half-modulators get the carrier voltage through separate compensating resistors R_s, the values of which were varied for the measurements.

If the carrier voltage is maintained constant, the distortion due to the reverse currents through the blocking rectifier elements remains unchanged even though the resistor values are varied. The distortion attenuation caused by the conducting
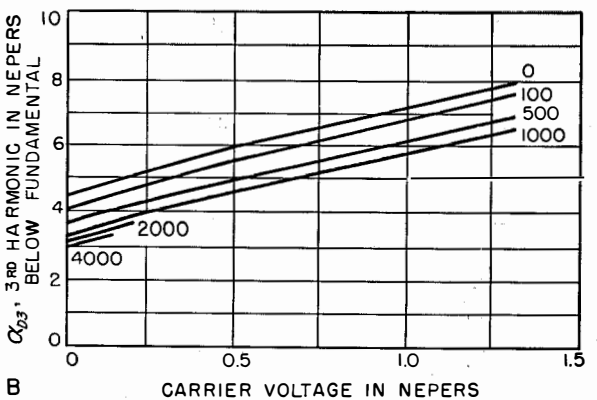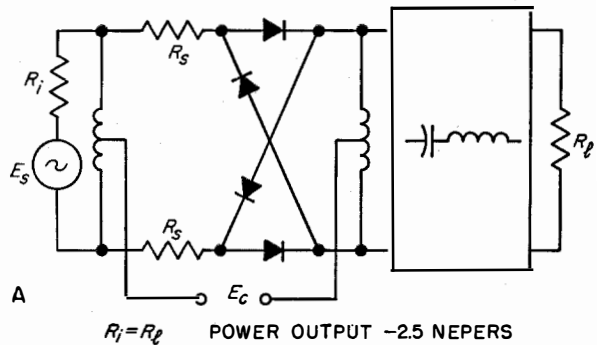

Figure 5—Measured distortion attenuation as a function of carrier voltage level for indicated values of R_s in ohms.

rectifier elements, however, decreases noticeably as the value of R_s is increased. This should be expected because the reduction in the carrier voltage at the conducting rectifier element is not compensated for by a corresponding reduction in signal voltage at the element. Here, too, the attenuation plotted against carrier power (Figure 7) shows a marked effect of the linearizing action.

This example shows the principle on which all discussed systems of linearization are based: the reverse distortions are prevalent in germanium rectifiers for matched loads. The conducting rectifier element contributes only a small proportion of the total distortion. In view of the above discussion, it is possible to increase the forward distortion somewhat by the insertion of input resistances that reduce the carrier voltage across the conducting element. Since only the conducting element determines the carrier power requirements, it is possible to save carrier power, which may be used to increase the total carrier voltage at the modulator. The improvement in

$R_i = R_\ell$ POWER OUTPUT –2.5 NEPERS

A

B

Figure 6—Measured distortion attenuation as a function of carrier voltage level for various values of R_s in ohms.

linearization brought about by increasing the carrier voltage more than compensates for the increase in forward distortion. The linearizing action, then, consists in a more-appropriate distribution of all distortion among conducting and blocking elements. If this process is exag-
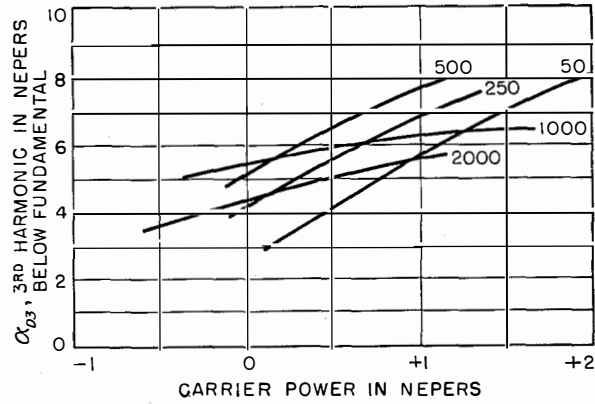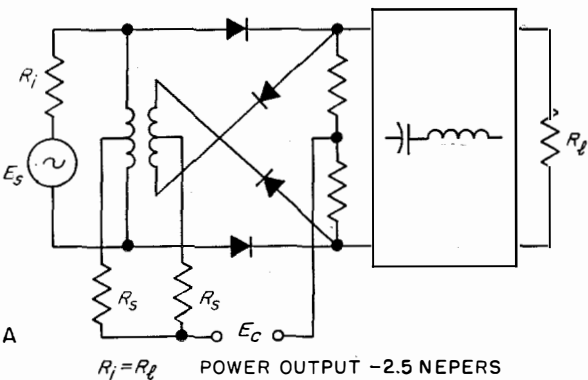

Figure 7—Measured distortion attenuation of the circuit of Figure 6 as a function of carrier power level for values of R_s in ohms as indicated.

gerated, the forward distortion will increase more rapidly than the reverse distortion decreases, and the total distortion will increase. Therefore, the attenuation plotted against carrier power for various values of the parameter R_s shows an optimum value of R_s.

In the split-ring circuit, the advantage stems from the fact that the carrier voltage applied to the conducting element is not reduced at the expense of modulator attenuation because the resistance R_s is not in the signal circuit. The attenuation is raised by only the small amount attributable to the change in switching ratio.

Another method of distortion suppression in ring modulators is based on the value of the load resistance R_l. As is evident from (6) and (7), the forward and reverse distortions are affected oppositely by changes in R_l but not to the same degree. Since the distortions vary as the square of the signal voltage applied to the rectifier element, the sum of these two distortions will also vary with the load resistance. Maximum distortion attenuation will be obtained when both types of distortion are equal. Results of measurements on germanium modulators show that this maximum occurs with undermatching, from which it is to be concluded that at the
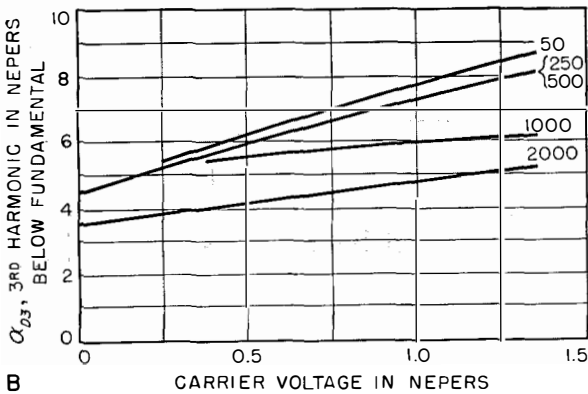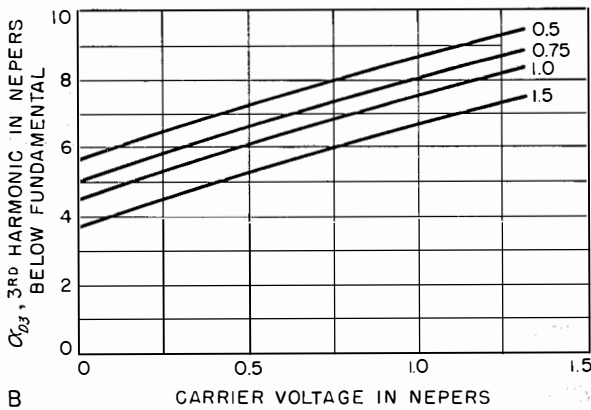
A

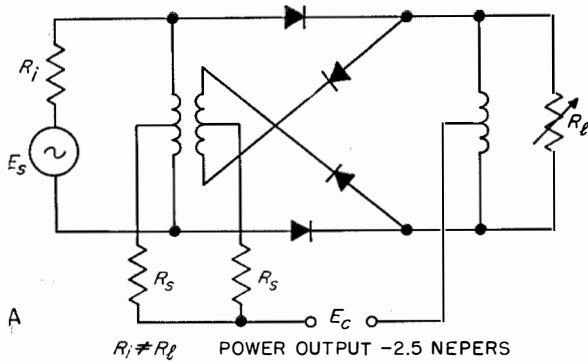$R_i \neq R_\ell$ POWER OUTPUT −2.5 NEPERS

B

Figure 8—Above, measured distortion attenuation as a function of carrier voltage level for the values of R_ℓ/R_i indicated. $R_s = 400$ ohms.

Figure 9—At right and below, measured distortion attenuation as a function of carrier voltage level for the indicated values of R_ℓ'/R_i. $R_s = 400$ ohms.

proper matching condition the reverse distortion predominates. Proper matching is defined as the condition in which the internal resistance R_i of the signal-current source, the load resistance R_ℓ, and the input and output resistances of the modulator ring are all equal. Undermatching is the condition in which the load resistance is of a smaller value than the other resistances.

Figures 8 and 9 show the measurement results for a split-ring modulator. The circuit in Figure 8 has a resistor as R_ℓ, while R_ℓ in Figure 9 is a filter circuit. For the resistive load of Figure 8, the qualitative laws can still be traced; this is not so for Figure 9, where the signal-voltage component across each element can be predicted only when an impedance curve of the filter circuit is available. It is clear, however, that in the more-common practice of a reactive load, a better linearizing action is possible than with a resistive load.

B

A

$R_i = R_\ell \neq R_\ell'$ POWER OUTPUT −2.5 NEPERS

$R_\ell' < R_i$ UNDERMATCHED

$R_\ell' = R_i$ MATCHED

$R_\ell' > R_i$ OVERMATCHED
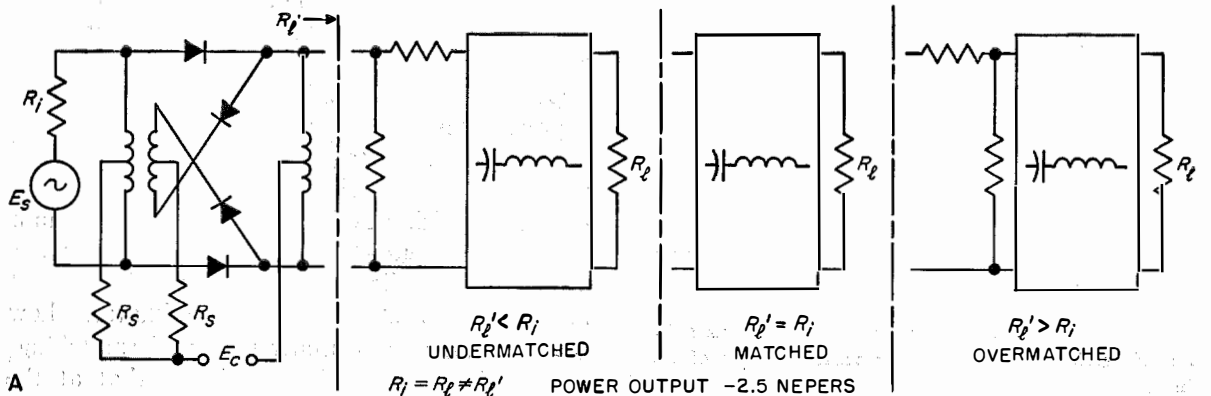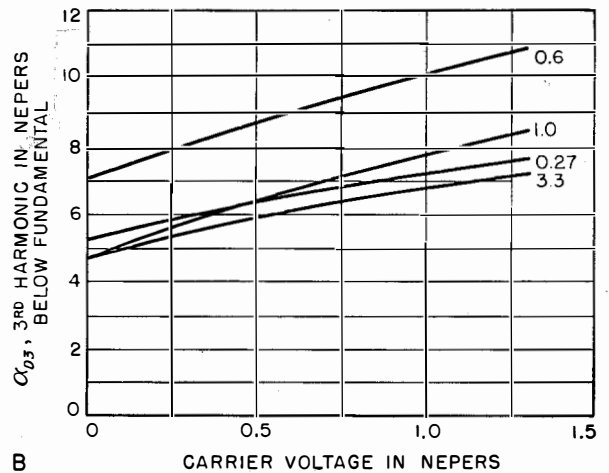
The optimum load resistance will, naturally, depend on all parameters that can influence the forward and reverse distortions; both should be of equal value for best results.

In practice, it will often be necessary to use several of the methods discussed here simultaneously because the circuit is affected by other factors, too. For instance, the degree of efficiency or tolerances for a required symmetry of the transformers may influence the design. The circuit of Figure 3, for instance, might be improved by providing a more-suitable terminal resistance; or, the arrangement of Figure 6 may be expanded by inserting resistances in series with the rectifier elements. The results of measurements show, moreover, that any distortion in a ring modulator that cannot be affected by circuit symmetry, can be linearized by up to 5 nepers through appropriate circuit considerations. This value refers to the distortion attenuation of the matched, not-linearized, modulator at constant signal and carrier power levels. For zero power levels at the modulator output terminals and the carrier input terminals, the value of the attenuation α_{D3} is about 2.5 nepers.

Data for suppression of distortions at other signal levels are derived from the square-law equation of signal level and cubic distortion. The distortion attenuation increases at about twice the rate of signal-level reduction. For germanium rectifier elements operated at approximately zero level, the distortion attenuation increases at about three times the rate of carrier-level reduction. For ordinary carrier-telephony service with the customary carrier power level of $+0.7$ neper and a usually required output level of -3.5 nepers, it is possible to obtain distortion attenuation of more than 11 nepers.

Since the methods of linearizing action discussed here are designed to affect the generation of distortion in the nonlinear rectifier element, they cover not only cubic distortions but also tend to suppress the squared modulation output, especially the second-order sidebands that are already reduced by the symmetry of the ring-modulator circuit.

Microstrip Applied to Band-Pass Microwave Filters*

By MAURICE ARDITI and JACK ELEFANT

*Federal Telecommunication Laboratories, a division of International Telephone
and Telegraph Corporation; Nutley, New Jersey*

MICROSTRIP[1-3] is a wide-band transmission system in which electromagnetic waves are propagated through a dielectric medium bonded by a strip conductor on one side and a conducting ground plane on the other side as is illustrated in Figure 1.

A transverse electromagnetic mode can propagate in microstrip only if the surrounding dielectric is uniform and infinite and the system is lossless. However, practical microstrip lines may consist of a solid dielectric on which a conductive strip is printed; there is an air region above them. Since these lines involve composite dielectrics, they cannot support a pure transverse electromagnetic mode. Nevertheless, both theory and experiments indicate that the field and power flow are concentrated in the dielectric between the conductors and that the assumption of a single infinite dielectric leads to useful results even though it is not rigorous. A first-order theory based on this assumption was described in a previous paper.[2]

The present paper deals with an experimental investigation of the principal characteristics of microstrip. The phase velocity and attenuation of the dominant mode have been measured for various geometries of the lines over a wide frequency range. The characteristics of various types of obstacles in the line, as defined by their scattering-matrix coefficients or equivalent circuits, have been determined and are shown in some examples. From the values of the suscept-
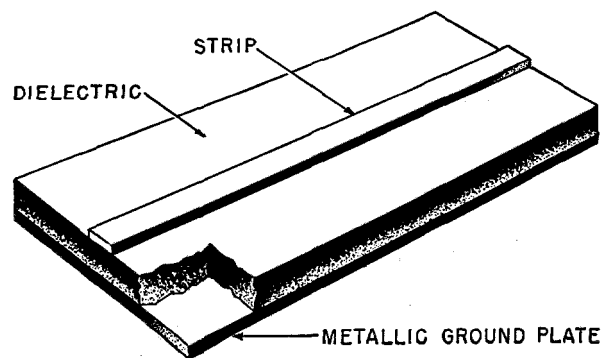

Figure 1—Microstrip line.

ances of obstacles and the characteristics of the lines, a resonant section can be designed. This design theory agrees well with the results of an experimental investigation.

1. Characteristics of Microstrip

1.1 EXPERIMENTAL MEASUREMENTS

Since the geometry of microstrip is rather unconventional, the usual measurement techniques must be modified to obtain the phase velocity and attenuation characteristics of the line or the characteristics of obstacles in the line. For example, a probe can be used only to obtain information on the field distribution in a region far from the main power flow. Also a slotted section probing through the ground plane under the strip conductor can alter the normal mode of propagation of energy.

For these reasons, it has been found convenient to make all impedance measurements by connecting the microstrip line through a transducer to a waveguide or to a coaxial slotted line.

* Abridgment of a paper, "Characteristics of Microwave Printed Lines (Microstrip) with Application to the Design of Band-Pass Microwave Filters," presented at the joint meeting of the Washington Section of the Institute of Radio Engineers and the American Section of the International Scientific Radio Union at Washington, District of Columbia, on April 23, 1952.
   [1] D. D. Grieg and H. F. Engelmann, "Microstrip—A New Transmission Technique for the Kilomegacycle Range," *Electrical Communication*, volume 30 pages 26–35; March, 1953: also, *Proceedings of the IRE*, volume 40, pages 1644–1650; December, 1952.
   [2] F. Assadourian and E. Rimai, "Simplified Theory of Microstrip Transmission Systems," *Electrical Communication*, volume 30, pages 36–45; March, 1953: also, *Proceedings of the IRE*, volume 40, pages 1651–1657; December, 1952.
   [3] J. A. Kostriza, "Microstrip Components," *Electrical Communication*, volume 30, pages 46–54; March, 1953: also, *Proceedings of the IRE*, volume 40, pages 1658–1663; December, 1952.

The reflections from the microstrip line are then measured in the standard manner. After correction for the effect of the junction, the parameters necessary to determine the various characteristics of the microstrip line can be obtained. Although the method has been described originally by Deschamps[4-8] for the determination
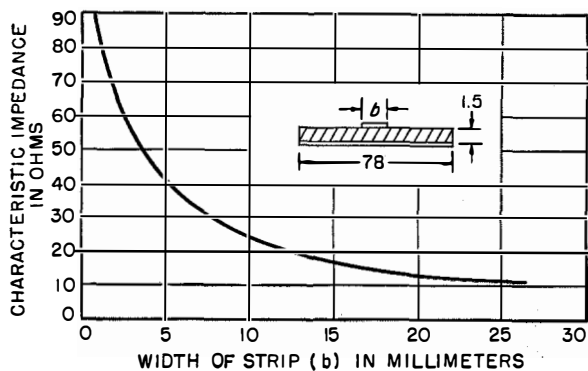

Figure 2—Characteristic impedance for microstrip as a function of the width of the strip. Fiberglas *G-6* dielectric is used. Dimensions are in millimeters.

of the reflection coefficients and attenuation losses of a closed waveguide junction, its application to microstrip is justified as long as the main power flow along the line is confined in one dominant mode, and in general this has been found to be true. A brief resume of Deschamps' method is given in the appendix.

[4] G. A. Deschamps, "Application of Non-Euclidean Geometry to the Analysis of Waveguide Junctions," presented at the joint meeting of American Section of the International Scientific Radio Union and the Institute of Radio Engineers in Washington, District of Columbia, on April 23, 1952. Published in part in footnote references 5–8.

[5] G. A. Deschamps, "Determination of the Reflection Coefficients and Insertion Loss of a Waveguide Junction," *Electrical Communication*, volume 31, pages 57–62; March, 1954: also, *Journal of Applied Physics*, volume 24, pages 1046–1050; August, 1953.

[6] G. A. Deschamps, "Geometric Viewpoints in the Representation of Waveguides and Waveguide Junctions," *Proceedings of the Symposium on Modern Network Synthesis*, Polytechnic Institute of Brooklyn, New York; September 30, 1952: pages 277–295.

[7] G. A. Deschamps, "New Chart for the Solution of Transmission-Line and Polarization Problems," *Electrical Communication*, volume 30, pages 247–254; September, 1953: also, *Transactions of the IRE Professional Group on Microwave Theory and Techniques*, volume 1, pages 5–13; March, 1953.

[8] G. A. Deschamps, "Accurate Comparison of High Standing-Wave Ratios and Its Application to the Determination of the Attenuation Constant of a Waveguide," presented at the 3rd Conference on Ultra-High-Frequency Measurements in Washington, District of Columbia, on January 16, 1953: unpublished.

1.2 Propagation Constants

The following results have been obtained experimentally with microstrip.

A. Over a wide range of frequencies, the phase velocity v is constant to within experimental errors that are less than 0.5 percent; that is, microstrip is nondispersive.

B. In general, the wavelength in microstrip is higher than the value λ_0 corresponding to a transverse electromagnetic mode of propagation between infinite parallel plates. For a given thickness of dielectric, the wavelength decreases as the width of the strip conductor increases, approaching asymptotically the value λ_0 obtained for very wide strips.

C. The dominant mode propagating in microstrip is not a pure transverse electromagnetic mode. Consequently, the definition of the characteristic impedance of the line does not have the same meaning as it would have in a coaxial system. However, to a first approximation, a characteristic impedance could be defined as

$$Z_0 = 1/Cv, \tag{1}$$

where C is the measured electrostatic capacitance per unit length of microstrip and v the phase velocity along the microstrip. The characteristic impedance as a function of the width of the strip is shown in Figure 2. For purposes of comparison with the theoretical curves presented[2] earlier, the experimental results of the ratio of Z_0/Z_0' versus b/h have been plotted in Figure 3.
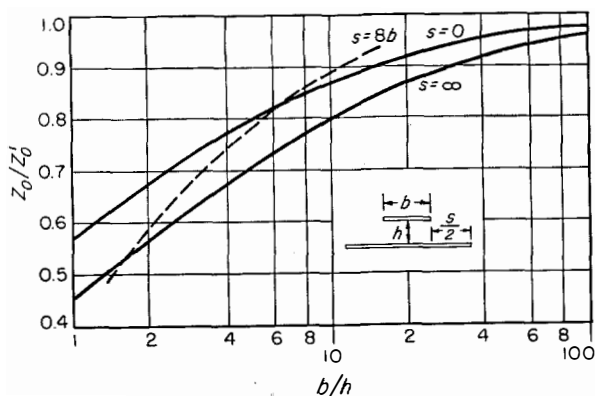

Figure 3—Theoretical limits of the characteristic impedance for a wide strip of zero thickness above a finite ground plane are shown by the solid lines. Experimental values are given by the broken-line curve.

Z_0' is the characteristic impedance corresponding to a constant field in the absence of fringing and leakage flux $Z_0' = (h/b)(\mu/\epsilon)^{1/2}$. It can be seen that the agreement with the first-order theory is quite good.

D. It was found that the attenuation along the microstrip line is constant with the exception of a small region near the transducer. Also, for practical lines, the experimental value of the attenuation constant of the dominant mode agrees closely with the value given[2] by the first-order theory. In the case of 50-ohm microstrip lines printed on Teflon-impregnated Fiberglas $\frac{1}{16}$ inch (1.6 millimeters) thick, the Q of the line is about 560 at 6000 megacycles per second, corresponding to an attenuation of 1.4 decibels per meter.
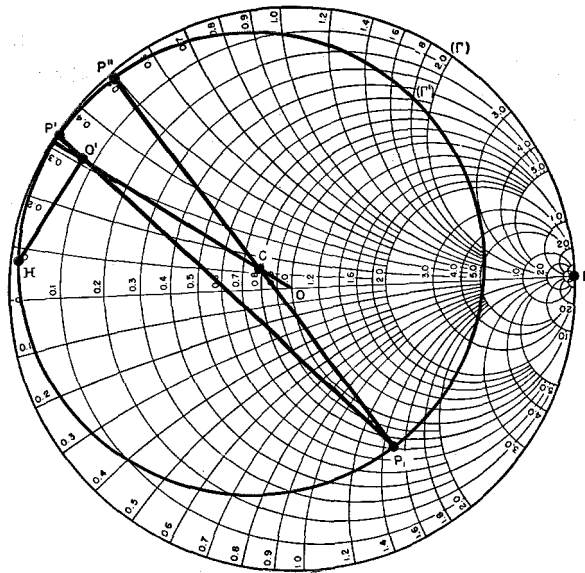

Figure 4—Circle diagrams for a transverse post in microstrip. $S_{11} = -\,0.725 + j0.49$, $\pm S_{12} = 0.232 + j0.437$, and $S_{22} = -\,0.790 + j0.303$.

2. Characteristics of Obstacles

The characteristics of various obstacles in microstrip have been studied,[9] but only two examples will be described here.

[9] M. Arditi, "Experimental Determination of the Properties of Microstrip Components," *Electrical Communication*, volume 30, pages 283–293; December, 1953: also, *Convention Record of the 1953 IRE National Convention*, Part 10, pages 27–37.

2.1 Step Discontinuity

Experiments show[9] that the equivalent circuit of a microstrip step discontinuity is an ideal transformer if the losses in the line are small. In a first approximation, the square of the turns ratio n^2 of the equivalent transformer is equal to Z_2/Z_1, where Z_2 and Z_1 are the values of the characteristic impedance of the lines on either side of the discontinuity.

2.2 Transverse Posts

At a given frequency, the susceptance resulting from a transverse post in the line is a function of the diameter of the post and the location of it across the line.[9] Due to radiation losses, which can be appreciable for large post diameters, it is desirable to specify the susceptances by the scattering-matrix coefficients in which the reference plane is taken as the axis of the post. As shown[4-8] by Deschamps, the power and phase relations expressed by the scattering coefficients can be deduced from the circle diagram shown in Figure 4. In this diagram, circle Γ' of radius R is the image of the unit circle, O' is the image of O, and P' is the image of P through the post. This circle diagram can be obtained by moving a short-circuit behind the post and by measuring for each position of the short-circuit the reflection coefficient as referred to the axis of the post. A good short-circuit is obtained by soldering a large conductive plate between the strip conductor and the ground plane at the end of the line. Other methods for obtaining the circle diagram without destroying the microstrip sample can be found in the references listed in footnotes 4 through 8 and in the appendix.

Introducing the notation $(x)_{db}$ to mean $-20 \log_{10} |x|$, the insertion loss of the post is given[4-8] by

$$(S_{12})_{db} = (O'H)_{db} - (R)_{db}/2. \qquad (2)$$

An exact equivalent circuit, including the radiation loss in the post, can be derived[4-8] from the circle diagram. When the losses are small, an equivalent shunt inductive susceptance can be deduced (see Figure 5). For large values of susceptances, a frequency-resonant method may be easier to use to determine the values of the scattering-matrix coefficients, as will be shown later.

Knowing the scattering-matrix coefficients and assuming that the reflection factor measured at the output side of the obstacle is W_2, the transformed reflection factor W_1, which appears on the input side, can be computed from the equation

$$W_1 = S_{11} + \frac{S_{12}^2 W_2}{1 - S_{22}W_2}. \qquad (3)$$

3. Design of Resonant Sections

By placing two obstacles at the proper distance, a microstrip section that is resonant at a given frequency can be obtained.
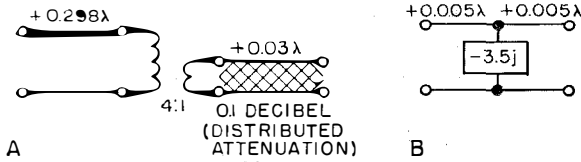

A

B

Figure 5—A is the exact equivalent circuit including losses deduced from Figure 4 and B is the approximate equivalent circuit neglecting the losses for a post transverse to a microstrip line.

The use of wave matrix for the analysis of microwave filters has already been described[10],[11] and could be readily applied here. However, as an illustration of Deschamps' methods, the analysis will be carried out here through simple geometrical constructions, thus avoiding to a large extent the use of complicated equations. It will be assumed that the scattering-matrix coefficients of the obstacles are independent of frequency in the pass band of the filter and also, because of the nondispersive properties of microstrip, the angular length of the line between the two obstacles will be made a direct function of frequency.

The analysis will now proceed by steps to show the transitions with previously well-known constructions.

A. Assuming first that the obstacle is a lossless susceptance of normalized value $-jb$, in the Smith chart the image of the unit circle Γ through the obstacle is the unit circle itself, O' is the image of O representing the reflectance of

[10] G. L. Ragan, "Microwave Transmission Circuits," McGraw-Hill Book Company, New York, New York; 1948: pages 551–554.
[11] J. Hessel, G. Goubau, and L. R. Battersby, "Microwave Filter Theory and Design," *Proceedings of the IRE*, volume 37, pages 990–1000; September, 1949.

a matched load, and P' is the image of P. (The reference plane is taken at the axis of the obstacle, which is assumed to be infinitely thin; see Figure 6.) Assuming, furthermore, that these points do not change with frequency (a valid assumption over a short frequency range), the locus of the input reflectance at a given point in the line at a distance θ from the obstacle (terminated into a matched load) is a circle Γ_2.

B. By placing two such obstacles at a distance L from each other (see Figure 7), the locus of the input reflectance versus frequency is a circle Γ_3, the image of circle Γ_2 through the second obstacle. This circle can be obtained easily through simple transmission-line theory. At some frequency, the circle Γ_3 passes through the center O of the Smith chart (resonance point). The center C of circle Γ_3 is on the line $O'OB$ and is defined by the following relations shown in Figure 7.

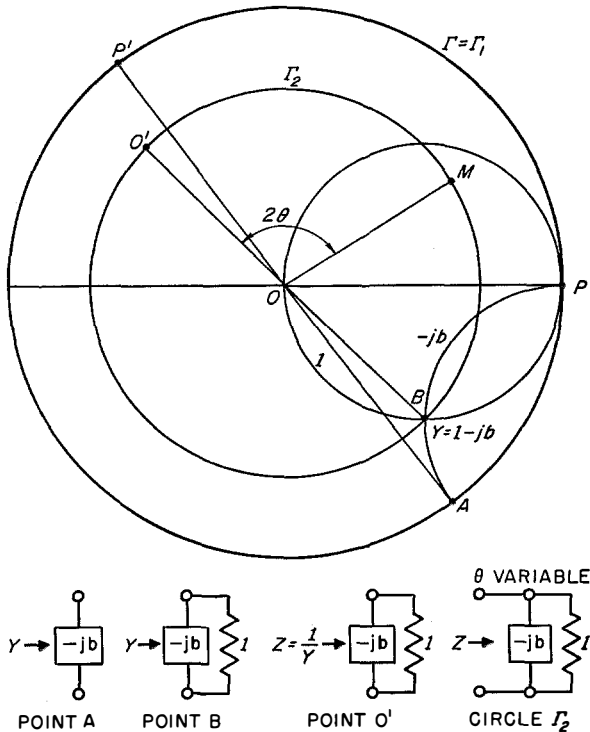$$OC = OH/2 \qquad (4)$$

with

$$HF/HG = (O'F/O'G)^2. \qquad (5)$$

Figure 6—Smith chart representation of the input reflectance of a shunt susceptance across a matched load.

At a given frequency, the reflection coefficient is given by the vector OD and the transmission coefficient by the vector ED orthogonal to OD.

For large values of the susceptance b, the circle Γ_3 has a radius almost equal to half the radius of the unit circle (see Figure 8). On this circle, the points marked 1, 2, 3, . . . correspond to the input reflectance at various frequencies. Also in the case of large values of b, the points E, H, and O' almost merge with the point-G intersection of the line OO' with the unit circle. Moreover, it can be shown[12,13] that the projections from this point of 1, 2, 3, . . . on an axis perpendicular to the line OO' give a linear scale of frequencies 1', 2', 3', . . . Thus, the transmission characteristics will be known at any frequency if measurements of the input reflectance are made at only two values of frequency. Also in this case, certain well-known[10] equations

[12] H. M. Barlow and A. L. Cullen, "Microwave Measurements," Constable and Company, Limited, London; 1950.
[13] W. Altar, "Q Circles, a Means of Analysis of Resonant Microwave Systems," *Proceedings of the IRE*, volume 35, pages 355–361 and pages 478–484; April and May, 1947.

are obtained. At resonance,

$$b \tan \theta = -2, \tag{6}$$

3-decibel bandwidth,

$$\Delta f = \frac{4}{\pi} \frac{f_0}{b^2}, \tag{7}$$

and the double-loaded Q_L of the resonant section,

$$Q_L = \pi b^2/4. \tag{8}$$

The input voltage standing-wave ratio and the transmitted and reflected powers can be deduced from this diagram and have been plotted in Figure 9 for the particular case of $|b| = 3$.

It can be seen that when the susceptances b are lossless, the curves are symmetrical. This is not always the case if losses are present.

C. When the resonant section is made with two obstacles that are lossy and in the general case are nonreversible, the frequency response and insertion loss can be obtained through similar geometrical constructions, which have been derived[4–8] by Deschamps and provide some simplification over the analytical computations.
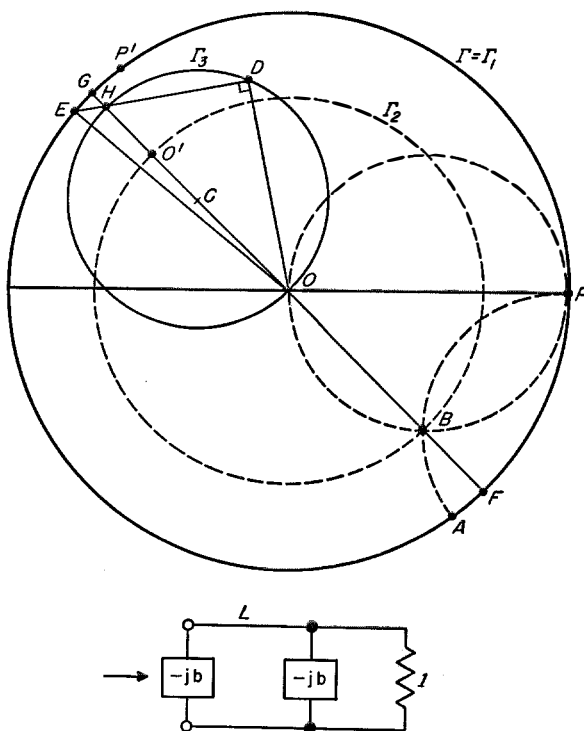

Figure 7—Frequency response of a resonant section made with two lossless susceptances.
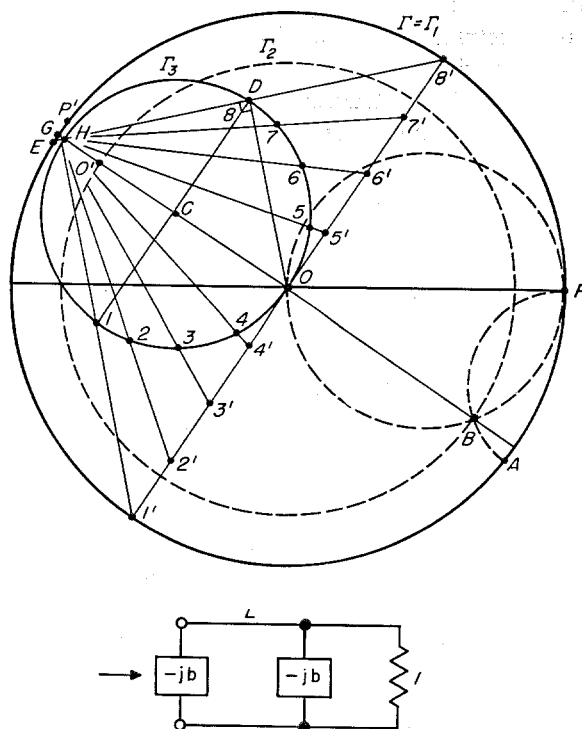

Figure 8—Frequency response and Q of the resonant section for large values of lossless susceptances ($|b| = 3$).
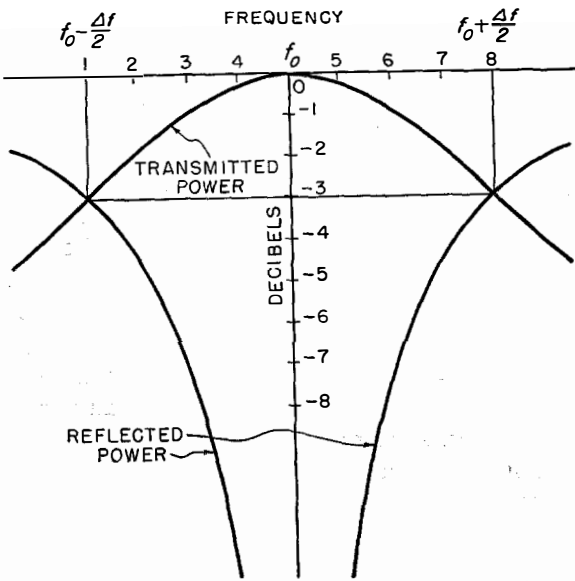
Figure 9—Reflected and transmitted power passing through a resonant section for the case of a lossless susceptance $|b| = 3$.

In Figure 10, the obstacle A is defined by its scattering-matrix coefficients S_{11}, S_{12}, and S_{22} or by the circle Γ_1, the image of Γ through the obstacle; the point O', the iconocenter or image

of $\bullet$; and the point P', the image of P. The locus of the input reflection coefficient when the frequency is varied is a circle Γ_3, the image of circle Γ_2 through the obstacle. Points of the circle Γ_3 can be obtained by using the following relations[5] deduced from (3). The reflection coefficient is

$$\mathbf{OM} = W = S_{11} + \frac{S_{12}{}^2 S_{11} \exp\left[-2j\theta\right]}{1 - S_{11}S_{22} \exp\left[-2j\theta\right]}, \quad (9)$$

and the transmission coefficient,

$$t = \frac{S_{12}{}^2 \exp\left[-j\theta\right]}{1 - S_{11}S_{22} \exp\left[-2j\theta\right]}, \quad (10)$$

with

$$\theta = 360° \; Lf/constant.$$

The circle Γ_3 can also be constructed very simply with Deschamps' hyperbolic protractor.[7,14]

At any given frequency,

$$\text{dissipated power} = 1 - |W|^2 - |t|^2. \quad (11)$$

The dissipated power can be computed from the

---

[14] G. A. Deschamps, "Hyperbolic Protractor for Microwave Impedance Measurements and Other Purposes," International Telephone and Telegraph Corporation, New York, New York; 1953.
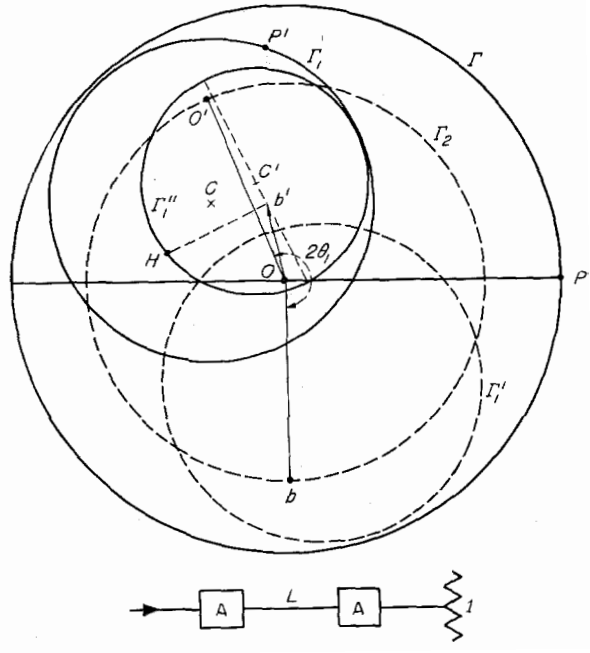

Figure 10—Frequency response of a resonant section with lossy nonreversible obstacles.

Figure 11—Insertion loss of a resonant section with lossy nonreversible obstacles.

above equations, but here again simple geo-metrical constructions[5] can give this value easily. The vector **OM** gives W directly. The trans-mission coefficient t is given by the following
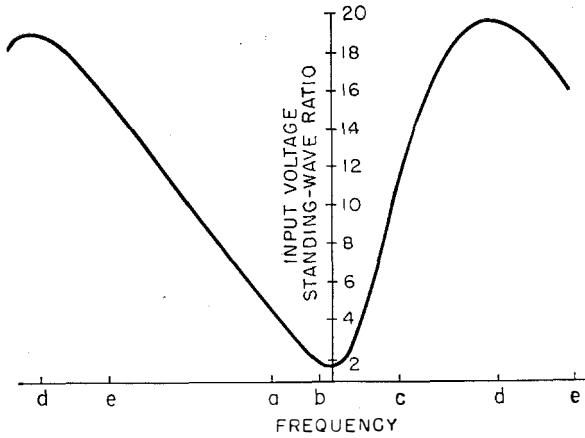

Figure 12—Input voltage standing-wave ratio plotted against frequency for a resonant section for lossy non-reversible obstacles.

construction shown in Figure 11. At the fre-quency f_1 (point b) for which

$$\theta_1 = 360° \ Lf_1/constant,$$

the circle Γ_1 is rotated around point O through an angle $2\theta_1$ to circle Γ_1'. The circle Γ_1'' is the
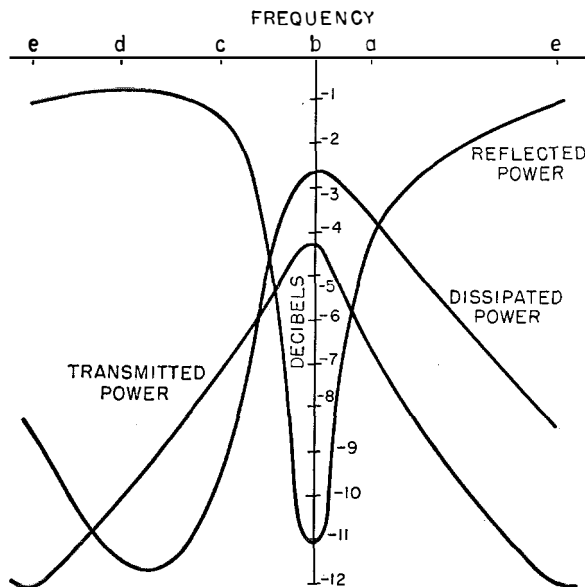

Figure 13—Relative reflected, transmitted, and dis-sipated powers in a resonant section for lossy non-reversible obstacles.

image of circle Γ_1' through the obstacle and the transmission coefficient is given by

$$t_{\mathrm{db}} = (b'H)_{\mathrm{db}} - (R)_{\mathrm{db}}/2, \qquad (12)$$

where $(x)_{\mathrm{db}}$ means $-20 \log_{10} |x|$ and R is the radius of circle Γ_1'' (see reference 5).

The input voltage standing-wave ratio, the transmitted and reflected power, and the dis-sipated power, deduced from the diagram of Figure 10 are shown in Figures 12 and 13. The curve for the transmitted power is symmetrical as should be expected from (10). The asymmetry of the curves of input voltage standing-wave ratio and reflected power versus frequency should be noted. It could be more or less pronounced depending on the particular values of the scattering-matrix coefficients of the obstacles.

D. As a practical example, the case of posts transverse to the microstrip will be considered.

The posts are 0.05 inch (1.3 millimeters) in diameter and located in the middle of a strip conductor 0.24 inch (6.1 millimeters) wide printed on *G-6* Fiberglas stock $\frac{1}{16}$ inch (1.6 millimeters) thick. At a frequency of 4900 megacycles per second and with the reference planes taken at the axis of the post, the scattering-matrix coefficients of the post as deduced from the circle diagram Γ_1 of Figure 14 are

$$
\begin{aligned}
S_{11} &= - \ 0.80 + j0.52 \\
\pm \ S_{12} &= \quad 0.17 + j0.23 \\
S_{22} &= - \ 0.77 + j0.55.
\end{aligned}
$$

The locus of the input reflection coefficient versus frequency of 2 such posts (located in the line and 14 millimeters apart, the line being terminated in a matched load) is the circle Γ_3. The experimental results shown in Figure 15 are in good agreement with the computed values shown in Figure 14. Similarly, the insertion loss at the center frequency has been found ex-perimentally to be about 1.5 decibels and is also in agreement with the computed value.

In Figure 16, the input voltage standing-wave ratio has been plotted against frequency together with a similar curve in the case of lossless susceptances $|b| = 6.5$. The increase in band-width due to the losses introduced by the ob-stacles and by the line is noticeable. The double-loaded Q_L in this case is of the order of 26 and the unloaded Q_0 is equal to 164.

3.1 DISCUSSION

In the case of a lossless obstacle having a large value of susceptance, the coefficient S_{11} can be obtained more accurately by using a frequency-resonance method.

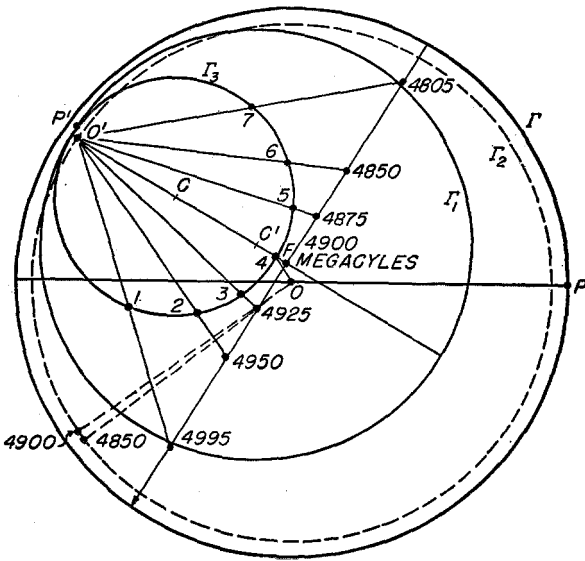If a resonant section is made with two identical

Figure 14—Frequency response and Q of a resonant section for lossy obstacles.
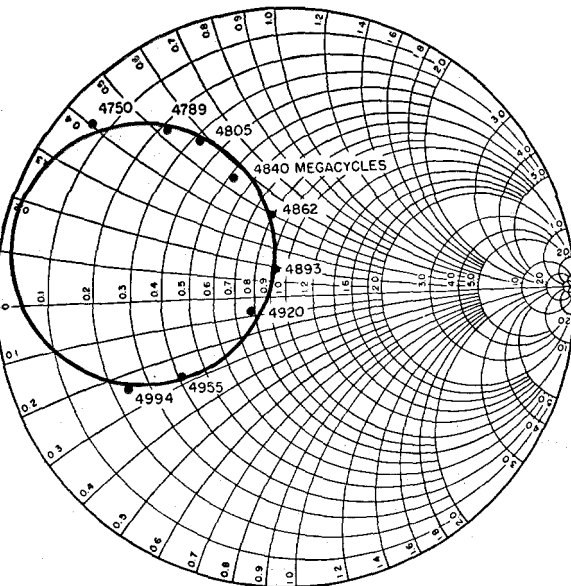

Figure 15—Frequency response and Q of a resonant section obtained experimentally.
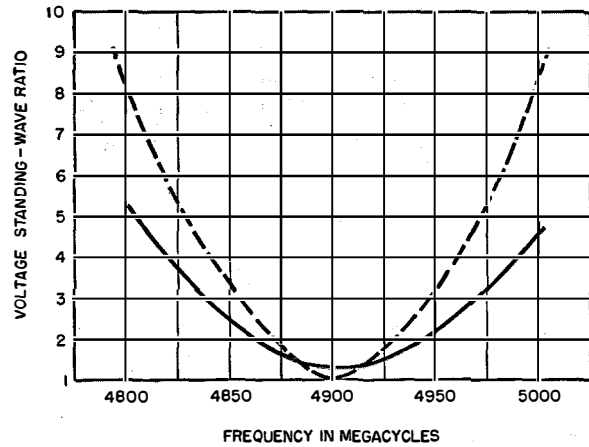

Figure 16—Input voltage standing-wave ratio plotted against frequency for a resonant section.

obstacles separated by a length of line L, from the relation

$$\Delta f = \frac{4}{\pi} \frac{f_0}{b^2} \qquad (7)$$

one can deduce easily

$$|S_{11}| = 1 \bigg/ \left(\pi \frac{\Delta f}{f_0} + 1 \right)^{\frac{1}{2}}, \qquad (13)$$

where Δf is the 3-decibel bandwidth and f_0 is the frequency at resonance.

A somewhat similar relation is obtained in the case of a lossy, nonreversible obstacle. For large values of susceptances ($|b| \geqslant 4$, for instance) the projection of points 1, 2, 3, . . . on an axis perpendicular to the line CO' defines a linear scale of frequencies and it has been shown by Deschamps that to a good approximation the distance $O'F$ is such that (see Figure 17)

$$O'F = 2R[A/(A+1)], \qquad (14)$$

where $2R$ is the diameter of circle Γ_3 and A is given by the relation

$$A = \frac{\lambda_0}{L} \frac{f_0}{\pi \Delta f}, \qquad (15)$$

λ_0 being the wavelength in microstrip at frequency f_0 and Δf, the 3-decibel bandwidth.

Usually the position of the point F is well defined experimentally. Then it is easy to obtain $OO' = S_{11}$ from the triangle $OO'F$, where OF and the angle β are obtained experimentally and $O'F$ is given by the above relation. This is the frequency-resonance method previously mentioned in section 2.2.

4. Conclusions

The Deschamps method is particularly well adapted to microstrip, since it gives directly the most-important parameters of the line or of obstacles in the line, independent of any equivalent circuit representation and arbitrary definition for the characteristic impedance of the line.

The examples discussed here should not be considered as the optimum performances that can be obtained with microstrip. Lines with lower insertion loss and obstacles having larger susceptances and less radiation loss have been developed already and it is hoped to give the results of some practical application in the near future.

5. Acknowledgment

The authors acknowledge the many original contributions of G. A. Deschamps during all phases of this work.
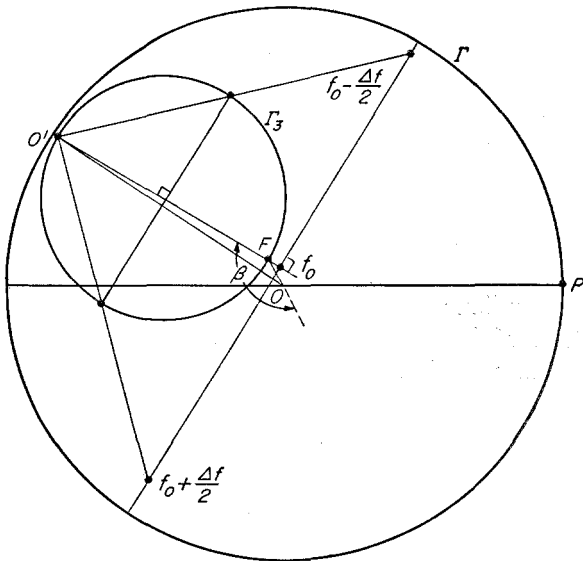

Figure 17—Frequency-resonant method for accurate determination of S_{11}.

6. Appendix

6.1 APPLICATION OF DESCHAMPS' METHOD TO MICROSTRIP

Recently, a method has been described[5] for the determination of the reflection coefficient and insertion loss of a junction in closed waveguides. Essentially, in this method the length of the line

after the junction is varied over half a wavelength by moving a short-circuit and the corresponding reflection coefficient is measured at the input of the junction in the standard manner. The successive positions of the short-circuit are arranged to differ by $\lambda/8$. When plotted on the complex plane, these reflection coefficients fall on a circle, assuming the losses in the line to be
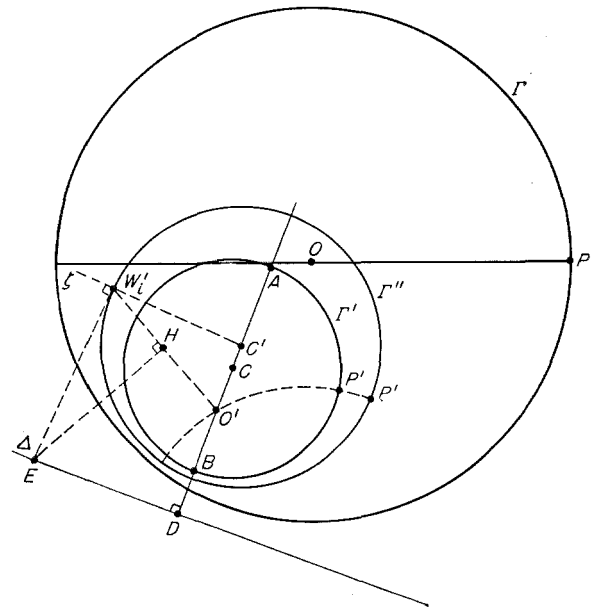
Figure 18—Γ'', image of a unit circle Γ through the junction. Γ'' is deduced from the circle Γ' of a lossy load, point W_i' corresponding to a lossless short-circuit, and the iconocenter O'.

small within half a wavelength. The chords that join opposite points intersect at a point that is related[5] in a simple manner to the reflection and transmission coefficient of the junction.

This method has been adapted to microstrip. The specimen is connected through a junction to an ordinary coaxial or waveguide standing-wave machine. A good short-circuit is provided at the end of the line by soldering a large conductor plate between the strip conductor and ground plane.

This method, however, destroys the microstrip sample and there is no possibility of checking the measurements later. The following suggestion was made by Deschamps and the method thus modified has proved to be very practicable for the measurement of characteristics in microstrip.

It is possible to obtain the circle diagram Γ'' corresponding to the displacement of a good short-circuit without having to cut the end of the line continuously. To this effect and with reference to Figure 18, the reflection coefficient W_i', given by a good short-circuit for one position in the line, is compared with the circle diagram Γ', obtained by moving a given reflective load around this position. Knowing the iconocenter O' of circle Γ' and point W_i', the circle Γ'' can be constructed easily.

A constant reflective load can be obtained with a microstrip stub in shunt across the main line. Behind this obstacle, a matched load is provided so that no microwave energy that may pass through the obstacle is reflected back (see Figure 19). The obstacle is made of a copper foil secured to a piece of polyethylene tape. The obstacle is simply pressed against the strip conductor and maintained in place by the tape. The whole assembly is easy to move and to locate accurately.

6.2 Note on Figure 18

For Figure 18, the measured quantities are W_i', the reflectance measured for one position of a good short-circuit in the line; Γ', the circle diagram of center C obtained by moving a reflective load around this position; and O', the iconocenter or image of the matched load.

The problem is to construct a circle Γ'' having a center C' and corresponding to the continuous displacement of a good short-circuit in the line. There are three steps in the solution.

A. Draw line Δ, a radical axis, perpendicular to line $O'C$ at D.

$$\overline{DO'}^2 = DB \times DA.$$

B. Obtain point E at intersection of Δ and the EH perpendicular bisector of $O'W_i'$.

C. Draw line ζ orthogonal to EW_i' at W_i'. The center C' of circle Γ'' is at the intersection of $O'C$ and ζ.

This construction is based on the properties that the radical axis Δ is the locus of the centers of a system of circles each orthogonal to all member circles of the family of circles defined by Γ' and O'.

Figure 19—Experimental setup.

Coaxial Line with Helical Inner Conductor*

By WILLIAM SICHAK

Federal Telecommunication Laboratories, a division of International Telephone and Telegraph Corporation; Nutley, New Jersey

TO OBTAIN an approximate solution for the fields in a coaxial line with a helical inner conductor, the helix is replaced by a fictitious surface that is conducting only in the helix direction, an approximation used in the early work on traveling-wave tubes. Maxwell's equations are solved for the lowest "mode" (all fields independent of angle) when the medium inside the helix has permittivity and permeability different from that of the medium surrounding the helix. Equations for the velocity along the axis, characteristic impedance, attenuation constant, and Q are given.

The significant parameter is $(2\pi Na)(2\pi a/\lambda)$, where N = number of turns per unit length, a = helix radius, and λ = wavelength. When this parameter is considerably less than 1, the velocity and characteristic impedance depend only on the dimensions. The dielectric inside the helix has only a second-order effect, while the dielectric outside the helix has a first-order effect. The wave appears to propagate along the helix wire with the velocity of light only when the outer conductor is very close to the helix; as the outer-conductor diameter is increased, the apparent velocity along the wire gradually increases and reaches a limiting value when the outer conductor is infinitely large. For the shapes generally used, the apparent velocity along the wire is rarely more than 30-percent greater than the velocity of light, but with an infinitely large outer conductor this velocity can be 2 or 3 times the velocity of light.

When $(2\pi Na)(2\pi a/\lambda)$ is greater than 1, the wave appears to propagate along the helix wire with the velocity of light, and the characteristic impedance depends only on the ratio of wavelength to helix radius. Introducing higher-dielectric-constant material inside or outside of the helix has a first-order effect, and the effect is the same whether the material is inside or outside the helix.

The outer-conductor loss is appreciable, about one-fourth to one-half the helix loss for the usual shapes with low velocities along the axis. The unloaded Q's can be about the same as with conventional coaxial lines. The Q does not depend on the length of the resonator if $(2\pi Na)(2\pi a/\lambda)$ is less than about 0.5, so that for frequencies below about 500 megacycles per second, the volume is considerably less than the volume of a conventional coaxial-line resonator. A few measurements to check the formulas for Q are presented.

• • •

Coaxial lines with helical inner conductors are used in many applications—in traveling-wave tubes, as delay lines, high-Q resonators, and high-characteristic-impedance transmission lines, and in extending microwave impedance-matching techniques to frequencies as low as 300 kilocycles. An analysis of this transmission line is given in this paper. The equations reduce to those previously published when A) the number of turns per unit length goes to zero (the standard coaxial line) and B) the outer conductor is removed (the helix used in traveling-wave tubes). The assumption that the electromagnetic wave travels along the helix wire with a velocity very close to that of light is not true except in extreme cases so that formulas based on this assumption may be in error.

Maxwell's equations are solved by replacing the helix with a fictitious surface that is conducting only in the helix direction. This method has been successfully used in the early work on traveling-wave tubes.[1,2] All fields are assumed to be independent of angle (the lowest "mode"). These assumptions have been questioned on

---

[1] J. R. Pierce, "Traveling-Wave Tubes," D. Van Nostrand Company, Incorporated, New York, New York; 1950: page 229. See also J. R. Pierce, "Theory of Beam-Type Traveling-Wave Tubes," *Proceedings of the IRE*, volume 35, pages 111–123; February, 1947.

[2] L. L. Chu and J. D. Jackson, "Field Theory of Traveling-Wave Tubes," *Proceedings of the IRE*, volume 36, pages 853–863; July, 1948.

---

sound theoretical grounds, but the results given here are good enough for most engineering applications. The details of the derivation are given in the appendix.

After this paper was written, a translation of a paper[3] originally published in Russian was obtained. It presents a general solution of the problem, emphasizing the high-frequency behavior with an electron beam. There is no discussion or derivation of characteristic impedance, velocity, or Q, the main points of this paper. Another paper[4] gives an expression for the velocity and an approximate expression for the characteristic impedance.

1. Velocity

When the dielectrics on both sides of the helix are identical, the velocity along the axis is given by

$$(c/V)^2 = 1 + (M\lambda/2\pi a)^2, \quad (1)$$

[3] L. N. Loshakov, "Propagation of Waves along a Coaxial Spiral Line in the Presence of an Electron Beam," *Journal of Technical Physics*, volume 19, pages 578–595; May, 1949.

[4] C. O. Lund, "Broadband Transition from Coaxial Line to Helix," *RCA Review*, volume 11, pages 133–142; March, 1950.
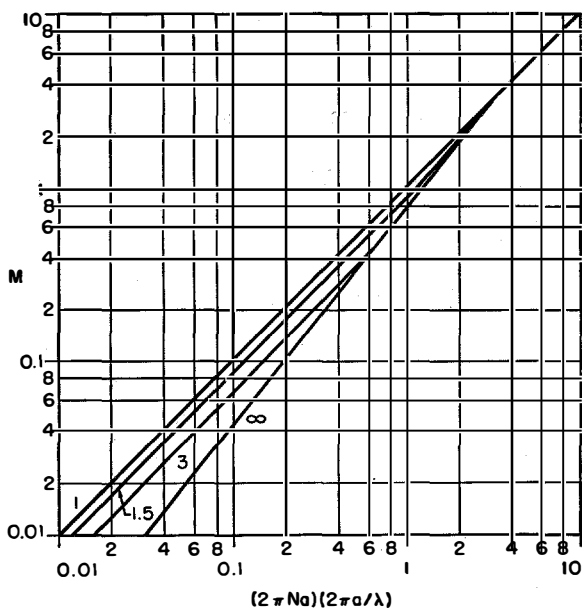
Figure 1—M plotted against $(2\pi Na)$ $(2\pi a/\lambda)$ for the indicated values of b/a.

$$(2\pi Na)\frac{2\pi a}{\lambda} =$$

$$M\frac{J_0(jM)}{J_1(jM)}\left[\frac{\dfrac{H_0^{(1)}(jMb/a)}{J_0(jMb/a)} - \dfrac{H_0^{(1)}(jM)}{J_0(jM)}}{\dfrac{H_1^{(1)}(jMb/a)}{J_1(jMb/a)} - \dfrac{H_1^{(1)}(jM)}{J_1(jM)}}\right]^{1/2} \cdot \quad (2)$$

All symbols are defined in section 5.

These equations can be solved by plotting $(2\pi Na)(2\pi a/\lambda)$ against M, with b/a as a pa-
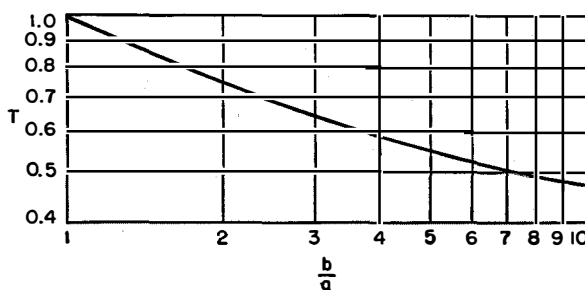

Figure 2—T in (3) is a function of b/a.

rameter as shown in Figure 1 for $\epsilon_1 = \epsilon_2$. Then if N, a, and λ are known, the velocity can be obtained from the first equation.

When the diameters are small $(b/\lambda < V/2\pi c)$, the above equations simplify to

$$\left(\frac{c}{V}\right)^2 \approx 1 + \frac{[1 - (a/b)^2](2\pi Na)^2}{2\ln(b/a)}$$
$$= 1 + T^2(2\pi Na)^2. \quad \Bigg\}(3)$$

T versus b/a is plotted in Figure 2. Usually $(2\pi Na)^2$ is large, so that

$$c/V \approx T(2\pi Na)$$
$$\approx (2\pi Na)(a/b)^{1/2}. \quad \Bigg\}(4)$$

The last approximation becomes inaccurate for large values of b/a. The factor T is, for $(2\pi Na) \gg 1$, the ratio of the velocity of light to the velocity of the wave along the wire. This ratio does not depart markedly from 1 for most practical cases, but in the case of helical antennas[5] this ratio can be larger than 2.

When the diameters are large $(b/\lambda > V/c)$, the equations reduce to

$$(c/V)^2 \approx 1 + (2\pi Na)^2 = 1/\sin^2\psi. \quad (5)$$

[5] A. G. Kandoian and W. Sichak, "Wide-Frequency-Range Tuned Helical Antennas and Circuits," *Electrical Communication*, volume 30, pages 294–299; December, 1953: also, *Convention Record of the 1953 IRE National Convention*, volume 1, pages 42–45.

www.americanradiohistory.com

For this case (usually encountered in traveling-wave tubes), the wave travels along the wire with the velocity of light. When the diameters are small and the dielectric inside the helix is different from the dielectric outside the helix, the velocity is very nearly the same as if the dielectric were uniform throughout. On the other hand, for large diameters,

$$\frac{c_2}{V} \approx (2\pi Na) \left(\frac{\epsilon_1 + \epsilon_2}{2} \right)^{\frac{1}{2}}. \qquad (6)$$

This case is interesting because the velocity is the same whether the dielectric is inside the helix or outside of it and, in addition, does not depend on the ratio of diameters.

2. Characteristic Impedance

The voltage is the integral of E_{r2} from $r = a$ to $r = b$. The current is given by

$$I = 2\pi a H_{\theta 2}(r = a) - j\omega\epsilon_1 \int_0^a E_{x1}(2\pi r)dr,$$

$$Z_0 = \frac{c}{V} 30\pi J_0{}^2(jM) \left| \frac{H_0{}^{(1)}(jMb/a)}{J_0(jMb/a)} - \frac{H_0{}^{(1)}(jM)}{J_0(jM)} \right|. \qquad (7)$$

Figure 3 shows how the characteristic impedance varies with M and b/a for $\epsilon_1 = \epsilon_2$.
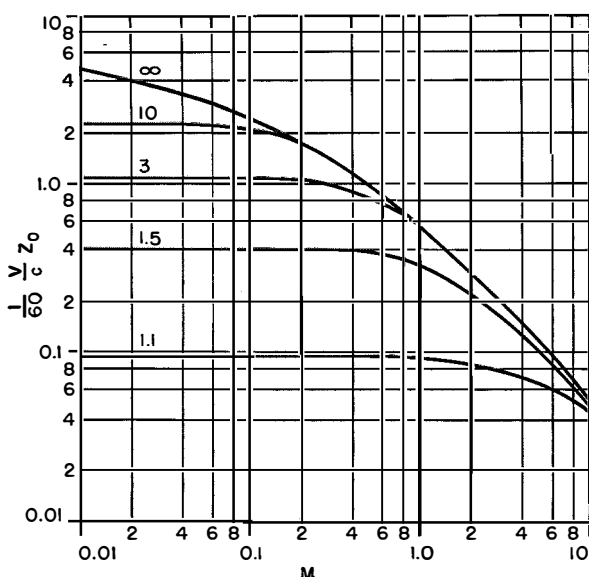

Figure 3—Relation of M to $(1/60)$ $(V/c)Z_0$ for indicated values of b/a.

When the diameters are small, this equation reduces to

$$Z_0 \approx \frac{c_2}{V} \left(\frac{\epsilon_0}{\epsilon_2} \right)^{\frac{1}{2}} 60 \ln \left(\frac{b}{a} \right). \qquad (8)$$

Using (3), this can be written

$$Z_0 \approx 120\pi Na \left[\frac{(1 - a^2/b^2) \ln (b/a)}{2} \right]^{\frac{1}{2}} \left(\frac{\epsilon_0}{\epsilon_2} \right)^{\frac{1}{2}}$$
$$= 120\pi NaT \, (\epsilon_0/\epsilon_2)^{\frac{1}{2}} \ln (b/a). \qquad (9)$$

As Winkler[6] has shown, the maximum value when holding N and a constant is obtained with $b/a = 2.06$.

This approximation holds when the curves in Figure 3 have zero slope. For the usual values of b/a (1.5 or greater), M must be less than about 0.4.

For $b/a = \infty$ and $\epsilon_1 = \epsilon_2$, the characteristic impedance is

$$Z_0 = (c/V)30\pi J_0(jM)H_0{}^{(1)}(jM). \qquad (10)$$

For $M < 0.5$,

$$Z_0 \approx 60 \frac{c}{V} \ln \frac{1.12}{M}. \qquad (11)$$

For $M > 0.5$,

$$Z_0 \approx \frac{c}{V} \frac{30}{M} \approx \frac{30\lambda}{2\pi a}. \qquad (12)$$

The last approximation holds when $c/V \gg 1$.

The standard formula for the inductance of a long solenoid can be obtained by treating the solenoid as a short length of short-circuited line and using (10) and (29).

3. Losses and Q

3.1 Outer-Conductor Losses

The power loss in the outer conductor can be calculated since the tangential magnetic field is known.[7] The power lost per square meter of surface is

$$P_L = \pi b(H_x{}^2 + H_\theta{}^2)Z_{\text{wall}}. \qquad (13)$$

[6] M. R. Winkler, Discussion on "High Impedance Cable," by H. E. Kallman, *Proceedings of the IRE*, volume 35, page 1097; October, 1947.
[7] R. I. Sarbacher and W. A. Edson, "Hyper- and Ultra-High Frequency Engineering," John Wiley and Sons, Incorporated, New York, New York; 1943: page 262.

The attenuation constant is

$$\alpha = \frac{P_L}{2P_{inc}} = \frac{P_L}{2I^2 Z_0}. \qquad (14)$$

For small diameters and high velocity ratios (the usual case of interest),

$$H_z \gg H_\theta,$$

$$I \approx 2\pi a H_{\theta 2}(r = a), \qquad (15)$$

$$\alpha \approx \frac{Z_{wall}}{4\pi b Z_0}\left(\frac{a}{b}\right)^2 (2\pi N a)^2. \qquad (16)$$

A result similar to (16) has been obtained by Bogle.[8] The factor $Z_{wall}/(4\pi b Z_0)$ is the attenuation constant due to the outer conductor in an ordinary coaxial line.
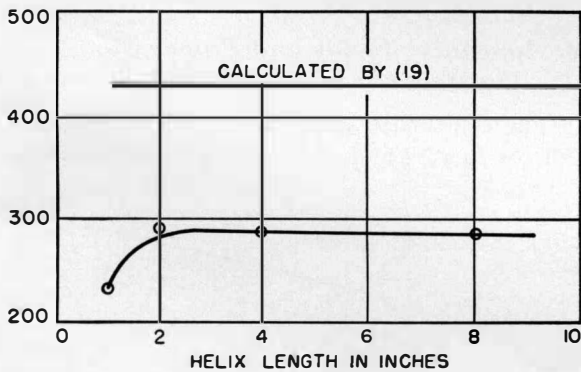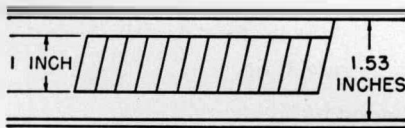

Figure 4—Experimental and calculated values of Q versus helix length. In the experimental helix, $Nd = 1/3$ and there were 116 turns with one end connected to the outer conductor.

3.2 Helix Losses

The procedure used to calculate the outer-conductor losses leads to erroneous results when applied to the helix because the boundary conditions of the helix are not satisfied exactly. An approximate result can be obtained by assuming that the resistance of the helix is the same as an

isolated conductor of the same diameter.

$$\alpha \approx \frac{Z_{wall}(2\pi N a)}{4\pi d Z_0} = \frac{Z_{wall}(2\pi N a)^2}{8\pi^2 a Z_0(Nd)}. \qquad (17)$$

The factor $(2\pi Na)$ is introduced because the unit of length is taken along the axis rather than along the helix wire.

This approximation does not take into account the proximity effect (apparent increase of resistance in a conductor due to the proximity of other conductors).

3.3 The Q

The unloaded Q using copper conductors is given by[9]

$$Q \approx \beta/2\alpha. \qquad (18)$$

For small diameters, this becomes

$$Q \approx \frac{120\pi a(1 - a^2/b^2)f_{mc}^{1/2}}{\frac{1}{2\pi Nd} + \left(\frac{a}{b}\right)^3}. \qquad (19)$$

This equation indicates that the optimum value of (Nd) is one as large as possible due to the approximations used in deriving these equations. However, it is known from experimental data that the optimum value of (Nd) is between 0.3 and 0.4.

The optimum value of b/a depends on (Nd). Using $(Nd) = 0.35$ and $b/a = 2.23$, the Q is

$$Q_{opt} \approx 250 b f_{mc}^{1/2}. \qquad (20)$$

For a coaxial line with $b/a = 3.6$

$$Q_{opt} \approx 210 b f_{mc}^{1/2}. \qquad (21)$$

These optimum Q's have been derived without regard to the resulting volume, subject only to the restriction that $(2\pi Na)(2\pi a/\lambda)$ be less than 0.5–1.0. The quantity $Q/volume$ is a maximum for $(Nd) = 0.35$ when $b/a = 1.57$.

$$Q_{opt} \approx 200 b f_{mc}^{1/2}. \qquad (22)$$

4. Experimental Results

According to (19), the Q does not depend on the length or volume of the resonator. Measurements were made on a series of resonators with the same helix and outer-conductor diameters but with different wire diameters and turns per

[8] A. G. Bogle, "Effective Inductance and Resistance of Screened Coils," *Journal of the Institution of Electrical Engineers*, volume 87, pages 299–316; September, 1940.

[9] "Reference Data for Radio Engineers," Federal Telephone and Radio Company, New York, New York, third edition; 1949: pages 304–319.

inch in the helix, but holding the product (Nd) constant. The coils ranged in length from 1 inch to 8 inches (2.5 to 20 centimeters). The resonant frequencies were near 9 megacycles. Q versus helix length is shown in Figure 4. Over most of the range, the Q is constant and equal to about two-thirds of the calculated values. Some of the discrepancy between measurement and theory is due to the use of commercial copper, to the method of soldering the helix to the outer conductor, and to the use of a solid polystyrene form for winding the helices. The shortest helix has a characteristic impedance less than the others (because $(2\pi Na)(2\pi a/\lambda)$ is about 1), so that its Q should be smaller.

5. Glossary

a = mean radius of helix

b = outer-conductor radius

$$B = \frac{p_1 \tan \psi J_0(p_1 a)}{j\omega\mu_1 J_1(p_1 a)}$$

c = velocity of light

d = radius of helix wire

$$D = \frac{J_0(p_1 a)}{- GJ_0(p_2 a) + N_0(p_2 a)}$$

$E_x,$

$E_r,$

E_θ = electric field in the indicated direction

f = frequency

f_{mc} = frequency in megacycles

$$F = \frac{p_2 \tan \psi J_0(p_1 a)}{j\omega\mu_2\left[- HJ_1(p_2 a) + N_1(p_2 a)\right]}$$

$$G = \frac{N_0(p_2 b)}{J_0(p_2 b)}$$

$$H = \frac{N_1(p_2 b)}{J_1(p_2 b)}$$

$H_x,$

$H_r,$

H_θ = magnetic field in the indicated direction

$H_0^{(1)},$

$H_1^{(1)}$ = Hankel functions of the first kind

I = current

$J_0,$

J_1 = Bessel functions of the first kind

$M = |pa|$

N = number of turns per unit length

$N_0,$

N_1 = Bessel functions of the second kind

$p^2 = \gamma^2 + \omega^2\epsilon\mu$

P_{inc} = incident power

Q = quality factor

V = velocity along the axis

Z_0 = characteristic impedance

$Z_{\text{wall}} = (\pi f\mu/\sigma)^{1/2}$

α = attenuation constant

$\beta = 2\pi/\lambda_a$ = phase constant along the axis

$\beta_0 = 2\pi/\lambda$ = free-space phase constant

$\gamma = \alpha + j\beta$ = propagation constant

ϵ = permittivity

λ = free-space wavelength

μ = permeability

σ = conductivity

$\omega = 2\pi \times$ frequency

6. Appendix—Fields and Propagation Constants

The coordinate system is shown in Figure 5. All conductors and dielectrics are assumed loss-

OUTER CONDUCTOR RADIUS B

HELICAL SHEATH RADIUS A

REGION 2

REGION 1

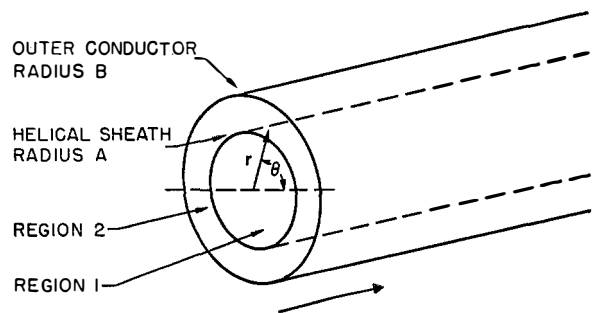Figure 5—Coordinate system. ψ is the angle between a turn of the helix and the cross-sectional plane of the helix.

less and the fields are independent of θ. Inside the helix, the longitudinal fields are taken to be of the form

$$\left.\begin{array}{l} E_{x1} = J_0(p_1 r), \\ H_{x1} = BJ_0(p_1 r). \end{array}\right\} \quad (23)$$

Bessel functions of the second kind are not used because they go to infinity at $r = 0$.

Between the helix and the outer conductor, the longitudinal fields are taken to be of the form

$$E_{x2} = D[- GJ_0(p_2 r) + N_0(p_2 r)],$$
$$H_{x2} = F[- HJ_0(p_2 r) + N_0(p_2 r)].$$
$$\tag{24}$$

The boundary conditions $E_{x2} = 0$ and $\partial H_{x2}/\partial r = 0$ at $r = b$ have been applied in the above equations.

By using Maxwell's equations [10] the remaining fields can be determined.

Inside the helix $(r \leqslant a)$,

$$E_{r1} = \frac{\gamma_1}{p_1} J_1(p_1 r),$$

$$E_{\theta 1} = \frac{(-)Bj\omega\mu_1}{p_1} J_1(p_1 r),$$

$$H_{r1} = \frac{B\gamma_1}{p_1} J_1(p_1 r),$$

$$H_{\theta 1} = \frac{j\omega\epsilon_1}{p_1} J_1(p_1 r).$$
$$\tag{25}$$

Outside the helix $(a \leqslant r \leqslant b)$,

$$E_{r2} = \frac{D\gamma_2}{p_2} [- GJ_1(p_2 r) + N_1(p_2 r)],$$

$$E_{\theta 2} = \frac{- Fj\omega\mu_2}{p_2} [- HJ_1(p_2 r) + N_1(p_2 r)],$$

$$H_{r2} = \frac{F\gamma_2}{p_2} [- HJ_1(p_2 r) + N_1(p_2 r)],$$

$$H_{\theta 2} = \frac{Dj\omega\epsilon_2}{p_2} [- GJ_1(p_2 r) + N_1(p_2 r)].$$
$$\tag{26}$$

The factor $\exp[j(\omega t - \gamma x)]$ multiplying the right-hand sides of all of the above equations has been omitted.

[10] See page 243 of footnote reference 7.

The boundary conditions at the helical sheet $(r = a)$ are

$$E_{x1} = E_{x2},$$
$$E_{\theta 1} = E_{\theta 2},$$
$$\frac{E_{x1}}{E_{\theta 1}} = \frac{E_{x2}}{E_{\theta 2}} = - \cot \psi,$$
$$(H_{x1} - H_{x2}) + (H_{\theta 1} - H_{\theta 2}) \cot \psi = 0.$$
$$\tag{27}$$

For a nontrivial (that is, one in which the coefficients B, D, and F are not zero) solution to exist, the following equation must hold:

$$\omega^2 \frac{\mu^2}{p^2} \cot^2 \psi$$
$$\times \left\{ \frac{\epsilon_2}{p_2} \left[\frac{-GJ_1(p_2 a) + N_1(p_2 a)}{-GJ_0(p_2 a) + N_0(p_2 a)} - \frac{\epsilon_1 J_1(p_1 a)}{p_1 J_0(p_1 a)} \right] \right\}$$
$$= - \left(\frac{\mu_2}{\mu_1} \right) \left(\frac{p_1}{p_2} \right) \frac{J_0(p_1 a)}{J_1(p_1 a)}$$
$$+ \left[\frac{-HJ_0(p_2 a) + N_0(p_2 a)}{-HJ_1(p_2 a) + N_1(p_2 a)} \right]. \tag{28}$$

This equation determines the propagation constant when the dimensions, dielectric constants, et cetera, are specified. When the outer conductor is removed, the equation reduces to that given by Harris.[11] When the dielectric on both sides of the helix is identical and the outer conductor is removed, the equation becomes

$$\frac{\beta_0^2 \cot^2 \psi}{p^2} = - \frac{J_0(pa)H_0^{(1)}(pa)}{J_1(pa)H_1^{(1)}(pa)}. \tag{29}$$

This result is the same as that given by Pierce,[1] and by Chu and Jackson.[2]

[11] L. A. Harris, H. R. Johnson, A. Karp, and L. D. Smullin, "Some Measurements of Phase Velocity along a Helix with Dielectric Supports," Massachusetts Institute of Technology Radiation Laboratory Report 93: January 21, 1949.

United States Patents Issued to
International Telephone and Telegraph System
August–October, 1954

UNITED STATES patents numbering 31 were issued between August 1 and October 31, 1954 to companies in the International System. The inventors, titles, and numbers of these patents are given below; summaries of several that are of more-than-usual interest are included. In cases where corresponding Canadian patents have already issued, their numbers are given in parentheses.

H. H. Adelaar, System for the Generation of Electric Pulses, 2,689,910.

A. J. Baracket and E. Stein, Automatic Synchronization, 2,686,833 (644,716).

J. I. Bellamy, Impulse-Repeating Electromagnetic Relay, 2,689,883.

J. I. Bellamy and P. W. Hemminger, Receiver for Remote Supervisory and Control Systems, 2,688,738.

H. Bosse, Slot Antenna, 2,686,265.

H. Boyer, Block Coupler, 2,686,841.

W. C. Bruckman and M. W. Kretichman, Washing-Machine Support, 2,687,861.

M. P. G. Capelli, Radio Altimeter, 2,686,302 (609,614).

A. M. Casabona, Null-Type Glide-Slope System, 2,685,688 (655,752).

E. Christensen, Automatic Telecommunication System with Absent-Subscriber Service, 2,686,842.

G. Deakin, Traffic-Recording System for Automatic Telephone Exchange, 2,686,836.

M. den Hertog, Group-Selection Control Circuit, 2,686,839 (169,273).

M. den Hertog, Identification Circuit for Automatic or Semiautomatic Telephone Systems, 2,686,840.

M. den Hertog, C. de Zeeus, and H. H. Adelaar, Means for Automatically Detecting a Change of Condition in Any One of a Number of Electrical Circuits from a Common Circuit, 2,688,662 (610,228).

E. L. Earle, General-Purpose Relay, 2,686,850.

G. C. Hartley, F. H. Bray, and M. C. Branch, Register Translator for Telecommunication Switching Systems, 2,686,224 (597,150).

W. Hauer, Circuit Arrangement for Communication Systems, Particularly Private Automatic Telephone Branch Exchanges, 2,690,478.

G. H. Hough and T. M. Jackson, Gaseous Electric-Discharge Tube, 2,686,273 (624,908).

J. B. Lair, Impulse-Storing and Distributing Circuit, 2,691,727.

G. X. Lens, Sorting Machine for Letters or Similar Flat Objects, 2,689,657 (623,914).

M. R. Mauge, Switching System for Grouped Telephone Lines, 2,692,917.

A. J. Montchausse, Crossbar Multiselector Arrangement, 2,691,700 (630,286).

A. J. Montchausse, Multiswitch Apparatus Controlled by Crossbars, 2,686,226.

A. D. Odell, Electrical Switching Circuit, 2,688,695.

D. C. Rogers and W. W. Marsh, Thermionic Cathode, 2,686,272 (626,223).

L. E. Setzer and C. B. Watts, Jr., Automatic Approach Control, 2,689,345.

R. Urtel, Horizontal-Line Registration for Pickup Tubes, 2,691,743.

A. R. Vallarino and S. W. Lewinter, Radio Dispatching System, 2,685,642.

S. van Mierlo, Electronic Switching, 2,688,661.

E. P. G. Wright, D. A. Weir, and J. Rice, Means for Checking Recorded Information, 2,688,656 (608,264).

H. N. Wroe, Telephone Signaling Arrangement, 2,686,228 (627,411).

Radio Dispatching System[1]

A. R. Vallarino and S. W. Lewinter

2,685,642—August 3, 1954

This patent covers a radio system for dispatching and following the movement of vehicles such as taxicabs or police patrol cars in separate zoned areas. Only three frequencies are used and the areas are so positioned that no contiguous areas operate on the same frequency channel. A central dispatching station is used to transmit frequencies in radial sector-shaped zones. This central dispatching area may be then surrounded by other zones that do not have contiguous boundaries operating on the same frequency.

Gaseous Electric-Discharge Tube

G. H. Hough and T. M. Jackson

2,686,273—August 10, 1954

A gaseous discharge tube is described having several spaced cathodes and a common anode, the cathodes being in the form of metallic strips mounted in a common plane and having substantially equal spacing between adjacent strips. The anode is a metallic strip spaced from these cathodes and at right angles thereto. A shielding means is provided between pairs of cathodes to reduce the ionization coupling between the cathodes of each pair.

Sorting Machine for Letters or Similar Flat Objects[2]

G. X. Lens

2,689,657—September 21, 1954

A sorting device for letters is in use in the Belgian Post Office in Antwerp and other places. It consists essentially of an endless conveyor arrangement with carriers that move past receptacles for the letters, which are disposed in the carriers in vertical position. The letters will be properly dropped into the various receptacles in a substantially vertical direction.

[1] A. R. Vallarino and S. W. Lewinter, "Radio Dispatching System for Operation of a Large Taxicab Fleet," *Electrical Communication*, volume 30, pages 55–60; March, 1953: also, *Electrical Engineering*, volume 71, pages 232–235; March, 1952.

[2] S. Scheuer, C. B. Neyt, and L. J. G. Nijs, "Electromechanical Distributor for Sorting Mail," *Electrical Communication*, volume 28, pages 163–170; September, 1951.

Automatic Synchronization

A. J. Baracket and E. Stein

2,686,833—August 17, 1954

An automatic synchronization system for television monitoring use in which a control voltage is produced in response to the presence or absence of synchronizing pulses in the video picture source; there is also provided an independent source of synchronizing pulses together with a gating means to permit these independent pulses to pass if the synchronizing pulses are not present in the applied video signal.

Null-Type Glide-Slope System

A. M. Casabona

2,685,688—August 3, 1954

A null-type glide-slope system having an additional feature that tends to eliminate ambiguities that might be encountered in the glide slope. The original glide-slope array comprises two antennas, one spaced at a height H and the other at a height $H/2$ above ground plane and energized to produce different sidebands characteristic of the glide-slope signals. The ambiguities are removed by providing two other antennas energized 180 degrees out of phase with energy of the carrier frequency plus one sideband only and spaced above and below the lower of the other two antennas at heights of $2H/3$ and $H/3$, respectively.

Automatic Approach Control

L. E. Setzer and C. B. Watts, Jr.

2,689,345—September 14, 1954

An automatic approach-control arrangement for aircraft in which the usual controls for correcting the departure of the craft from the desired beacon course line are supplied and in addition thereto, there is derived a third signal indicative of the direction of departure off-course, but substantially independent of the degree of this departure. This third signal is combined in opposition to the guiding signals to provide the resultant control voltage. By this means the degree of correction is reduced as the proper course is approached so that course swings are reduced.

Contributors to This Issue
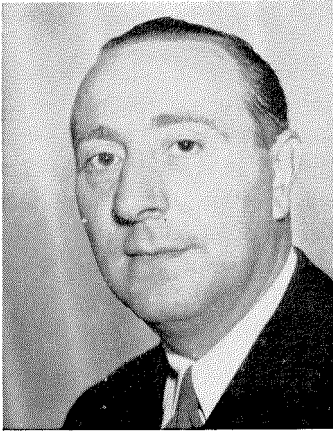
MAURICE ARDITI

MAURICE ARDITI was born on March 1, 1913, in Paris, France. In 1933, he received a degree in engineering physics at the Ecole de Physique et Chimie Industrielle of Paris, in 1934 a degree in electrical engineering at Ecole Supérieure d'Electricité, and in 1935 an M.S. degree in physics and chemistry from Sorbonne University, Paris.

From 1936 to 1939, Mr. Arditi did research work in physical chemistry at Paris University. In 1939, he joined the laboratories of Le Matériel Téléphonique, Paris, working on secondary emission, electron multipliers, and electron optics. He joined Federal Telecommunication Laboratories, New York, in 1944 and resumed work on special switching tubes. From 1947 to 1951, he was active in the field of microwave receivers for radio links and is presently engaged in the development of the microstrip line. Some of his studies on this subject are reported in the present issue.

Mr. Arditi is a Senior Member of the Institute of Radio Engineers.

• • •

STERLING O. BICKEL was born in Union City, Indiana, on January 18, 1921. He served with the Army Engineer Corps and was released in 1947. In 1949, Mr. Bickel received B.S. degrees in radio and in administrative engineering from Tri-State College, Angola, Indiana.

Mr. Bickel was with the Magnavox Company until 1951, at which time he joined Capehart–Farnsworth Company as a tube-reliability engineer in guided missiles. Some of his work on subminiature-tube reliability is reported on in this issue.

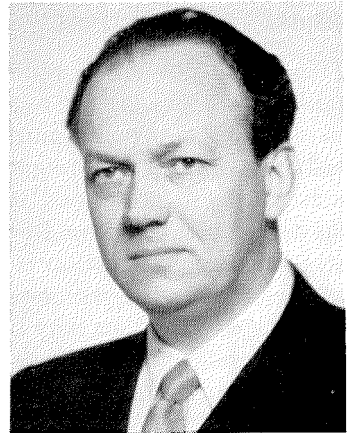Mr. Bickel is an Associate Member of the Institute of Radio Engineers.

• • •

AMUND BRAATEN was born on May 11, 1905 in Oslo, Norway. He studied electrical engineering at the Technical University of Norway, graduating in 1929.

Following graduation, he joined the Standard laboratories in Hendon, England, returning to Norway in 1931, where for a brief time he served as a member of the staff at the Technical University.

Mr. Braaten rejoined the International System in 1932 as engineer of manufacture and cable engineer at Standard Telefon og Kabelfabrik A/S. He was promoted to chief engineer in 1941, to works manager in 1946, and to managing director in 1953. He reports in this issue on the new high-voltage cable-testing facilities recently installed at Oslo.

• • •

LEOPOLD CHRISTIANSEN was born in Kiev, Russia, on December 2, 1913. He studied at the Technical University of Stuttgart, at the Rensselaer Polytechnic Institute of Troy, New York, and at the Technical University of Dresden, where he received his diploma and his doctorate.
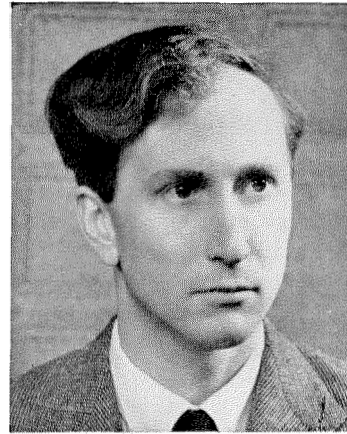

AMUND BRAATEN

STERLING O. BICKEL
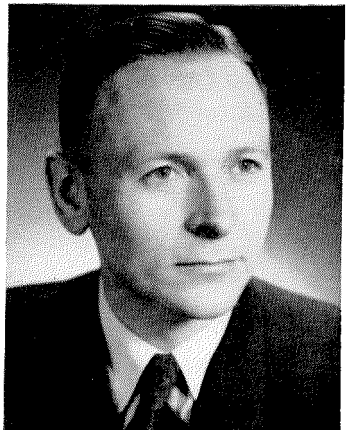
LEOPOLD CHRISTIANSEN
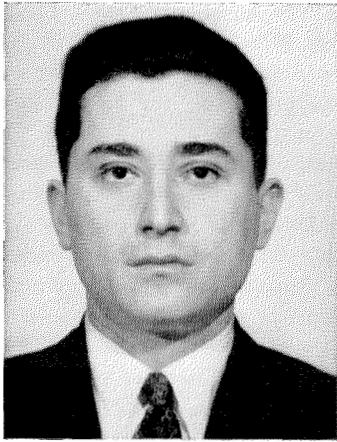
City of New York in 1944 and a master's degree in 1951 from Polytechnic Institute of Brooklyn.

After several years with the Board of Transportation of New York City, he joined the staff of Federal Telecommunication Laboratories in 1951. A report on some of his work on microstrip lines is included in this issue of *Electrical Communication*.

Mr. Elefant is now associated with Airborne Instrument Laboratories of Mineola, New York.

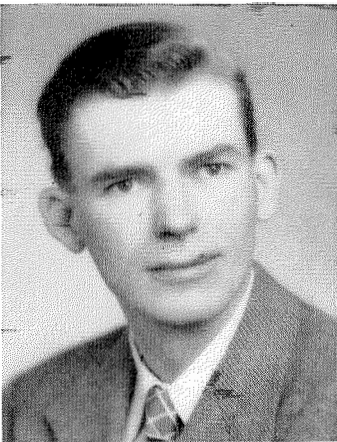JACK ELEFANT

• • •

D. S. RIDLER

He worked first at the Institute of Electrical Engineering of the Technical University of Dresden. In 1948, he joined the Standard Elektrizitäts-Gesellschaft AG (division of Mix & Genest). Since that time, he has been engaged in the development of various carrier-frequency telephony systems.

In this issue, he is author of a paper on distortion in carrier-frequency modulators.

• • •

JACK ELEFANT was born in New York City on October 8, 1923. He received a bachelor's degree in electrical engineering from the College of the

HENRY G. NORDLIN was born in Saint Paul, Minnesota, on September 1, 1921. He received the B.E.E. degree from the University of Minnesota in 1943 and has since completed his studies for an M.S. degree in electrical engineering at Stevens Institute of Technology.

He joined the Federal Telephone and Radio Company in 1943 and is now a project engineer in the chemical and physical division of Federal Telecommunication Laboratories.

Mr. Nordlin is a Senior Member of the Institute of Radio Engineers.

• • •

WILLIAM SICHAK was born on January 7, 1916, in Lyndora, Pennsylvania. He received the B.A. degree in physics from Allegheny College in 1942.

From 1942 to 1945, he was engaged in developing microwave radar antennas at the Radiation Laboratory of Massachusetts Institute of Technology. Since then, he has been with Federal Telecommunication Laboratories, working on microwave antennas and allied equipment. In this issue, he is author of a paper on coaxial lines with helical inner conductors.

Mr. Sichak is in charge of the antennas and components division in the laboratories. He is a Member of the

HENRY G. NORDLIN

D. S. RIDLER was born in London, England, in 1921. He joined the telephone switching division of Standard Telephones and Cables, Limited, in 1939 and later transferred to Standard Telecommunication Laboratories, Limited, where he has been engaged in work on the design and application of digital devices.

Mr. Ridler is the coauthor of the paper in this issue on the application of functional diagrams to electronic telegraph circuits. He is an Associate Member of the Institution of Electrical Engineers.

WILLIAM SICHAK

Institute of Radio Engineers and of the American Physical Society.

* * *

E. P. G. WRIGHT joined the equipment engineering branch of the Western Electric Company in London in 1920, and in 1926 took charge of project engineering when the company became associated with the International System. In 1928, Mr. Wright was transferred to the laboratories to work on switching problems. He was in charge of switching-system design for Stand-

E. P. G. WRIGHT

ard Telephones and Cables, Limited, from 1932 until the war, when he was assigned to special duties on radio production and test-equipment design.

Mr. Wright is an author of the paper in this issue on functional diagrams for the design of telegraph circuits.

Mr. Wright served as a member of the British Telephone Technical Development Committee from its inception until 1939. He is a member of the Institution of Electrical Engineers and was awarded the Fahie Premium for papers on the bypath system and voice-frequency signalling and dialling.

INTERNATIONAL TELEPHONE AND TELEGRAPH CORPORATION

MANUFACTURE AND SALES

North America

UNITED STATES OF AMERICA —

Divisions of International Telephone and Telegraph Corporation

Capehart–Farnsworth Company; Fort Wayne, Ind ana

Federal Telephone and Radio Company; Clifton, New Jersey

Kellogg Switchboard and Supply Company; Chicago, Illinois

Federal Electric Corporation; Clifton, New Jersey

International Standard Electric Corporation; New York, New York

International Standard Trading Corporation; New York, New York

K llogg Credit Corporation; Chicago, Illinois

CANADA — (*See British Commonwealth of Nations*)

British Commonwealth of Nations

ENGLAND —

Standard Telephones and Cables, Limited; London

Creed and Company, Limited; Croydon

International Marine Radio Company Limited; Croydon

Kolster-Brandes Limited; Sidcup

CANADA — Standard Telephones & Cables Mfg. Co. (Canada), Ltd.; Montreal

AUSTRALIA —

Standard Telephones and Cables Pty. Limited; Sydney

Silovac Electrical Products Pty. Limited; Sydney

Austral Standard Cables Pty. Limited; Melbourne

NEW ZEALAND — New Zealand Electric Totalisators Limited; Wellington

Latin America and West Indies

ARGENTINA — Compañía Standard El ctric Argentina, S.A.I.C.; Buenos Aires

BRAZIL — Standard Electrica, S.A.; Rio de Janeiro

CHILE — Compañía Standard Electric, S.A.C.; Santiago

CUBA — Standard Products Distributing Company; Havana

MEXICO — Standard Electrica de Mexico, S.A.; Mexico City

PUERTO RICO — Standard Electric Corporation of Puerto Rico; San Juan

Europe

AUSTRIA — Vereinigte Telephon- und Telegraphenfabriks A. G., Czeija, Nissl & Co.; Vienna

BELGIUM — Bell Telephone Manufacturing Company; Antwerp

DENMARK — Standard Electric Aktieselskab; Copenhagen

FINLAND — Oy Suomen Standard Electric AB; Helsinki

FRANCE —
Compagnie Générale de Constructions Téléphoniques; Paris
Le Matériel Téléphonique; Paris
Les Téléimprimeurs; Paris

GERMANY —
Standard Elektrizitäts–Gesellschaft A.G.; Stuttgart
Divisions
Mix & Genest; Stuttgart
Süddeutsche Apparatefabrik; Nürnberg
C. Lorenz, A.G.; Stuttgart
G. Schaub Apparatebau; Pforzheim

ITALY — Fabbrica Apparecchiature per Comunicazioni Elettriche; Milan

NETHERLANDS — Nederlandsche Standard Electric Maatschapp j N.V.; The Hague

NORWAY — Standard Telefon og Kabelfabrik A/S; Oslo

PORTUGAL — Standard Eléctrica, S.A.R.L.; Lisbon

SPAIN —
Compañía Radio Aérea Marítima Española; Madrid
Standard Eléctrica, S.A.; Madrid

SWEDEN — Aktiebolaget Standard Radiofabrik; Stockholm

SWITZERLAND — Standard Telephone et Radio S.A.; Zurich

TELEPHONE OPERATIONS

BRAZIL — Companh a Telefônica Nacional; R o de Janeiro

CHILE — Compañía de Tel fonos de Chile; Sant ago

CUBA — Cuban American Telephone and Telegraph Company; Havana

CUBA — Cuban Telephone Company; Havana

PERU — Compañía Peruana de Teléfonos Limitada; Lima

PUERTO RICO — Porto Rico Telephone Company; San Juan

CABLE AND RADIO OPERATIONS

UNITED STATES OF AMERICA —
American Cable & Radio Corporation; New York, New York
All America Cables and Radio, Inc.; New York, New York
The Commercial Cable Company; New York, New York
Mackay Radio and Telegraph Company; New York, New York

ARGENTINA —
Compañía Internacional de Radio; Buenos Aires
Sociedad Anónima Radio Argentina; Buenos Aires (*Subsidiary of American Cable & Radio Corporation*)

BOLIVIA — Compañía Internac onal de Radio Boliviana; La Paz

BRAZIL — Companhia Radio Internacional do Brasil; Rio de Janeiro

CHILE — Compañía Internacional de Rad o, S.A.; Santiago

CUBA — Radio Corporation of Cuba; Havana

PUERTO RICO — Radio Corporation of Porto Rico; San Juan

RESEARCH

UNITED STATES OF AMERICA —
Divisions of International Telephone and Telegraph Corporation
Farnsworth Electronics Company; Fort Wayne, Indiana
Federal Telecommunication Laboratories; Nutley, New Jersey
International Telecommunication Laboratories, Inc.; New York, New York

ENGLAND — Standard Telecommunication Laboratories, Limited; London

FRANCE — Laboratoire C ntral de Té écommunications; Paris

ASSOCIATE LICENSEES FOR MANUFACTURE AND SALES IN JAPAN

Nippon Electric Company, Limited; Tokyo

Sum tomo Ele tric Industries, Limited; Osaka